47047

National Library of Canada
Bibliothèque nationale du Canada

Canadian Theses Division
Division des thèses canadiennes

Ottawa, Canada
K1A 0N4

PERMISSION TO MICROFILM — AUTORISATION DE MICROFILMER

• Please print or type — Écrire en lettres moulées ou dactylographier

Full Name of Author — Nom complet de l'auteur

Francis Stuart Foster

Date of Birth — Date de naissance	Country of Birth — Lieu de naissance
July 29 52	Canada

Permanent Address — Résidence fixe

12 Laurier Av
Toronto Ont

Title of Thesis — Titre de la thèse

The development of new ultrasonic imaging techniques for the early detection of breast cancer.

T 1

University — Université

Toronto

Degree for which thesis was presented — Grade pour lequel cette thèse fut présentée

Ph. D.

Year this degree conferred — Année d'obtention de ce grade	Name of Supervisor — Nom du directeur de thèse
~~1979~~ 1980	John W. Hunt

Permission is hereby granted to the NATIONAL LIBRARY OF CANADA to microfilm this thesis and to lend or sell copies of the film.

The author reserves other publication rights, and neither the thesis nor extensive extracts from it may be printed or otherwise reproduced without the author's written permission.

L'autorisation est, par la présente, accordée à la BIBLIOTHÈQUE NATIONALE DU CANADA de microfilmer cette thèse et de prêter ou de vendre des exemplaires du film.

L'auteur se réserve les autres droits de publication; ni la thèse ni de longs extraits de celle-ci ne doivent être imprimés ou autrement reproduits sans l'autorisation écrite de l'auteur.

Date	Signature
Dec 14 / 79	Stuart Foster

NL-91 (4/77)

Reproduced with permission of the copyright owner. Further reproduction prohibited without permission.

National Library of Canada

Cataloguing Branch
Canadian Theses Division

Ottawa, Canada
K1A 0N4

Bibliothèque nationale du Canada

Direction du catalogage
Division des thèses canadiennes

NOTICE

The quality of this microfiche is heavily dependent upon the quality of the original thesis submitted for microfilming. Every effort has been made to ensure the highest quality of reproduction possible.

If pages are missing, contact the university which granted the degree.

Some pages may have indistinct print especially if the original pages were typed with a poor typewriter ribbon or if the university sent us a poor photocopy.

Previously copyrighted materials (journal articles, published tests, etc.) are not filmed.

Reproduction in full or in part of this film is governed by the Canadian Copyright Act, R.S.C. 1970, c. C-30. Please read the authorization forms which accompany this thesis.

THIS DISSERTATION
HAS BEEN MICROFILMED
EXACTLY AS RECEIVED

AVIS

La qualité de cette microfiche dépend grandement de la qualité de la thèse soumise au microfilmage. Nous avons tout fait pour assurer une qualité supérieure de reproduction.

S'il manque des pages, veuillez communiquer avec l'université qui a conféré le grade.

La qualité d'impression de certaines pages peut laisser à désirer, surtout si les pages originales ont été dactylographiées à l'aide d'un ruban usé ou si l'université nous a fait parvenir une photocopie de mauvaise qualité.

Les documents qui font déjà l'objet d'un droit d'auteur (articles de revue, examens publiés, etc.) ne sont pas microfilmés.

La reproduction, même partielle, de ce microfilm est soumise à la Loi canadienne sur le droit d'auteur, SRC 1970, c. C-30. Veuillez prendre connaissance des formules d'autorisation qui accompagnent cette thèse.

LA THÈSE A ÉTÉ
MICROFILMÉE TELLE QUE
NOUS L'AVONS REÇUE

NL-339 (3/77)

Reproduced with permission of the copyright owner. Further reproduction prohibited without permission.

THE DEVELOPMENT OF NEW ULTRASONIC IMAGING TECHNIQUES FOR THE EARLY DETECTION OF BREAST CANCER

by

Francis Stuart Foster

A Thesis

Submitted in Conformity

with the

Requirements for the Degree of

Doctor of Philosophy

in the

University of Toronto

Department of Medical Biophysics

University of Toronto

November, 1979

© F. S. Foster 1979

Reproduced with permission of the copyright owner. Further reproduction prohibited without permission.

UNIVERSITY OF TORONTO

SCHOOL OF GRADUATE STUDIES

PROGRAM OF THE FINAL ORAL EXAMINATION

FOR THE DEGREE OF DOCTOR OF PHILOSOPHY

OF

FRANCIS STUART FOSTER

10:00 a.m., Friday, December 14, 1979

Room 307, 63 St. George Street

THE DEVELOPMENT OF NEW ULTRASONIC IMAGING TECHNIQUES FOR THE EARLY DETECTION OF BREAST CANCER

Committee in Charge:

Professor R. Volpe, Chairman
Professor M.J. Bronskill
Professor A.J. Cousin
Professor J. Cunningham
Professor J. Hunt, Supervisor
Professor H.E. Johns
Professor F.P. Ottensmeyer
Professor R.C. Waag, External Examiner
Professor G.F. Whitmore

Reproduced with permission of the copyright owner. Further reproduction prohibited without permission.

Title: The Development of New Ultrasonic Imaging Techniques for the Early Detection of Breast Cancer

Author: F. S. Foster

Supervisor: J. W. Hunt

ABSTRACT

Ultrasound is the basis of a varied and rapidly expanding group of medical diagnostic procedures. Although the breast is well situated and contains no structures that obstruct the propagation of ultrasound, this organ has proved to be one of the most difficult to adequately image. Investigation in this field has recently been stimulated by reports indicating that a significant decrease in mortality due to breast cancer could be achieved using a safe effective screening procedure. While mammography is an effective means of detecting small breast tumours, many critics feel that its use would result in as many new breast cancers as were detected in the screening program. For this reason the use of ultrasound is a particularly appealing alternative. A number of groups have demonstrated the capability of ultrasound in breast imaging but several problems remain to be solved before it can be used in routine clinical imaging or as a screening tool. Two of the most fundamental problems are addressed in this thesis. The first concerns the improvement of lateral resolution throughout the image and the second relates to the development of a comfortable and effective clinical scanning procedure.

The lateral resolution is directly related to the focussing of the ultrasound beam. The physics of ultrasound focussing in breast and other human tissues is examined using a unique variable aperture, variable focal length transducer. Focussing is tested as a function of lens f-number (focal length/diameter), tissue type and thickness.

Reproduced with permission of the copyright owner. Further reproduction prohibited without permission.

The causes of defocussing are investigated and the crucial role of ultrasound attenuation and system bandwidth are discussed. A frequency of 3.5-4.0 MHz and an f-number of 2.0-3.0 are recommended for breast imaging.

The use of low f-number lenses results in a reduction of the region in which the image remains sharp (depth of field). One way to solve this problem is to divide the image range into a number of well focussed "zones", each scanned separately, and summed to generate the final image. An instrument called the Demonstration Scanner is used to assess the validity of this approach. Significant resolution gains are demonstrated and a rule for selecting zone width is derived.

A new concept in ultrasound image formation, called the Cylindrical Transducer Scatter Scanner, has been invented. With it, the depth of field problem is attacked directly by replacing the traditional point focus with a line focus generated by a cylindrical transducer. Right-angle scatter, detected by a transducer aimed along the axis of the cylinder, is used to generate the image. This approach achieves an extremely sharp focus, with a depth of field essentially equal to the length of the cylinder. The ultrasonic field of the cylindrical transducer is examined experimentally and theoretically. Preliminary images of simple phantoms and in vitro tissue samples are exceptionally encouraging and a program for the development of scatter imaging technology is described.

Breast II is a simple ultrasound breast scanner designed for clinical use. Emphasis is placed on the development of a comfortable and acceptable scanning procedure, not on resolution. The rationale behind this design is discussed. Clinical results indicate that a simple linear scanning regime is sufficient to provide high quality images of normal and pathological tissues. The design of Breast III, a zone focussed rectilinear scanner is outlined briefly.

Reproduced with permission of the copyright owner. Further reproduction prohibited without permission.

CURRICULUM VITAE

NAME: Francis Stuart Foster

ADDRESS: Physics Division
Ontario Cancer Institute
500 Sherbourne Street
Toronto, Ontario, Canada M4X 1K9

TELEPHONE: 416-724-0671 Ext. 663

DATE OF BIRTH: July 29, 1951

CITIZENSHIP: Canadian

EDUCATION: B.A.Sc. Engineering Physics,
University of British Columbia, 1974.

M.Sc. "The Design and Characterization of Short Pulse Ultrasound Transducers", Department of Medical Biophysics, University of Toronto, 1977.

Ph.D. nearing completion (see "Research Experience" for project description).

DISTINCTIONS: National Cancer Institute Studentship, April 1978 to present.

RESEARCH INTERESTS: Ultrasonic diagnostics.
New transducer materials and technology for improvement of image quality.
Interaction of ultrasound with tissue aimed at characterization of normal and abnormal conditions.

PUBLICATIONS:

1) F.S. Foster and J.W. Hunt (1978): The design and characterization of short pulse ultrasound transducers. Ultrasonics 16; 116-122.

2) F.S. Foster and J.W. Hunt: The focussing of ultrasound beams through human tissue. Proc. 8th Int. Symp. Acoustical Imaging, Key Biscayne, Florida, 1978 (in press).

3) F.S. Foster and J.W. Hunt: Transmission of ultrasound beams through human tissue: focussing and attenuation studies. Ultrasound in Medicine and Biology (in press).

4) W.B. Taylor, J.W. Hunt, F.S. Foster and R. Blend: A high-resolution transrectal ultrasonographic system. Ultrasound in Medicine and Biology (in press).

Reproduced with permission of the copyright owner. Further reproduction prohibited without permission.

5) F.S. Foster, M. Arditi and J.W. Hunt: The cylindrical transducer scatter scanner. Submitted to the Journal of the Acoustical Society of America.

6) F.S. Foster: Portfolio of photographs, Photo Life Magazine, June 1978.

PATENT: Ultrasonic Imaging Device (cylindrical Transducer Scatter Scanner) Patent applied for April 26, 1979.

RESEARCH EXPERIENCE: 1) Ph.D. RESEARCH (aimed at studying the interaction of ultrasound with breast tissue and applying the knowledge gained to the design of a high resolution breast scanner for clinical use).
- development of a variable focal length ultrasound lens using liquid Freon (2)
- study of focussing of ultrasound beams in tissue, especially breast (2,3)
- effect of absorption, scattering and system bandwidth on focussing (3)
- development of a demonstration scanner image 10 cm of tissue in vitro using an f/1.8 to f/20.0 liquid Freon lens in conjunction with a 7.5 cm annular array (Object: find optimum f-numbers for detecting various lesions in tissue)
- invention and initial development of the cylindrical transducer scatter scanner (5)

2) TRANSDUCER TECHNOLOGY
- fabrication and testing of short-pulse (wideband) transducers (1)
- lens, both variable focus and fixed focus
- large aperture techniques
- annular array fabrication
- study of Poly Vinylidene Fluoride (PVF_2) transducers

3) ATTENUATION MEASUREMENTS
- computerized transient analysis approach using unipolar pulse transducers (3)
- continuous wave approach

4) PRACTICAL DESIGN OF CLINICAL ULTRASOUND SCANNERS
- transrectal scanner now in routine clinical use (4)
- simple breast scanner using a water bag coupling, initial clinical tests underway

Reproduced with permission of the copyright owner. Further reproduction prohibited without permission.

F. Stuart FOSTER

Major and Minor Fields and Principal Instructors:

Major Field: Radiation Physics (MBP 1003Y) - Dr. J. Cunningham

First Minor Field: Cellular Biophysics (MBP 1011B) - Dr. R. Phillips

Second Minor Field: Holography and Optical Signal Processing (ELE 1211Y) - Dr. K. Iizuka

Reproduced with permission of the copyright owner. Further reproduction prohibited without permission.

THE UNIVERSITY OF TORONTO LIBRARY

MANUSCRIPT THESIS

AUTHORITY TO DISTRIBUTE.

NOTE: The AUTHOR will sign in one of the two places indicated. It is the intention of the University that there be NO RESTRICTION on the distribution of the publication of theses save in exceptional cases.

(a) Immediate publication in microform by the National Library is authorized.

Author's signature Alison Lost .... Date Jan 25/80

or

(b) Publication by the National Library is to be postponed until Sept 1, 19.. (normal maximum delay is two years). Meanwhile this thesis may not be consulted in the University Library except with written permission on each occasion from me.

Author's signature Alison Lost ... Date Jan 25/80

This restriction is authorized for reasons which seem to me, as Head of the Graduate Department of ....., to be sufficient.

Signature of Graduate Department Head .....

Date .....

BORROWERS undertake to give proper credit for any use made of the thesis, and to obtain the consent of the author if it is proposed to make extensive quotations, or to reproduce the thesis in whole or in part.

Signature of borrower	Address	Date

FORM TO BE BOUND WITH TWO COPIES OF DOCTORAL THESIS FACING FRONT COVER

202 A

REVISED AUGUST 1973

Reproduced with permission of the copyright owner. Further reproduction prohibited without permission.

Of all the wonders of nature, ultrasound is perhaps the most remarkable, with the possible exception of a moose singing "Embraceable You" in spats.

-after Woody Allen.

Reproduced with permission of the copyright owner. Further reproduction prohibited without permission.

ACKNOWLEDGEMENTS

I gratefully offer thanks to:

John Hunt, for seasoning my graduate career with just the right amount of challenge, council, and friendship;

The staff and students of this Department whose suggestions and good humour helped maintain my equanimity and sanity: faulty socks notwithstanding;

The members of the machine shop and electronics group, who deserve much of the credit for the clinical prototype, Breast II;

Ralph Blend for providing valuable clinical input;

Marcel Arditi for his generous assistance on the theoretical aspects of the cylindrical scanner;

Art Worthington, for helping construct the electronics for the Demonstration Scanner;

Linda Comish, for not only typing the thesis but also correcting numerous spelling and grammatical errors;

The National Cancer Institute, for financial support; and especially

Michele Francoeur for brightening up my life during the course of this work.

Reproduced with permission of the copyright owner. Further reproduction prohibited without permission.

TABLE OF CONTENTS

CHAPTER 1	INTRODUCTION	1
	Importance of Early Detection	2
	Ultrasonography	4
	- Pulse Echo Imaging	4
	- Ultrasonography of the Breast	6
	Research Objectives	9
	- Focussing and Resolution	10
	- Effect of Tissue on Focussed Ultrasound Beams	11
	- Solutions to the Depth-of-Field Problem	12
	- Cylindrical Scanner for Breast Imaging	15
	- Clinical Pulse-Echo Prototypes	15
	References	17
CHAPTER 2	TRANSMISSION OF ULTRASOUND BEAMS THROUGH HUMAN TISSUE: FOCUSSING AND ATTENUATION STUDIES	21
	Introduction	22
	Equipment and Techniques	23
	- Focussing Experiments	23
	- System Characteristics	28
	- Attenuation Measurements	30
	Experimental Studies	32
	- Focussing in Water	32
	- Focussing Through Human Tissues	35
	- Attenuation Measurements	40
	Summary	47
	References	49

Reproduced with permission of the copyright owner. Further reproduction prohibited without permission.

CHAPTER 3 THE DEMONSTRATION SCANNER

Introduction 52

General Description 53

- Transducer (AR2) 54

- Freon Focussing System 57

- Gating 60

- Transducer Motion 62

Results 63

- Phantom Study 63

- Zone Width 64

- Tissue Study 68

Summary 69

Referehces 71

CHAPTER 4 THE CYLINDRICAL TRANSDUCER SCATTER SCANNER 72

Introduction 73

Basic Principles 74

Cylindrical Transducers: Practical Considerations 76

Electronics and Measurement Techniques 81

Ultrasound Field of the Cylindrical Transducer 82

- Central Region 82

- Edge Field 92

A Simple Scanner for B and C Mode Imaging 94

Summary and Conclusions 97

References 101

Reproduced with permission of the copyright owner. Further reproduction prohibited without permission.

CHAPTER 5	FUTURE OF THE CYLINDRICAL SCANNER	103
	Physics	104
	- Scattering in Breast Tissue	104
	- Artefact Reduction	105
	- New Geometries	106
	Transducer Materials	107
	Prototype Scanners	110
	Summary	115
	References	117
CHAPTER 6	CLINICAL PULSE-ECHO PROTOTYPES	118
	Scanning Approach	120
	Breast II	123
	Future Work	128
	Summary and Conclusions	131
	References	132
CHAPTER 7	CONCLUSIONS	133
APPENDIX	DEMONSTRATION SCANNER DETAILS	137
	Electrical Characteristics of AR2	138
	Transducer Motion	144
	Freon Pump Controller	144
	Signal Gating	145

Reproduced with permission of the copyright owner. Further reproduction prohibited without permission.

CHAPTER 1

INTRODUCTION

Reproduced with permission of the copyright owner. Further reproduction prohibited without permission.

I. IMPORTANCE OF EARLY DETECTION

Breast cancer kills more Canadian women than any other form of cancer (1). As well, this disease is responsible for the deaths of more women in the age group 40-44, than any other cause (2). Over the past 40 years, the overall death rates for other sites such as uterus and cervix have dropped significantly, while there has been no change in the rate for breast cancer. Surgery, radiotherapy, chemotherapy and hormone therapy seem to be unable to improve this situation.

The etiology of breast cancer is coupled with many factors (1,3-6). Particularly striking is the relationship between the survival rate and early diagnosis. The age-corrected survival rate for breast cancer seems to be closely allied with the size of the tumour at first diagnosis. According to Duncan and Kerr (5), a patient whose tumour has a size of 1 cm has a much greater probability of survival (over more than 20 years) than a patient whose tumour has a size of 3 cm (see Figure 1). Although their interpretation may be perfectly correct, many critics feel that

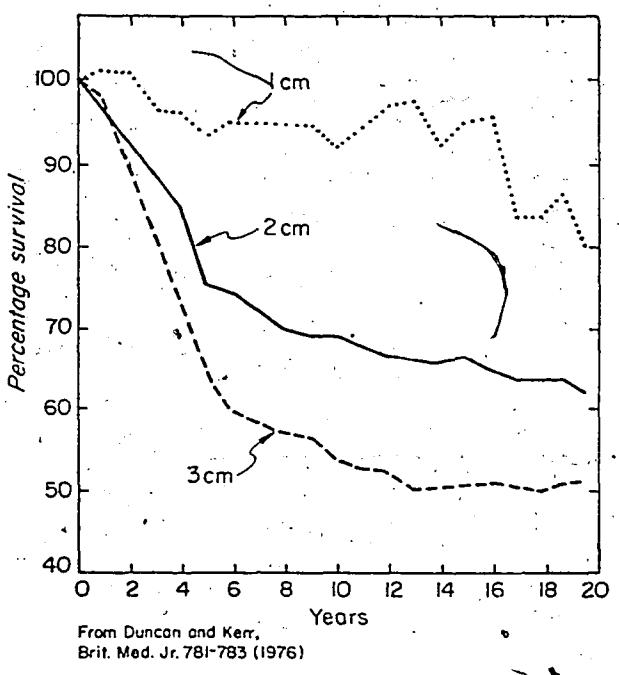

Figure 1. The age-corrected survival curves of women treated for breast cancers with sizes from 0.5-1.5 cm, 1.5-2.5 cm and 2.5-3.5 cm.

Reproduced with permission of the copyright owner. Further reproduction prohibited without permission.

experimental biases may account for some or all of the reported gain. The most important bias is called lead time, which may be succinctly stated as follows. If a tumour is detected 2 years earlier and if the patient lives two years longer from diagnosis, there is clearly no benefit from early detection. The true benefit of the early detection of breast cancer can only be assessed by means of properly controlled screening trials such as that performed by the Health Insurance Plan (HIP) of Greater New York (7) during the 1960's. The data from this randomized trial indicates that screening with mammography and physical examination would reduce breast cancer mortality of women over the age of 50 years by 40%. However, no decrease in mortality was found for women under the age of fifty.

The risk-benefit ratio for screening younger women is still hotly debated. Since the HIP study, radiation dosage in mammography has decreased markedly, while image definition has improved and radiologists have become more adept at reading mammograms. On the basis of the latter refinements, recent reports by the Breast Cancer Detection Demonstration Project of the USA (8,9) and Edinburgh screening trial (10) have suggested that mammography is now equally effective for all age groups. This optimism is not shared by everyone. Bailar (11) for example, has expressed an equally convincing contrary assessment. In his analysis he assumed a reasonable and conservative estimate of 2 rads per film set to the glandular tissue. Based on this dose and the recommendations of the Biological Effects of Ionizing Radiation (BEIR) report (12), Bailar concluded that mammography would take as many lives as it saves in a screening program, regardless of age.

In the midst of this controversy, the NCI and NIH of the United States have adopted an understandably conservative viewpoint. In the recently published NIH/NCI consensus on breast cancer screening (13) they endorsed mammography in combination with physical examination as an effective screening tool for women

Reproduced with permission of the copyright owner. Further reproduction prohibited without permission.

over the age of fifty, but did not recommend the use of mammography for screening asymptomatic women under the age of fifty (basically the same as the HIP study). Regardless of the outcome of the controversy, screening with mammography may never be accepted by the majority of North American women simply because of the potential hazard. Public apprehension over nuclear power is an analogous situation. The NIH/NCI consensus specifically recommends that more emphasis in research be placed on safe, non-invasive techniques such as ultrasound and thermography. Ultrasound is well suited to this task for several reasons: firstly, at diagnostic intensities ultrasound is safe; secondly, the application of new focussing techniques should allow the detection of minimal cancers deep within the breast; and finally, ultrasound offers the possibility of classifying tumours on the basis of echo patterns.

II. ULTRASONOGRAPHY

a) Pulse Echo Imaging

The term "ultrasonography" was coined by J.J. Wild and D. Neal (14) in 1951 to describe an ultrasonic echo ranging technique applicable to the examination of human tissues. In 1952, Wild and Reid (15) extended the concept to two dimensions and generated the first "echograms" of normal and diseased human tissue *in vivo*. The general method by which this visualization was accomplished closely parallels the system of underwater navigation called "sonar". An ultrasound transducer is excited with a short voltage pulse, causing the generation of an ultrasound pulse which propagates into the tissue at the speed of sound (see Figure 2). The frequency used is generally between 1 and 10 MHz and the physical length of the ultrasound pulse is on the order of 1-2 mm in tissue. The lateral dimension of the beam, δ, is controlled by the transducer size and focussing properties. These will be discussed in great detail later in this thesis. As the ultrasound pulse travels through tissue, encountering discontinuities such as organ boundaries and

Reproduced with permission of the copyright owner. Further reproduction prohibited without permission.

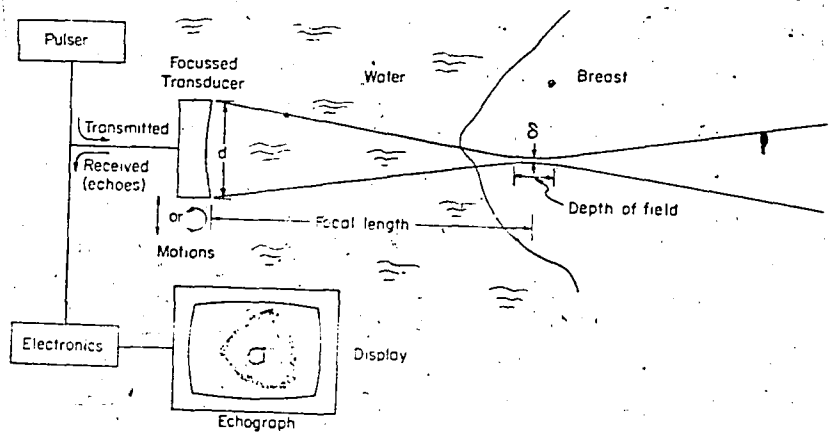

Figure 2. The principle of an ultrasound scanner is shown here. A short electrical pulse is used to excite a transducer producing an ultrasound pressure pulse that moves towards the breast. Whenever this wave interacts with different structures in the breast, reflections take place. These reflections are detected by the same transducer, received by the electronics, and displayed as a "line" on a video monitor. By scanning across the breast, a tomographical image is displayed.

blood vessels, echoes representing these interfaces are directed back towards the transducer. The transducer converts the echoes into electrical signals as a function of time. These signals are then displayed as bright spots on an oscilloscope. The distances between the bright spots on the oscilloscope are proportional to the distances between the corresponding structures in the tissue. Each pulse sent out by the transducer results in one line of image information. The orientation and position of the line on the oscilloscope is directly related to the orientation and position of the transducer, such that as the transducer is swept across the tissue, a tomographic image is generated.

In the past 25 years ultrasonography has evolved to the extent that it now makes an important contribution to medical imaging in almost every advanced radiology department in the world. The effect has been particularly revolutionary in obstetrics and dynamic imaging of the heart. An excellent review of the technology and clinical applications of ultrasound is "Biomedical Ultrasonics" by Wells (16).

Reproduced with permission of the copyright owner. Further reproduction prohibited without permission.

b) Ultrasonography of the Breast

The accurate diagnosis of lesions in the breast has been an important objective since the inception of ultrasonography. Wild's original scanner was first applied to breast visualization (17). The poor quality of images he obtained with this instrument (Figure 3a) were due to limitations in the mechanical aspects of the scanner and the high frequency (15 MHz) that was employed. The attenuation of ultrasound by breast at 15 MHz would limit visualization to only a few cm. Howry and Bliss (18) used frequencies in the low Megahertz region in an imaging system called the Somascope (tissue vision) which operated on the same principles as discussed above. The Somascope produced the first convincing images of tumours in excised breast tissue (Figure 3b) (19). By 1954, Wild had upgraded his system and was able to detect a small tumour behind the nipple in one subject (Figure 3c) (20). Kikuchi et al (21), DeLand (22) and Wells (23) each developed systems in the next decade-and-a-half that, while improving the image markedly, still did not have clinically acceptable resolution.

In 1972 the introduction of gray scale echography by Kossoff (24) greatly improved the diagnostic usefulness of echography by simply displaying echo amplitude as shades of gray. A wide range of improved breast scanning systems were subsequently developed by Jellins, Kossoff and co-workers (25), Kobayashi (26), Baum (27) and Fry (28). Increasing success was achieved in the accurate diagnosis of a large range of pathological differences in diseased breast. Figure 4 shows four breast scans from the excellent ultrasound group in Australia (25). On the top left is a compound echographical image of a young subject, showing the normal breast patterns due to the nipple, glandular ducts, chest wall, and adipose tissue. The top right photograph shows a small scirrhous carcinoma. This lesion (~0.5 cm) is characterized by the jagged appearance of the boundary. This carcinoma was able to be detected and diagnosed. The two bottom images show

Reproduced with permission of the copyright owner. Further reproduction prohibited without permission.

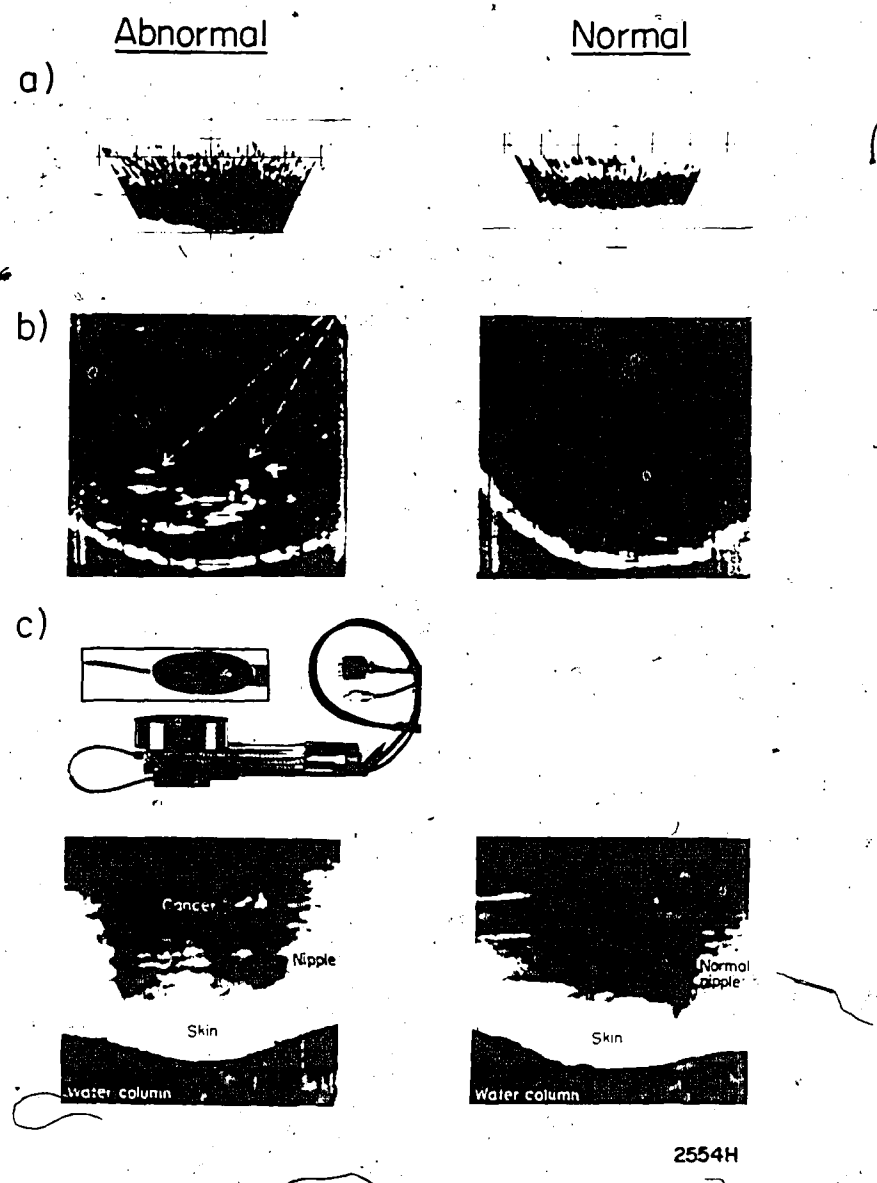

Figure 3. Early breast ultrasonograms: (a) Wild and Reid, 1952 (17), showing a carcinoma characterized by a general increase in echogenicity; (b) Howry et al, 1954 (19) in vitro. The normal breast scan shows no interior echoes while that for a large carcinoma shows many; (c) Wild and Reid, 1954 (20) detected a small cancer behind the nipple of one patient.

Reproduced with permission of the copyright owner. Further reproduction prohibited without permission.

Reproduced with permission of the copyright owner. Further reproduction prohibited without permission.

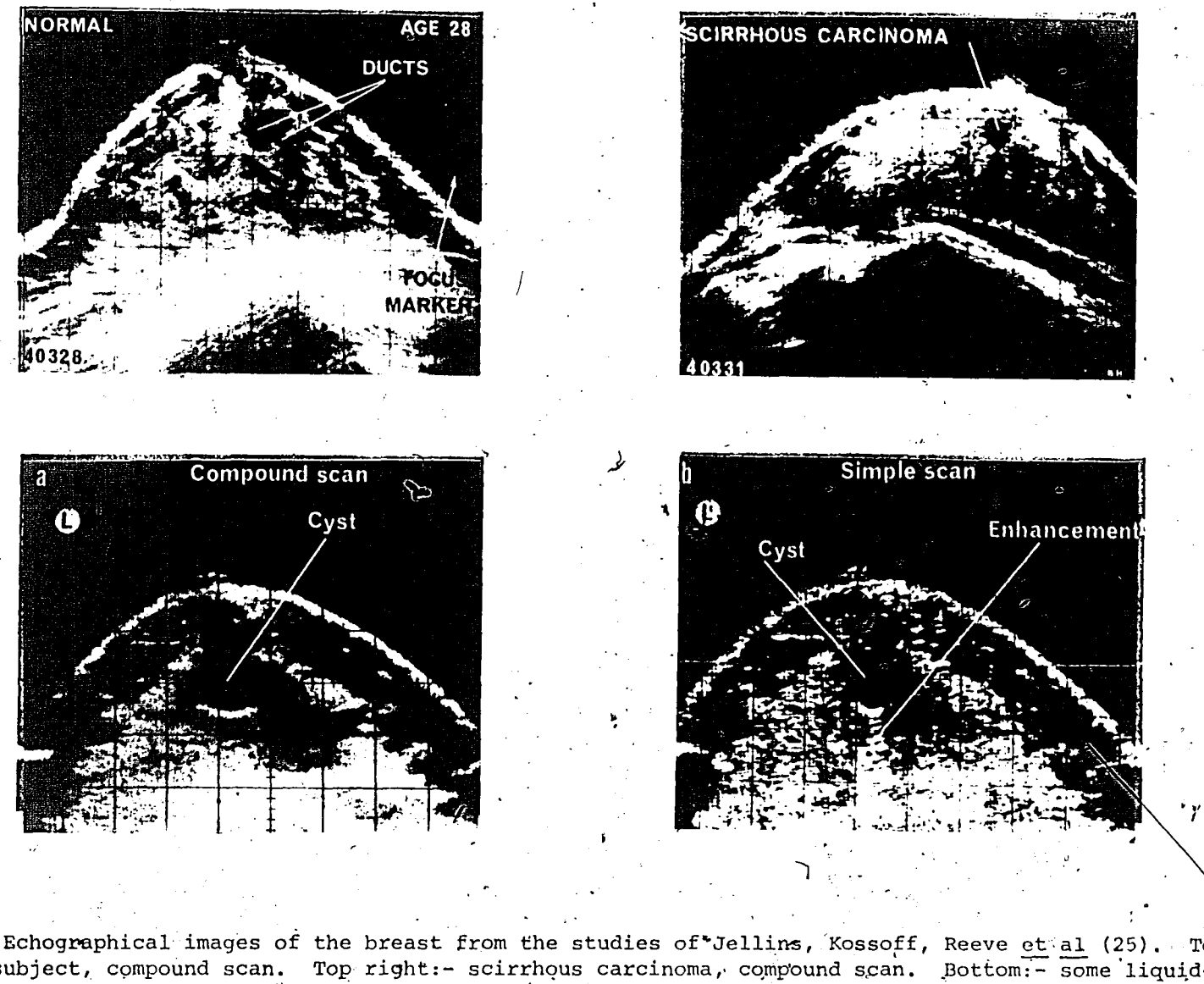

Figure 4. Echographical images of the breast from the studies of Jellins, Kossoff, Reeve et al (25). Top left:- normal subject, compound scan. Top right:- scirrhous carcinoma, compound scan. Bottom:- some liquid-filled cysts. Left:- compound scan. Right:- linear scan better indicates the enhancement of the ultrasound beyond the cyst. Similarly, a shadow below a tumour usually indicates a carcinoma.

similar scans of a cyst. On the left, the image was obtained by a compound scan, and shows the sharp boundaries, and echo-free regions characteristic of cysts. A somewhat different appearance is obtained by a simple linear scan (lower right). Fairly sharp boundaries are still observed, but as well, an enhancement of the echoes behind the cyst are observed. This appearance is useful to distinguish cysts from other benign lesions.

Based on this success, Wagai and Kobayashi were funded for a mobile system in Japan that was designed for general screening of the breast. Their studies were summarized in the recent book "Clinical Ultrasound of the Breast" (29).

Using ultrasound as a diagnostic tool, many investigators claim very high accuracies for malignant tumours. When Kobayashi (26) used three criteria (boundary echo and shape, internal echoes, and shadows beyond the lesions), he reported a diagnostic accuracy of 93%. Similarly Jellins et al (25) have indicated that the correct diagnosis of the malignancy is as good as 85% from five features of their echo patterns, and 98% for liquid filled lesions. These values of diagnostic accuracy are slightly inflated, since tumours at all stages were included. The accuracy for tumours in the T1 stage (primary with diameter less than 1.0 cm) was considerably lower. Encouraged by the results we began our own breast imaging project 2 years ago.

III. RESEARCH OBJECTIVES

The overall objective of our research program was to design a clinically useful ultrasound breast scanner with sufficient resolution to detect malignancies accurately in the T1 stage. My contributions towards this goal are in the following areas:

1. Investigation of the focussing and attenuation of ultrasound beams in human breast tissue (Chapter 2);

2. Development of methods for maintaining optimum focussing throughout the depth of tissue to be imaged (Chapters 3, 4 and 5); and

Reproduced with permission of the copyright owner. Further reproduction prohibited without permission.

3. Design of an efficient, accurate and comfortable scanning approach for clinical use (Chapter 6).

A large proportion of the work relates to the improvement of image resolution using ultrasound lenses. It is therefore vital to introduce the important parameters and terminology associated with the focussing of ultrasound and show how these effect the imaging process.

a) Focussing and Resolution

The focussing of light is a phenomenon with which most people are reasonably familiar. Fortunately, the formulae that describe the focussing of light waves can be applied to the focussing of ultrasound with virtually no alteration.

The ability of a lens to focus radiation is chiefly dependent on two parameters: λ, the wavelength of the radiation, and f-number, the ratio of the focal length to the lens diameter (30). A simple formula relating these two parameters for continuous wave (CW) radiation is:

$$\text{FWHM} = 1.41\lambda \text{ f-number} \qquad (1)$$

where FWHM refers to the full width at half maximum of the radiation amplitude distribution in the focal plane of the lens for a point object at infinity (ie. for plane waves). For example, consider the case of an eye observing a star. The lens of the eye has a diameter of about 5 mm and a focal length of 20 mm. Its f-number is therefore 4.0 (written f/4) and based on equation 1

$$\text{FWHM} = (1.41)\ (0.5\ \mu\text{m})\ (4.0) = 2.8\ \mu\text{m}$$

for green light. Thus the width of the image on the retina is approximately 2.8 μm across. The images of two such stars, separated by less than this distance would be difficult to resolve. In fact, FWHM is almost identical to the "Rayleigh resolution limit" given in most optics books (see for example, Born and Wolf (31)).

Reproduced with permission of the copyright owner. Further reproduction prohibited without permission.

We selected FWHM as an indication of the resolving capability of ultrasound lenses because it is readily measured experimentally..

A FWHM of 2.8 μm is enviably small. Comparable resolution with an f/4 ultrasound lens would require a frequency, $\nu = c/\lambda = 3.0$ GHz where c is the velocity of ultrasound in water. Ultrasound in the sub-GHz frequency range has been very successfully applied to acoustic microscopy (32) but, when it is necessary to penetrate 8.0 to 10.0 cm of breast tissue, frequencies no higher than about 5.0 MHz may be employed. This is due to the attenuating properties of the tissues as discussed in Chapter 2. If we accept the 5.0 MHz frequency limit, the maximum resolution expected in tissue becomes:

$$\text{FWHM} = (1.41)\ (c/\nu)\ (\text{f-number}) = (0.42)\ (\text{f-number})\ (\text{mm})$$

The ultrasound lenses presently used in conventional imaging systems have f-numbers ranging from 5 to 10. Consequently the maximum resolution at the focus ranges from ∿2.0 mm to 4.0 mm. One of the important contributions made in this thesis is the exploration of focussing in tissue at lower f-numbers (ie. between f/2 and f/5).

b) The Effect of Tissue on Focussed Ultrasound Beams (Chapter 2)

Thus far we have concerned ourselves with the focussing of continuous wave (CW) radiation by perfect lenses in non aberrating media. When ultrasound is focussed in tissue for the purpose of imaging, none of these conditions apply. It is rather like trying to focus light into pea soup[a]. To study this problem and determine the optimum f-number for breast imaging, a unique variable focal length (zoom) liquid Freon ultrasound lens was invented. Freon was chosen as the lens

[a] Such as that available at the Amsterdam Restaurant on Church Street.

Reproduced with permission of the copyright owner. Further reproduction prohibited without permission.

material when we discovered that it transmits ultrasound at a remarkably low velocity of 590 m/s. The acoustic refractive index, as defined by the ratio of the velocity of ultrasound in water to that in Freon, is 2.53. Such a high refractive index allows highly focussed beams to be formed by relatively thin spherical lenses. The construction, fabrication and testing of the Freon lens are discussed in Chapter 2. The focussing of ultrasound through human tissue was measured for a range of f-numbers from f/2 to f/10. The defocussing effects appeared to be due to two major mechanisms: (i) attenuation; and (ii) phase distortion of the converging wavefront due to refractive index variations in the tissue. Attenuation studies showed that the first mechanism was responsible for a large proportion of defocussing and could be controlled by the frequency bandwidth of the system. The second mechanism was important for heterogeneous tissues such as breast, where large fractions of the ultrasound energy were deflected off axis. Focussing properties were highly dependent on tissue type; however, for all tissues, optimum focussing was achieved below a focal-number of 3.

c) Solutions to the Depth-of-Field Problem

Demonstration Scanner (Chapter 3)

Most ultrasound imaging is carried out between f/5 and f/10 (16,33). The important consequence of going to lower f-numbers, as the focussing studies suggest, is loss of depth-of-field. This problem is illustrated in Figure 5. Here, a set of wires, spaced over a depth of 6 cm, are imaged at f/2.4. Note the excellent lateral resolution of the wires at the focal depth and the progressive degradation of the focus both in front and behind this point. As indicated in Figure 5, the degradation is almost wholly due to the physical convergence of the beam. To obtain a focussed image over a large depth, it is necessary to move the well focussed region throughout the depth of tissue to be imaged, while recording only the focussed information. To confirm the potential of this approach,

Reproduced with permission of the copyright owner. Further reproduction prohibited without permission.

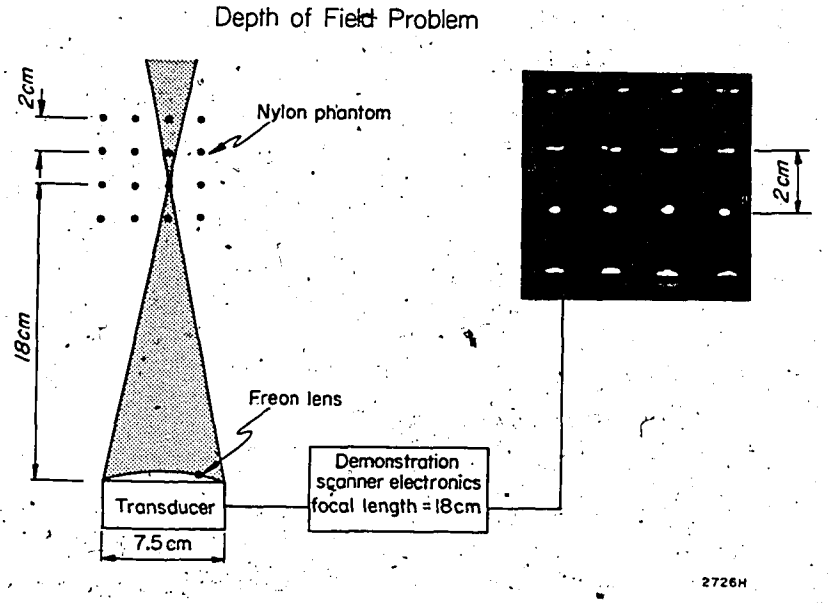

Figure 5. The depth-of-field problem. The beam is well focussed only near 18 cm. Nylon strings at 18 cm are well resolved but resolution degrades rapidly both in front and behind this distance. The image was made using the demonstration scanner (Chapter 3).

a "Demonstration Scanner" was constructed using the variable focal length property of the Freon lens (Chapter 3). Imaging studies with this device indicated that a significant improvement in image quality is obtained at the lower f-numbers as predicted.

Cylindrical Scanner (Chapters 4 and 5)

A unique and radically different approach to solving the depth-of-field problem is discussed in Chapter 4. The new device is called the Cylindrical Transducer Scatter Scanner, or just cylindrical scanner for brevity. It differs

Reproduced with permission of the copyright owner. Further reproduction prohibited without permission.

from conventional ultrasound scanners on two fundamental points: firstly, the beam is focussed into a line, not a point; and secondly, the image is based on ultrasound scattered at right angles in tissue in contrast to back scatter as in conventional ultrasonography. The cylindrical scanner employs separate transmitting and receiving transducers as shown in Figure 6. The transmitting transducer generates a cylindrical wavefront that converges to a line focus in the object. A receiving transducer aligned co-axially with the line focus, detects the ultrasound waves scattered at 90° from structures in the object. Because of the high degree of cylindrical focussing, the scatter is treated as if it arises from points on or very near the line focus. This allows the use of

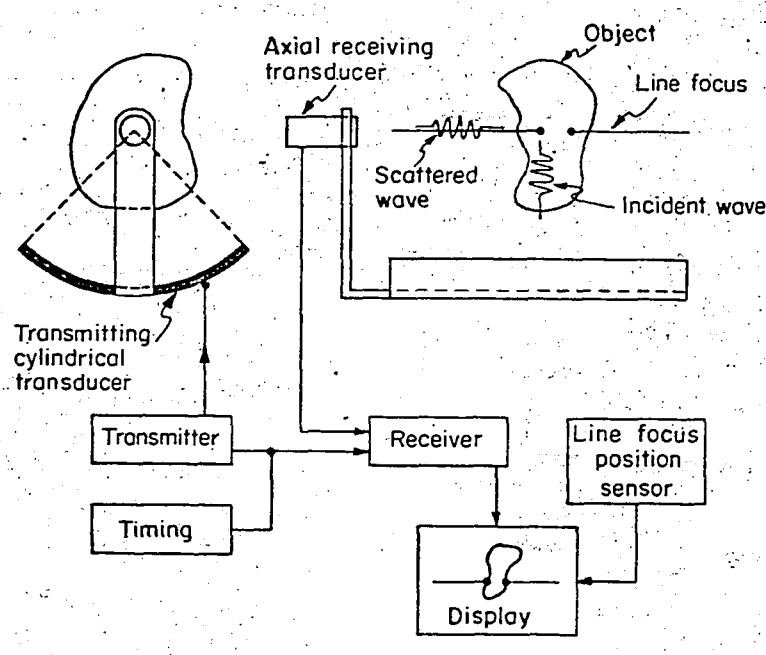

Figure 6. The cylindrical transducer transmits a pulse of ultrasound that converges to a line focus in the object to be imaged. A receiving transducer aimed along the line focus, detects some of the ultrasound scattered at an angle of 90° to the insonifying pulse. The receiver converts the scattered ultrasound into electrical signals for display. A tomographic image is generated by translating or rotating the two transducers as a unit, while appropriately displaying the scatter information.

Reproduced with permission of the copyright owner. Further reproduction prohibited without permission.

a ranging approach similar to that employed in conventional pulse-echo imaging. A tomographic image is generated by translating or rotating the two transducers as a unit while appropriately displaying the scatter information. This approach eliminates the depth-of-field problem inherent in pulse-echo imaging without sacrificing the speed or simplicity of the imaging process. The focussing properties of the cylinder greatly affect the resolving capability of the scanner. In Chapter 4 the focussing of cylindrical waves is examined in great detail from a theoretical point of view. A 120° cylindrical scanner was constructed and an experimental examination of its field was in close agreement with the theoretical predictions. Tissue and phantom images demonstrate remarkably improved resolution and depth-of-field compared to conventional pulse-echo images.

d) Cylindrical Scanner for Breast Imaging

Chapter 5 describes a plan to apply the cylindrical scanner to breast imaging. The proposed program is roughly divided into two parts:

1. The physics of image formation, involving basic studies of scatter, artefact generation, transducer materials and new geometries; and

2. Practical prototype development.

A large cylindrical transducer has been fabricated for the first breast prototype and has thus far produced exceptional images of *in vitro* tissue samples. However, before the device can be applied to breast imaging, a number of practical problems must be solved - especially in the areas of signal to noise, signal processing and mechanical design. The present status and future development of this exciting new imaging technique are discussed.

e) Clinical Pulse-Echo Prototypes (Chapter 6)

The success of any clinical or screening application of breast ultrasonography depends critically on the mechanical design of the instrument. It is especially important that the procedure be:

Reproduced with permission of the copyright owner. Further reproduction prohibited without permission.

1. Comfortable, even for elderly or sick patients;

2. Fast (∿5 min/examination); and

3. Simple to operate.

There are two schools of thought on how an ultrasound breast scanning procedure should be carried out. The first, championed by Jellins, Kossoff and co-workers (25) and Life Instruments Limited, involves the lowering of the unrestrained breast from above into an open water bath. Here, the woman is necessarily in the prone position. Transducers positioned in the water bath then scan the breasts according to some automated schedule. The second approach, used by Kobayashi (26) and Kelly-Fry (28), utilizes a transducer assembly scanned in a water bag that is lowered from above to make contact with the supine patients' breast. The advantages and disadvantages of both of these approaches are examined in Chapter 5. Our first clinical prototype (Breast II) was a modified version of the supine approach in which a sealed water bath was employed. This modification allows the use of a very flexible membrane to make contact with a large area of the breast. Breast II employs a conventional f/5 transducer and, although it does not deliver the highest resolution, it has given us valuable insight for the mechanical design and scanning arrangement for future prototypes. Specifically, Breast II satisfied us that the supine position was superior to the prone position and that a simple linear scanning regime was sufficient to provide high quality images of normal and pathological tissues. Breast II also served as an electronics proving ground. The focussing studies, demonstration scanner and Breast II prototype have each contributed to the Breast III scanner which we hope is going to provide safe, effective breast visualization for the early detection of cancer. The specifications and decision making process behind Breast III are discussed briefly.

Reproduced with permission of the copyright owner. Further reproduction prohibited without permission.

CHAPTER 1

REFERENCES

1. Patrick, H.: The diagnosis of breast cancer. CA 27: 209-232 (1977).

2. Strax, P.: The value of screening programs in the early detection of breast cancer. In: Clinical Uses of the Female Sex Hormones and Early Diagnosis and Treatment of Mammary Cancer. Proc. 2nd Annual Postgraduate Course. The Wilson Research Foundations, N.Y. Eds. R.A. Wilson and B.N. Craver, International Congress Series 258. pp. 34-44. Excerpta Medica, Amsterdam, 1972.

3. Seidman, H.: Screening for breast cancer in younger women: Life expectancy gains and losses. CA 28: 68-87 (1978).

4. Fisher, B., Slack, N.H., Bross, I.D.J. and Cooperating Investigators: Cancer of breast: size of neoplasm and prognosis. Cancer 24: 1071-1080 (1969).

5. Duncan, W. and Kerr, G.R.: The curability of breast cancer. Br. Med. J. Oct. 2, pp. 781-793 (1976).

6. Morgan, R.W. and Vikel, D.V.: Etiology of breast cancer. III. Opportunities for preventions. Can. Med. Assoc. J. 111: 1105-1107 (1974).

7. Strax, P., Venet, L. and Shapiro, S.: Value of mammography in reduction of mortality for breast cancer in mass screening. Am. J. Roentgenol. 117: 686-689 (1973).

8. Smart, C.R. and Beahrs, O.H.: Breast cancer screening results as viewed by the clinician. Cancer 43: 851-856 (1979).

9. Egeli, R.A. and Urban, J.A.: Mammography in symptomatic women 50 years of age and under, and those over 50. Cancer 43: 878-882 (1979).

10. Samuel, E.: Screening for breast cancer. Br. Med. J. 2: 175-178 (1978).

Reproduced with permission of the copyright owner. Further reproduction prohibited without permission.

11. Bailar, J.C.: Mammography - a contrary view. Ann. Intern. Med. 84: 77-84 (1976).

12. Advisory committee on the biological effects of ionizing radiation: the effects on populations of exposure to low levels of ionizing radiation. (BEIR Report) Washington, National Adacemy of Sciences, National Research Council, 1972.

13. NIH/NCI consensus development meeting on breast cancer screening. Preventative Medicine 7: 269-278 (1978).

14. Wild, J.J. and Neal, D.: Use of high frequency ultrasonic waves for detecting changes of texture in living tissues. Lancet 1: 655-657 (1951).

15. Wild, J.J. and Reid, J.M.: Application of echo ranging techniques to the determination of structure of biological tissues. Science 115: 226-230 (1952).

16. Wells, P.N.T.: Biomedical Ultrasonics (Academic Press, New York) Chapter 2, pp. 37-42, 1977.

17. Wild, J.J. and Reid, J.M.: Further pilot echographical studies on the histological structure of tumours of the living intact human breast. Am. J. Path. 28: 839-861 (1952).

18. Howry, D.H. and Bliss, W.R.: Ultrasonic visualization of soft tissue structures of the body. J. Laboratory and Clin. Med. 40: 579-592 (1952).

19. Howry, D.H., Stott, D.H. and Bliss, W.R.: The ultrasonic visualization of carcinoma of the breast and other soft tissue structures. Cancer 7: 354-358 (1952).

20. Wild, J.J. and Reid, J.M.: Echographic visualization of lesions of the living intact human breast. Cancer Res. 14: 277-283 (1954).

21. Kikuchi, Y., Uchida, R., Tanaka, K. et al: Early cancer diagnosis through ultrasonics. J. Acoust. Soc. Am. 29: 824-833 (1957).

Reproduced with permission of the copyright owner. Further reproduction prohibited without permission.

22. De Land, F.H.: A modified technique of ultrasonography for the detection and differential diagnosis of breast lesions. Am. J. Roent. Rad. Ther. Nucl. Med. 105: 446-452 (1969).

23. Wells, P.N.T. and Evans, K.T.: An immersion scanner for two-dimensional ultrasonic examination of the human breast. Ultrasonics 6: 220-228 (1968).

24. Kossoff, G., Garrett, W.J., Carpenter, D.A., Jellins, J. and Dadd, M.J.: Principles and classification of soft tissues by gray scale echography. Ultrasound in Med. Biol. 2: 89-105 (1976).

25. Jellins, J., Kossoff, G., Reeve, T.S. et al: (a) Ultrasonic gray scale visualization of breast disease. Ultrasound in Med. Biol. 1: 393-404 (1975). (b) Detection and classification of liquid-filled masses in the breast by gray scale echography. Radiology 125: 202-212 (1977).

26. Kobayashi, T.: Gray scale echography for breast cancer. Radiology 122: 207-214 (1977).

27. Baum, G.: Ultrasound mammography. Radiology 122: 199-205 (1977).

28. Kelly-Fry, E., Fry, F.J. and Gardner, G.W.: Recommendations for widespread application of ultrasound visualization techniques for examination of the female breast. In: Ultrasound in Medicine, Vol. III (Plenum Press, New York) 1977.

29. Kobayashi, T.: (a) Clinical ultrasound of the breast. (Plenum Press, New York) 1978. (b) Review: ultrasonic diagnosis of breast cancer. Ultrasound in Med. Biol. 1: 383-391 (1975).

30. Goodman, J.W.: Introduction to Fourier Optics. (McGraw-Hill, Toronto) p. 65, 1968.

31. Born, M. and Wolf, E.: Principles of Optics. (Pergamon Press, New York). p. 333, 1964.

Reproduced with permission of the copyright owner. Further reproduction prohibited without permission.

32. Kessler, L.W.: Review of progress and applications of acoustic microscopy. J. Acoust. Soc. Am. 55: 909-922 (1974).

33. Kossoff, G., Robinson, D.W. and Garrett, W.J.: Ultrasonic two-dimensional visualization for medical diagnosis. J. Acoust. Soc. Am. 44: 1310-1318 (1968).

Reproduced with permission of the copyright owner. Further reproduction prohibited without permission.

CHAPTER 2

TRANSMISSION OF ULTRASOUND BEAMS THROUGH HUMAN TISSUE: FOCUSSING AND ATTENUATION STUDIES

A summary of:

1. F.S. Foster and J.W. Hunt: The focussing of ultrasound beams through human tissue. Proc. 8th Int. Symp. Acoustical Imaging, Key Biscayne, Florida, 1978 (in press); and

2. F.S. Foster and J.W. Hunt: Transmission of ultrasound beams through human tissue: focussing and attenuation studies. Ultrasound in Medicine and Biology (in press).

Reproduced with permission of the copyright owner. Further reproduction prohibited without permission.

I. INTRODUCTION

At present, there is great interest in the improvement of resolution in medical ultrasonographic images. Although sub-millimeter resolution of deep-seated soft tissue structures may never be achieved, the present study of focussing shows good promise for low millimeter resolution through the use of low f-number (focal length/diameter) transducers in relatively homogeneous tissues.

Traditional contact ultrasound B-scanners, such as those used in the majority of clinical applications, employ small aperture (13-19 mm) single element transducers. The resolution of these devices has been discussed by many authors (eg. 1). In the range direction, resolution is limited by the pulse length (~2 mm). whereas the lateral resolution is governed by the diffraction and depth-of-field limitations (~4-20 mm, depending on the position in the field of the transducer). The improvement of lateral resolution to the level obtained in the range direction is contingent upon improved transducer focussing techniques.

Several groups have explored the potential of using large aperture (low f-number) transducers in improving the lateral resolution. One major problem with this technique is the poor depth-of-field provided by the highly convergent beam. Dietz et al (2) and Melton (3) have investigated the use of phased annular arrays as a means of overcoming this problem. Burckhardt et al (4) and Macovski and Norton (5) have also shown some success using the special properties of thin annuli. The improvement of lateral resolution depends on the transducer f-number and, to a certain extent, the properties of the tissue being imaged. Since low f-number systems do provide millimeter resolution in water, it is questionable whether a similar improvement could be obtained in soft tissue. Due to the complex arrangement of tissue along the path of the converging ultrasound

Reproduced with permission of the copyright owner. Further reproduction prohibited without permission.

beam, there may be a limit beyond which decreasing the f-number does not improve resolution. Ultimately, the limit of resolution must depend on the acoustical properties of the tissue such as spatial variations of refractive index, scattering properties, and as discussed later, attenuation. The severity of the effect of soft tissue interaction on the beams of conventional transducers was initially reported by Halliwell and Mountford (6). They investigated beam distortion and steering in the human calf. This work has been extended to other soft tissues by Banjavic (7) and Halliwell (8). We have made quantitative measurements of beam distortion as a function of f-number, tissue type, and tissue thickness. The results of the latter study indicate the necessity to measure focussing parameters in the actual tissue to be imaged, and not, as often occurs, in water.

The object of the present paper is to summarize our measurements of focussing in human tissue and to investigate the principle causes of defocussing: namely, attenuation and wavefront distortion due to refractive index variations. The crucial role of system bandwidth will also be explored.

II. EQUIPMENT AND TECHNIQUES

a) Focussing Experiments

The system used to perform the focussing measurements is shown in Figure 1. Basically, the experimental arrangement has four important components: (i) an ultrasound transmitter with variable aperture size; (ii) a lens with which the ultrasound is focussed at a given depth; (iii) a tissue container that separates the tissue (plus saline) from an environment of distilled water; and (iv) a small microphone that scans the distribution of ultrasound at the focal plane.

Reproduced with permission of the copyright owner. Further reproduction prohibited without permission.

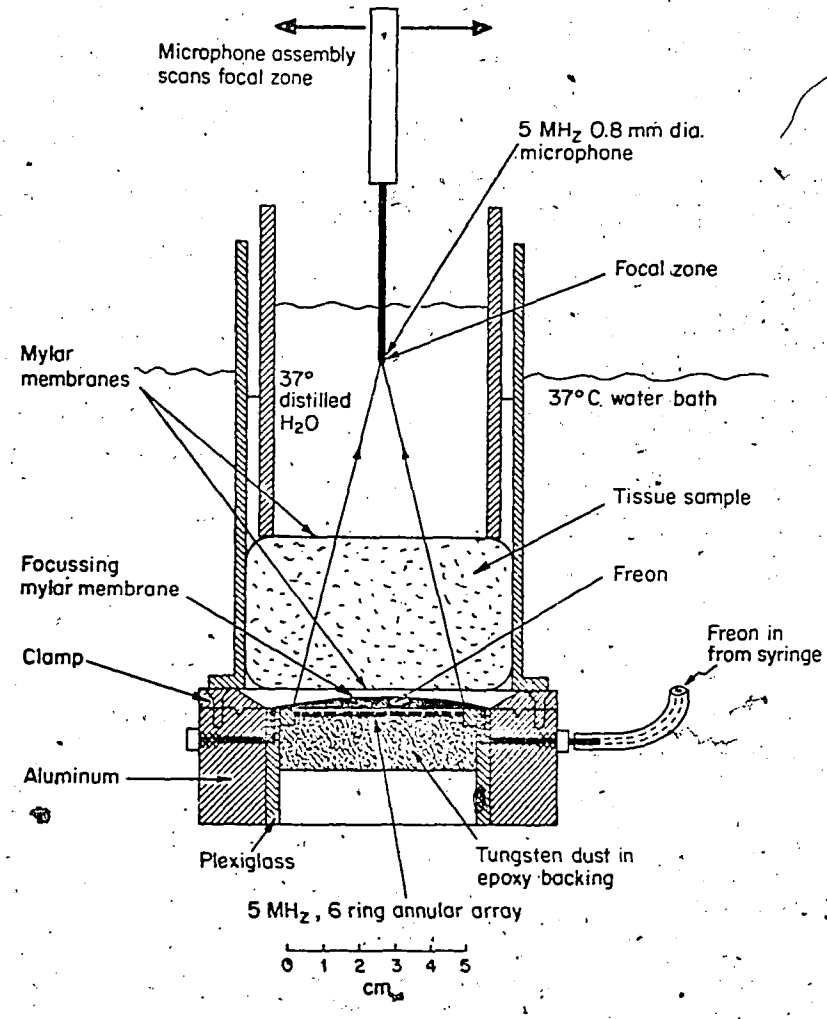

Figure 1. Cross-section of apparatus used in focussing experiments.

Reproduced with permission of the copyright owner. Further reproduction prohibited without permission.

The transmitter (AR1) is shown in Figure 2. The maximum diameter of this 6 ring annular array is 50 mm and it is focussed by means of a novel liquid Freon[a] lens. Freon has two special properties that make it an ideal lens material: exceptionally low velocity of sound (590 ms^{-1}) and high density (2.1 x 10^3 Kg m^{-3}). The low velocity of sound enables large apertures to be focussed by relatively thin lenses while the high density ensures an acoustical impedance similar to that of water. The focal length of AR1 can be altered by simply changing the amount

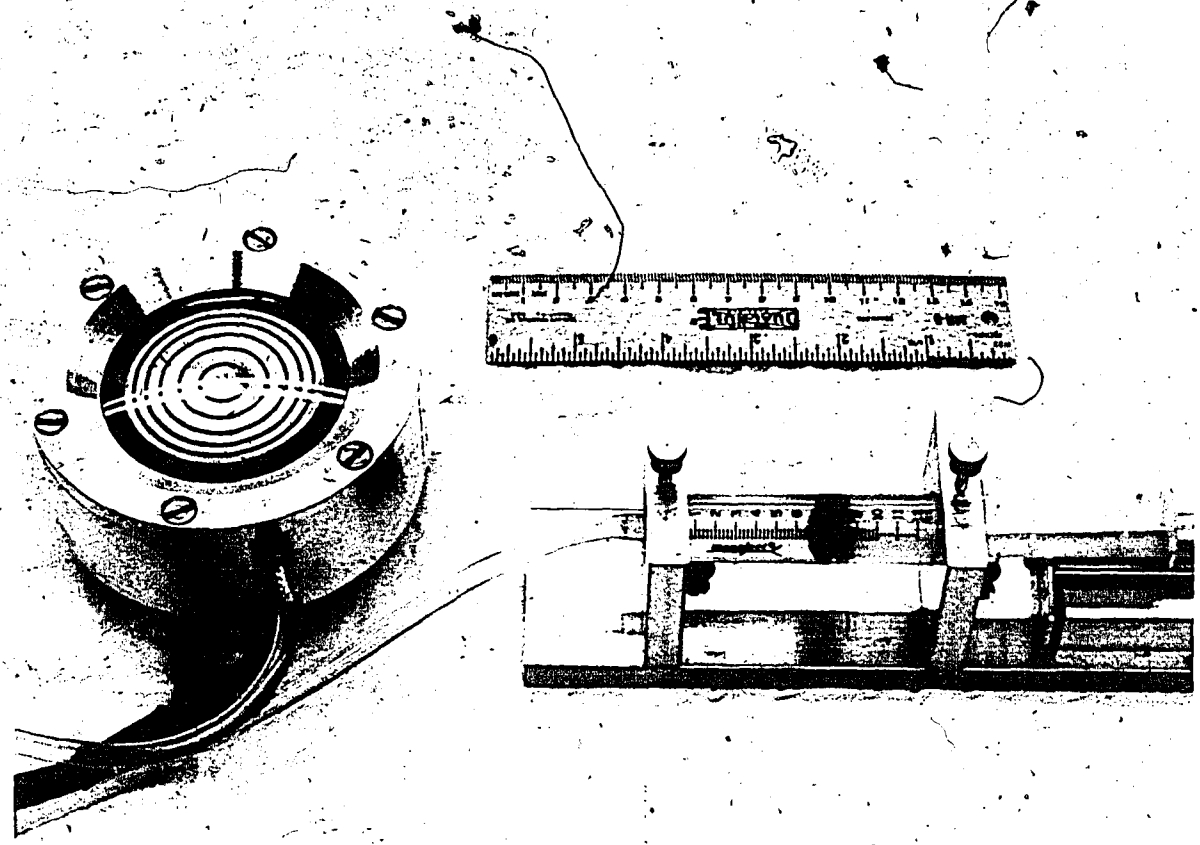

Figure 2. Transducer AR1: a 50 mm diameter annular array focussed by means of a liquid Freon lens. The syringe forces Freon in and out of the lens, changing the focal length.

[a] Dupont Freon 114B2, supplied by Columbia Organic Chemicals, Columbia, South Carolina.

Reproduced with permission of the copyright owner. Further reproduction prohibited without permission.

of Freon in the lens. If a thin spherical lens is assumed, the simple optical formula

$$f = \frac{r}{n - 1} \qquad (1)$$

may be used to predict the focal length, f, of the ultrasound lens. Here, r is the radius of curvature of the lens and n is the refractive index, as defined by the ratio of the velocity of sound in water to that in the lens. For Freon, n = 2.53 at 23°C. A calibration plot of Freon volume vs focal length is given in Figure 3. The theoretical curve was computed by first calculating r from the volume of Freon injected and then applying equation 1. The experimental points were obtained by measuring the distance from the transducer to the point at

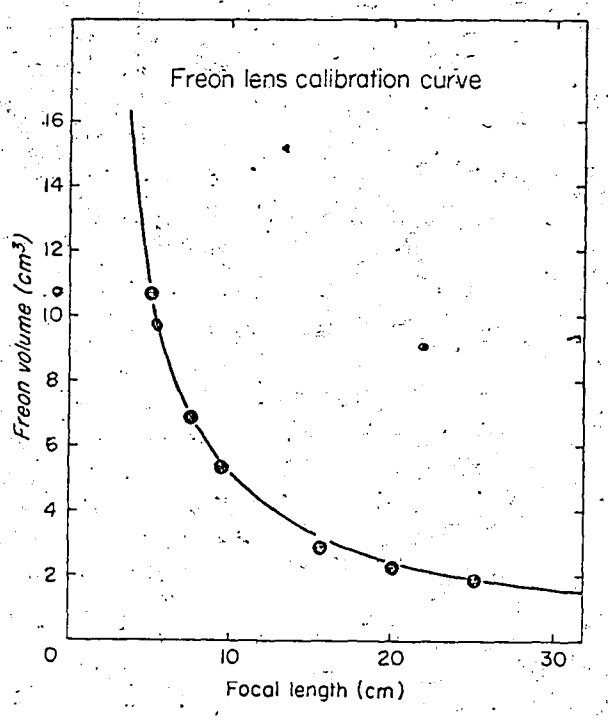

Figure 3. Freon lens calibration curve. Theoretical (——), Experimental (o o o).

Reproduced with permission of the copyright owner. Further reproduction prohibited without permission.

which the output of a small ultrasound microphone was at a maximum. Note that there is good agreement between experiment and theory.

As illustrated in Figure 1, samples were confined above the transmitter in a sealed Plexiglas container whose thin Mylar windows separated the tissue, plus phosphate buffered saline (PBS) from the distilled water in the tank. Above the upper surface, a 0.8 mm diameter phase sensitive piezoelectric microphone scanned the focal plane such that its output became the 'y' coordinate of an x-y display. The 'x' coordinate was proportional to the position of the microphone. An example of a typical beam profile is shown in Figure 4. Since this profile was the result

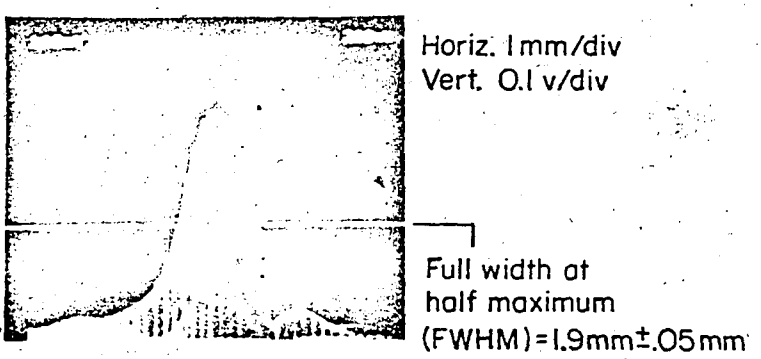

Figure 4. Distribution at the focal plane for an f/2 wideband ultrasound beam focussed through 1.2 cm of human liver at 37°C. The vertical axis represents the gated output of a 0.8 mm diameter microphone while the horizontal axis represents distance in the focal plane.

Reproduced with permission of the copyright owner. Further reproduction prohibited without permission.

of focussing a very short pulse (ie. a wide frequency spectrum), no side lobes were observed.

b) System Characteristics

Figure 5a shows the highly damped pulse transmitted by AR1, and its associated frequency spectrum. Good fidelity of the transmitted pulse shape was obtained by exciting the centre element with a step function of voltage and receiving the transmitted pulse in the far field with a thick (3 μs transit time) receiver. See Foster and Hunt (9) for details of this technique. The frequency spectrum of the transmitted pulse has a bandwidth of 5.1 MHz (-6 dB points) with an average frequency of 4.1 MHz.

The microphone consisted of a 0.8 mm diameter, 5 MHz disk of PZT5 (Vernitron Limited, Bedford, Ohio) mounted in the tip of an 18 gauge hypodermic needle. A 22 gauge varnished copper wire was inserted through the hypodermic needle to make contact with the back face of the disk and conductive epoxy was used to make an electrical connection between the front face and the body of the needle. The bandpass was from 3.5 to 6 MHz (-6 dB points), although the microphone was useful down to a frequency of 0.5 MHz. Measurements of microphone sensitivity as a function of angle at 3.8 MHz demonstrated an angular distribution with a FWHM (Full Width at Half Maximum) of 34° which is comparable to the 28.1° convergence of an f/2 beam.

Figure 5b shows the overall response of the transmitter, microphone, and amplifier used in the experiments. Note that the microphone and receiving circuits have narrowed the bandwidth of the transmitted pulse to 4 MHz with an average frequency of 3.8 MHz. The latter measurement was performed with the transducer at full aperture focussed at 10 cm. The microphone output consisted of one major oscillation followed by some lower amplitude ringing. The first oscillation was obtained by gating, as shown in Figure 5b and used in all measurements. This

Reproduced with permission of the copyright owner. Further reproduction prohibited without permission.

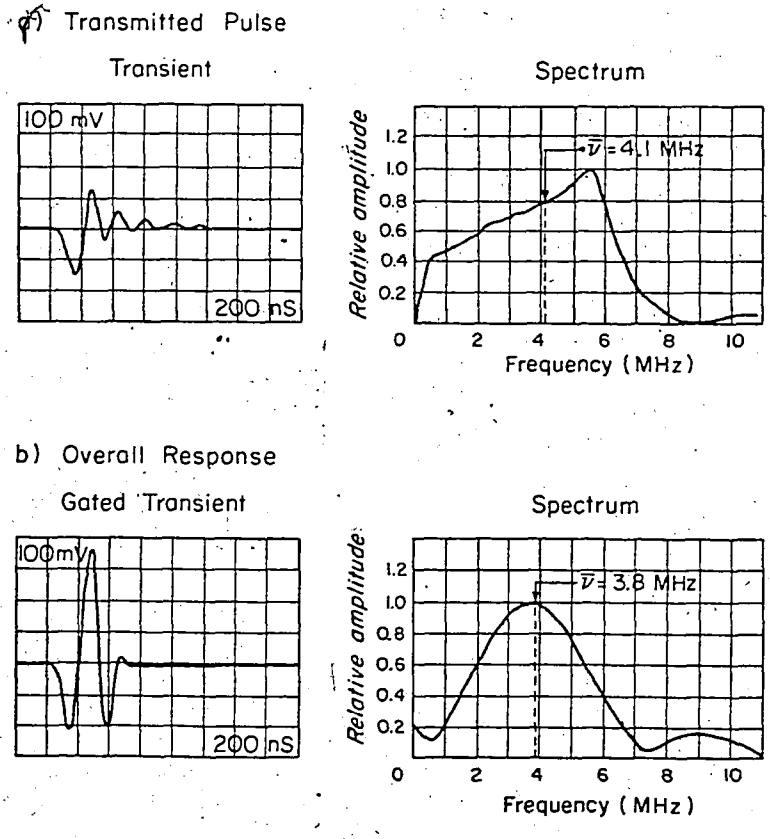

Figure 5. System characteristics. (a) The transmitted pulse was measured using a thick (3 μs transit time) receiver in the farfield of the centre transducer element. (b) The final signal used in focussing tests; after reception by the microphone, amplification and gating. The system was set at f/2 for this measurement.

Reproduced with permission of the copyright owner. Further reproduction prohibited without permission.

gating procedure did not alter the measured distributions but did remove the signal clutter of the distribution near the base line.

In several experiments the focussing of continuous wave (CW) ultrasound was studied. Here, the transducer was excited with a long radiofrequency burst (~10 μs) (Wavetek, San Diego, Calif.). A short section of the steady state microphone output was gated out and the beam profile was produced as described before.

c) Attenuation Measurements

Attenuation was measured as a function of frequency using a transient analysis technique at ultrasound intensities similar to those used in most diagnostic applications. A schematic of this approach is shown in Figure 6. First, the transmitting transducer, T, generates a unipolar ultrasound pulse (10), that propagates through a sample holder containing distilled water and is received in the farfield by a thick (3 μs transit time) transducer. This signal, $f_w(t)$, is digitized by a transient waveform recorder (Biomation 8100, Cupertine, Calif.) and transferred to a PDP 11-34 computer (Digital Corp., Maynard, Mass.). After averaging 5 to 10 transients the Fourier transform $F_w(\nu)$ is computed. The process is repeated with the actual tissue sample in the holder to generate the tissue spectrum $F_s(\nu)$. Attenuation is then computed using the formula:

$$A(\nu) = -20 \log \left[\frac{F_s(\nu)}{F_w(\nu)}\right]/(2.303\ \ell) \qquad (2)$$

where $A(\nu)$ is the attenuation in dB/cm and ℓ is the sample thickness. The attenuation of water has been neglected in equation 2 because it is extremely low (0.0022 dB/(cm - $(MHz)^2$) (10). Also, simple calculations based on reasonable values of tissue impedance, show that replacing the water in the sample holder with tissue, results in an error of about 1% which shows up as a constant offset in the computed attenuation. Tissue culture flasks (Falcon Plastics, Los Angeles,

Reproduced with permission of the copyright owner. Further reproduction prohibited without permission.

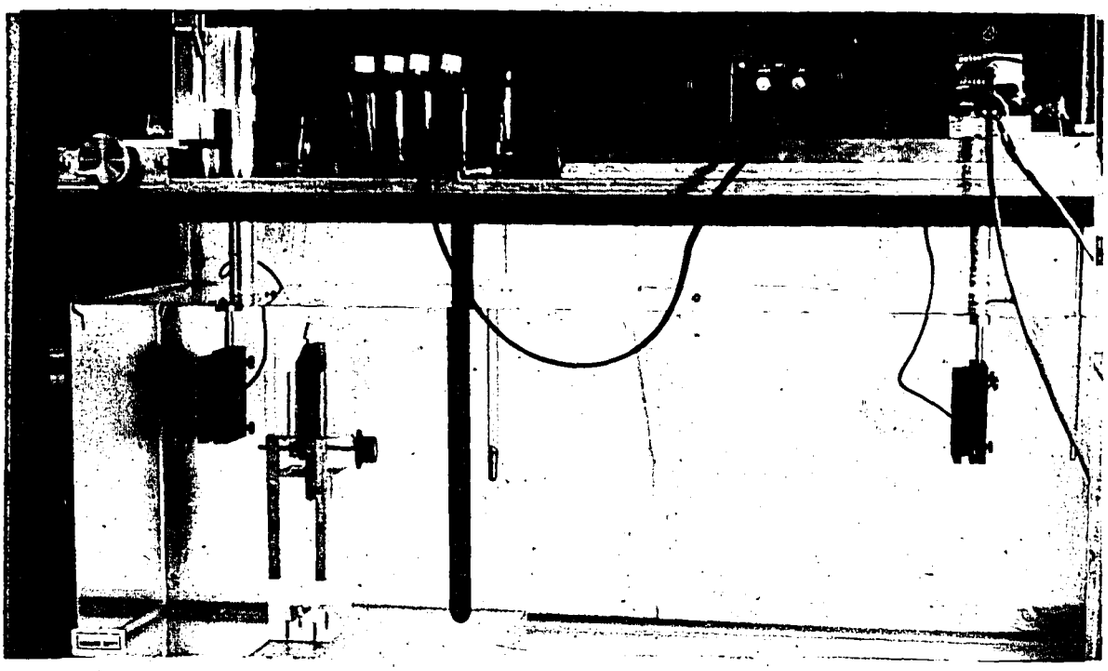

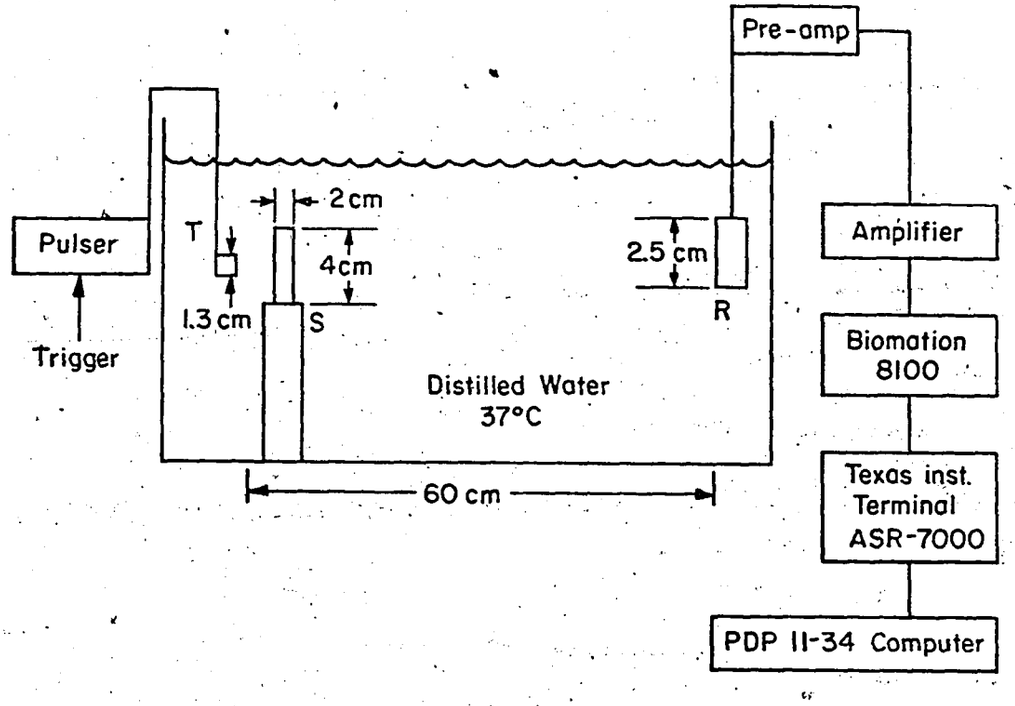

Figure 6. Schematic and photograph of attenuation measurement system. The transmitting transducer, T, generates a unipolar ultrasound pulse that propagates through the sample, S, and is received in the far field by a thick (3 μs transit time) transducer, R. The signal is digitized by a Biomation 8100 transient recorder and transferred to a PDP 11-34 computer for processing. By comparing the signal for the sample holder plus tissue to the signal for the sample holder plus water, attenuation is deduced over the range 0.5 to 6 MHz.

Reproduced with permission of the copyright owner. Further reproduction prohibited without permission.

Calif.) with ℓ = 2.0 cm, served as excellent sample holders. Sealed samples were made by sawing off the tops of the flasks, introducing the tissues, and regluing the tops in place. By placing the thick receiver well into the far field (60 cm from the transmitter), phase cancellation effects were minimized (11). System linearity was tested very simply by plotting CW input amplitude to the transmitter vs receiver amplifier output for a number of different frequencies. These plots showed excellent linearity over the full dynamic range of the system.

III. EXPERIMENTAL STUDIES

a) Focussing Experiments in Water

Tests of CW focussing are shown in Figure 7. AR1 was excited with 10 μs bursts of continuous waves with frequencies between 1 and 7 MHz. Simple Fraunhofer diffraction theory predicts that the full width at half maximum of the amplitude distribution at the focus is given by:

$$\text{FWHM} = 1.41\ (c/\nu)\cdot(z/d) = 1.41\ c\ (\text{f-number})/\nu \qquad (3)$$

where c is the velocity of ultrasound in water, ν is the frequency, z is the focal length, and d the diameter of the transducer. The 1.41 factor arises from consideration of the FWHM of the Bessel Function, $J_1(\pi x)/(\pi x)$, which occurs in the standard Fraunhofer analysis of diffraction. In general, the agreement is very good. Several factors are responsible for the small discrepancies observed at higher frequencies and lower f-numbers. They are (i) lens aberrations; (ii) reduced effective aperture due to the separations between rings (0.5-0.7 mm); (iii) absorption in the Freon lens; and (iv) effects due to the size and angular response of the microphone (0.8 mm diameter). Experimental and simulation studies indicate that the second factor, ie. reduction of the effective aperture, appears to explain most of the observed deviation.

Reproduced with permission of the copyright owner. Further reproduction prohibited without permission.

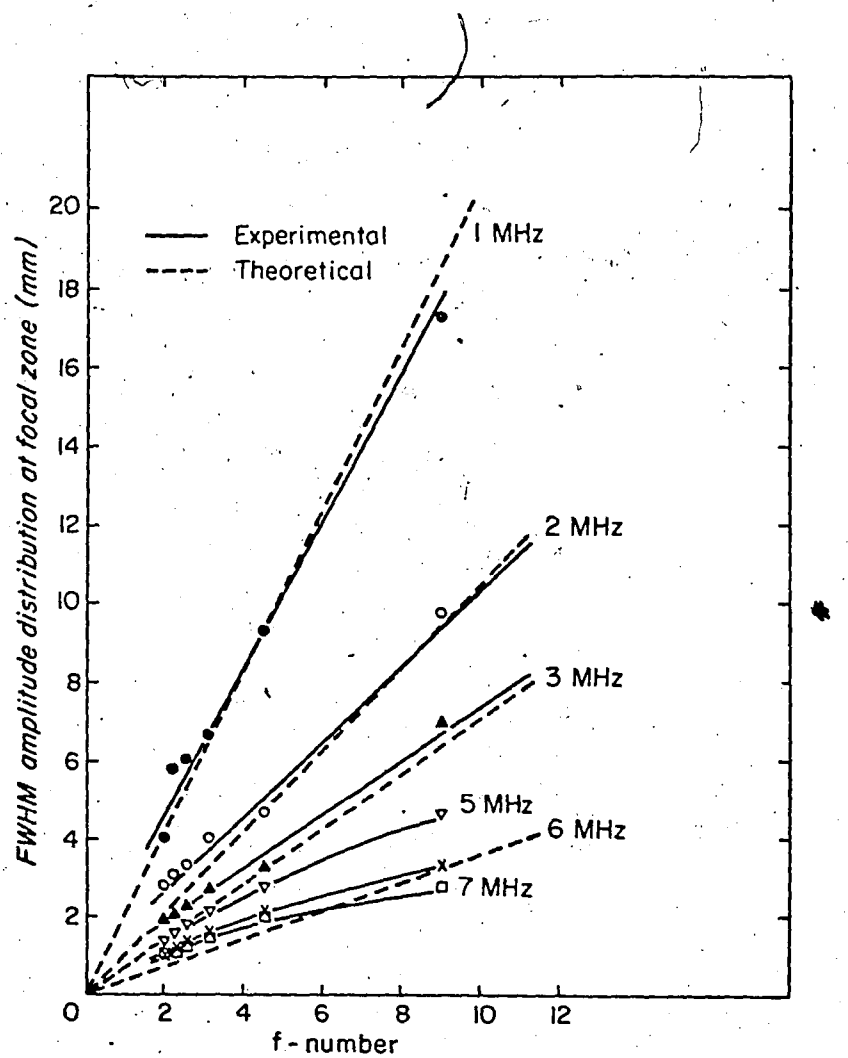

Figure 7. CW focussing properties of AR1.

Reproduced with permission of the copyright owner. Further reproduction prohibited without permission.

Focussing of the wideband pulse of AR1 (see Figure 5) is examined in Figure 8. Since the f-number is directly proportional to the FWHM, it is expected that equivalent f-numbers at different focal lengths will have the same FWHM's. As Figure 8 shows, this is true to a reasonable extent. Note that the calibration curve lies somewhat above the theoretical line predicted using equation 3. The theoretical result is based on an average frequency of 4.1 MHz and is therefore only approximate.

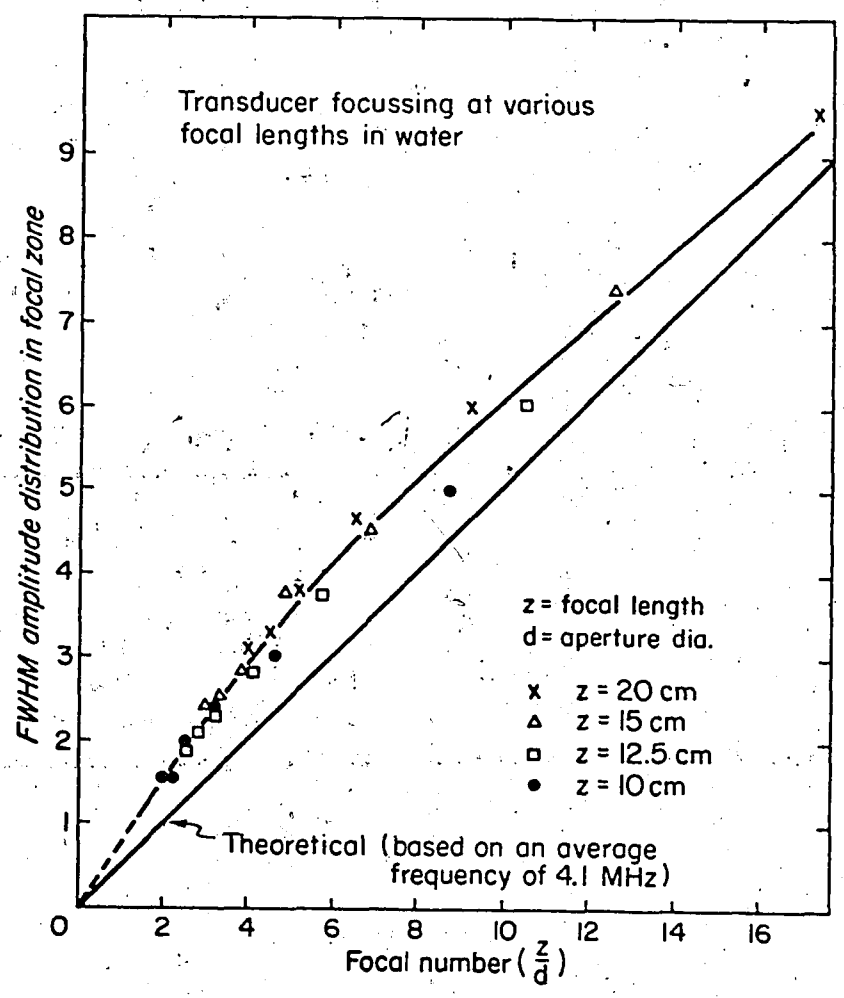

Figure 8. Test of wideband focussing in water. The focal length was adjusted between 10 cm and 20 cm by changing the amount of Freon in the lens. At each focal length FWHM's were obtained for each of the six available apertures. The theoretical curve was calculated using equation 3 assuming an average frequency of 4.1 MHz.

Reproduced with permission of the copyright owner. Further reproduction prohibited without permission.

b) Focussing Through Human Tissues

Fresh tissue samples were obtained as soon as possible after autopsy and submerged in PBS. Samples were stored at 4°C for no more than 36 hours and then heated to 37°C for the experiments. Figure 9 shows FWHM as a function of depth in normal liver tissue as measured with the system shown in Figure 1. In this experiment, liver slices were added in approximately 1.5 cm increments to a total depth of 8.5 cm. After each slice, Polaroid photographs were made of the ultrasound amplitude distribution for each of the six apertures available. The special advantage of this technique is that a wide range of apertures can be tested without

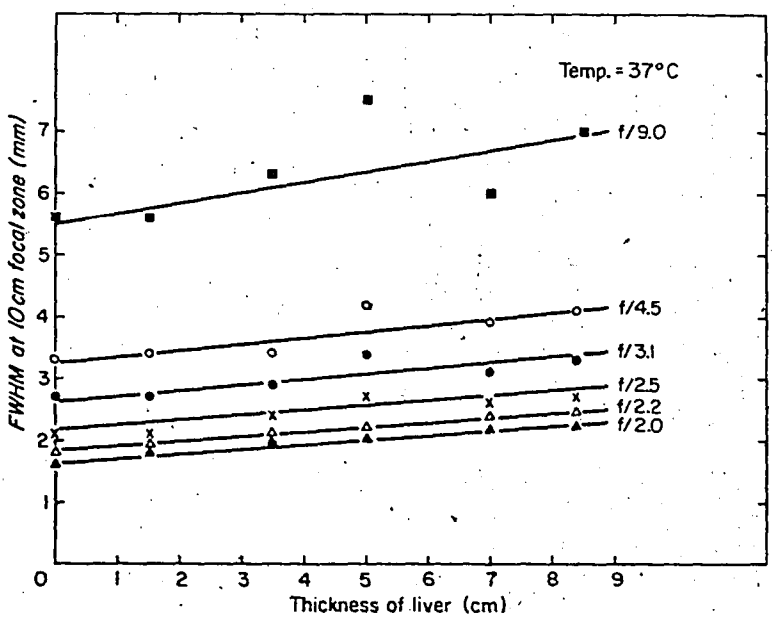

Figure 9. Focussing in normal human liver. The focal length was set at 10 cm. As slices of tissue were added the FWHM's were measured for each aperture of the annular array.

Reproduced with permission of the copyright owner. Further reproduction prohibited without permission.

changing transducers or altering tissue geometry. The results indicate that focussing ability decreases linearly with increasing thickness of intervening liver. Also, since the slopes of the lines are approximately equal, it appears that the loss of focussing with increasing thickness is independent of f-number. The fluctuations in the FWHM's for the small apertures were greater than those for the large apertures. The large fluctuations in focussing ability for small apertures were also reported by Banjavic et al (7) and Halliwell (8). Presumably the improvement noted at larger apertures is due to averaging effects imposed by the tissue on the propagating pulse. The spacing between slices of liver may cause a small reduction of ultrasound intensity but should not influence the focussing of the beam.

Whole organ studies of fresh human breast and brain have been performed using the experimental arrangement shown in Figure 10[a]. For the studies of the breast, the tissue floated against the upper Mylar membrane, and the nipple pointed down towards the transducer. This allowed the measurement of focussing properties in a geometry similar to that which would be employed in a breast imaging system. The results are shown in Figure 11. Focussing is quite poor in the thick part of the breast (geometry A) but still tends to improve as the f-number decreases. In the thinner but more curved portions of the breast (geometry B), focussing is improved. Refractive effects at the interface between the breast tissue and water may lead to a shift in the site of the centre of the focus as well as some deterioration in focussing. It is possible that by matching the velocity of ultrasound in the breast to that of PBS, further improvement could be obtained.

The brain study was performed on a sample approximately twice as thick as that used in the breast study. Figure 11 shows that the defocussing per centimeter

---

[a] For brain a larger sample holder was required.

Reproduced with permission of the copyright owner. Further reproduction prohibited without permission.

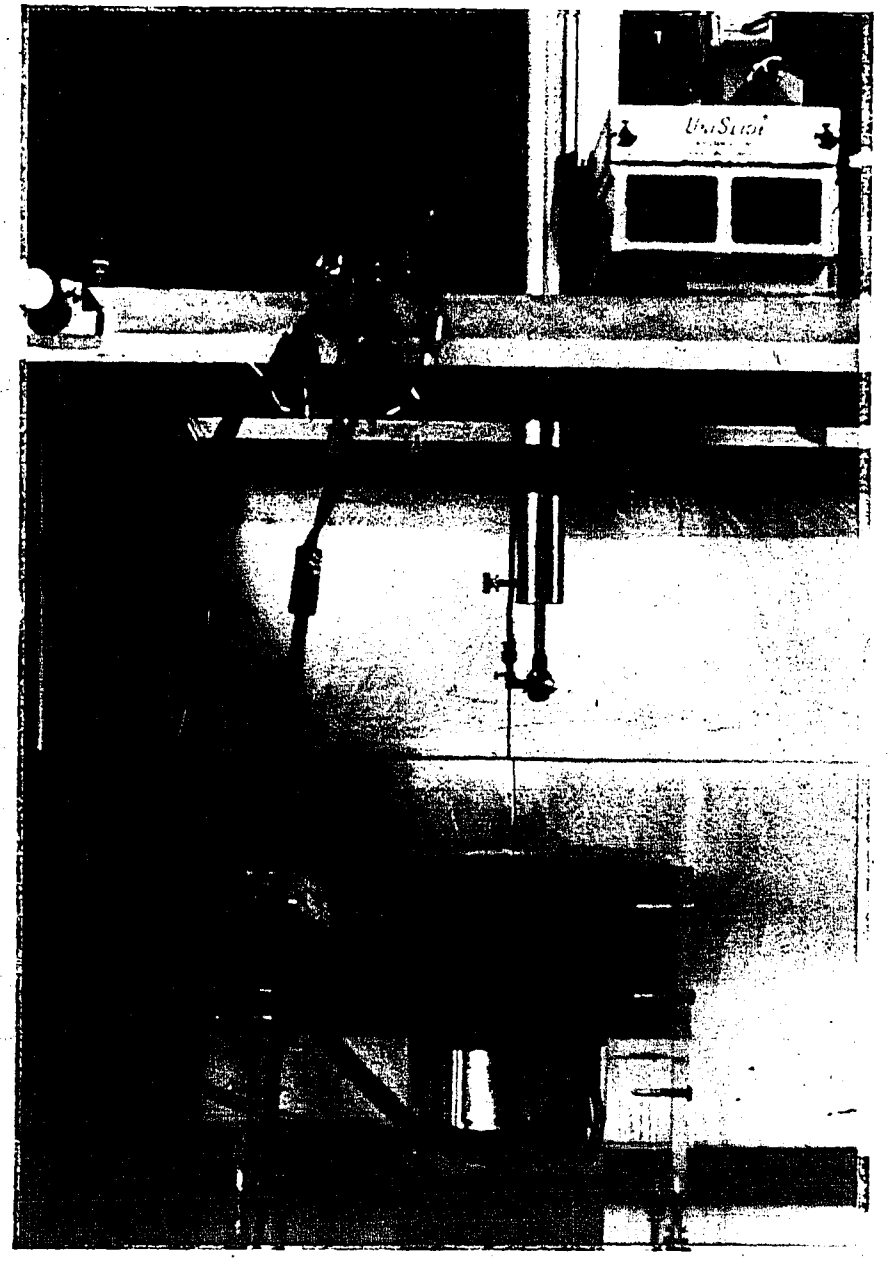

Figure 10. Photograph of the experimental arrangement for focussing studies of whole organs. A sealed container holds a fresh mastectomy above the transmitter, AR1. The beam is focussed through the sample and a microphone scans the focal plane for each of the six available apertures.

Reproduced with permission of the copyright owner. Further reproduction prohibited without permission.

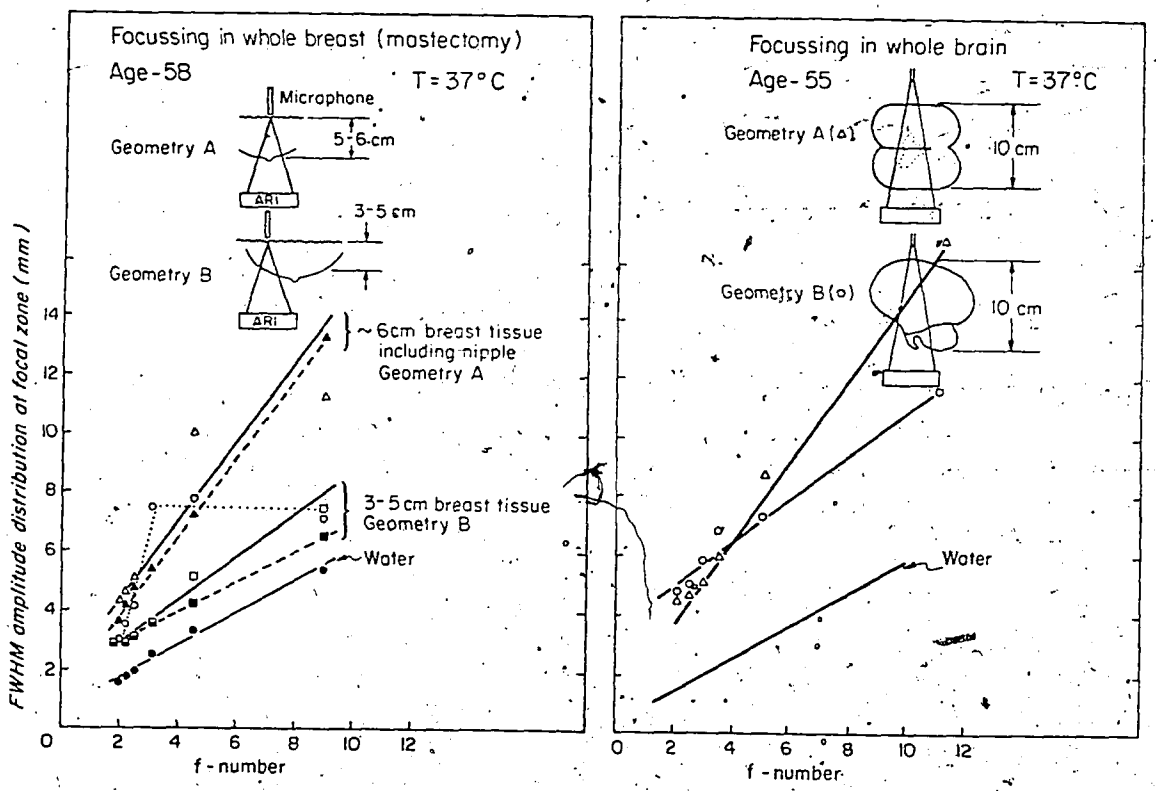

Figure 11. Focussing in whole fresh human breast and brain.

of tissue is significantly lower in brain. The experimental points show that there is little difference between the two geometries tested. In geometry A, the beam converges laterally in the brain, from left to right, and in geometry B, axially from bottom to top.

Figure 12 shows a summary of focussing results for 5 cm samples of various tissues. The focussing response of liver is shown as the lower shaded area. Note that the results for abnormal and normal liver are similar. The tumour sample[a] demonstrates a more rapid loss of resolution at high f-numbers when compared to liver. Both the liver and tumour plots indicate that better resolution can be

[a] Retroperitoneal mass associated with Hodgkin's disease (type undefined), firm in consistency, white in colour.

Reproduced with permission of the copyright owner. Further reproduction prohibited without permission.

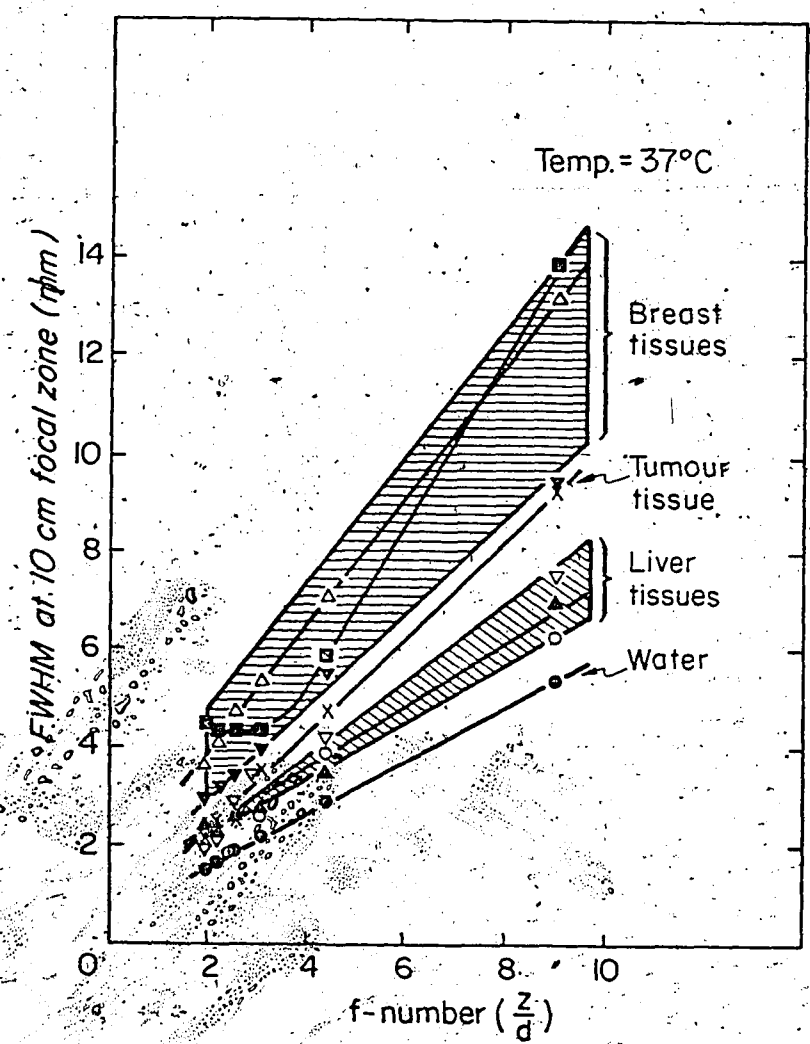

Figure 12. Focussing of the wideband pulse through 5 cm of selected human tissues. The focal length was 10 cm and the aperture was varied.

Legend:
- Water
- Liver C "Normal"
- Liver E (Metastasis Present)
- Liver D "Normal"
- Male Breast
- Tumour C
- Female Breast (4.3 cm) Age = 20
- Female Breast, Age = 58

Reproduced with permission of the copyright owner. Further reproduction prohibited without permission.

obtained by lowering the f-number below f/2. The results for three samples of breast tissue are shown as the upper shaded area. Here, again, focussing improves with decreasing f-number. Note that the beam tends to spread much more in breast than in liver. This is probably due to the increased inhomogeneity and attenuation of breast tissue. For one sample of male breast tissue there was no improvement of focussing below f/3. This was the only sample tested in which a focussing limit was observed.

c) Attenuation Measurements

From the onset of the focussing experiments it became clear that there was a general relationship between focussing and attenuation. To illustrate this, attenuation was measured as a function of frequency for many of the samples used in the focussing tests. The measurement technique was described in Section II and the tissues were handled as in the focussing experiments. Two examples of attenuation measurements are shown in Figure 13. Attenuation in castor oil served as a convenient standard and calibration check, demonstrating a value of 0.7 ± 0.1 dB/(cm - MHz$^{1.67}$). The error limits were based on the variation of data from three completely separate experiments. This result is in excellent agreement with that of Fry and Dunn (12) as shown in Figure 13a. This figure also shows the transients and their associated spectra from which the attenuation spectrum was obtained. Figure 13b shows the data and attenuation spectrum for a sample of liver containing multiple metastases. This measurement formed the upper bound of four transient studies for liver. Figure 14 shows a summary of attenuation data. The attenuation of ultrasound in liver is reasonably linear vs frequency over the range from 0.5 to 6 MHz, with a value of 0.7 ± 0.2 dB/(cm - MHz). Here, the ± 0.2 dB/(cm - MHz) limits include the error due to the measurement technique plus an estimated uncertainty due to natural variations of attenuation in normal liver. This value is somewhat less than the values of Chivers and Hill (13). The difference appears to be due to the temperature and condition of the

Reproduced with permission of the copyright owner. Further reproduction prohibited without permission.

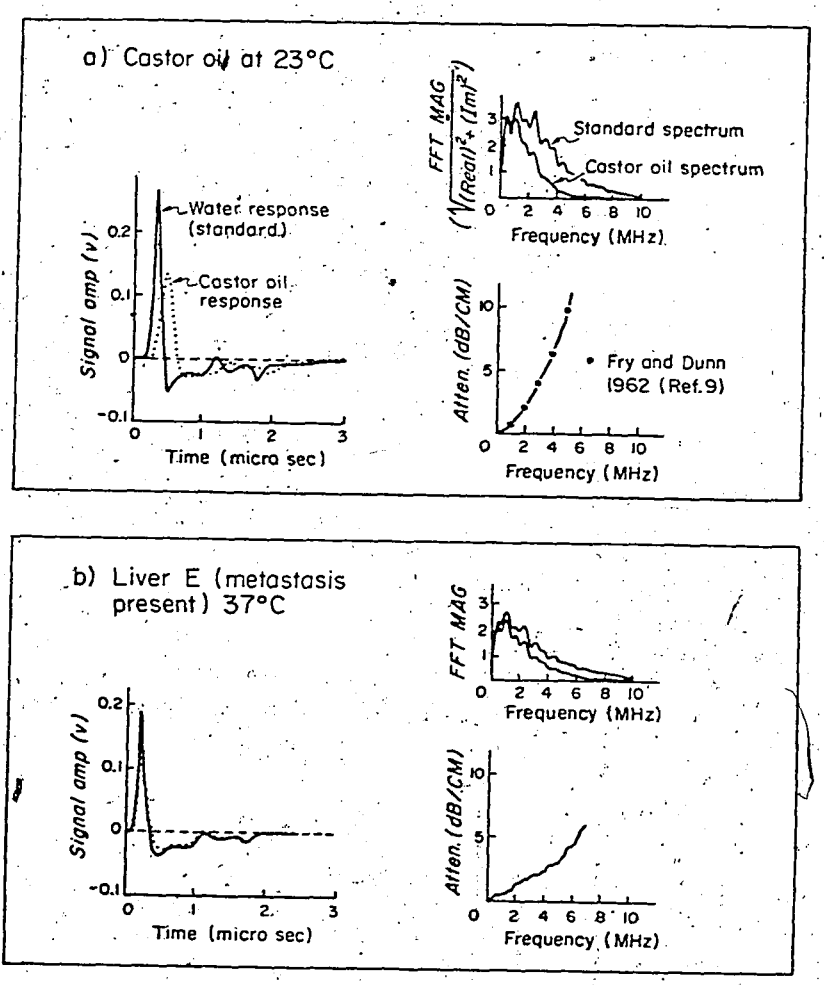

Figure 13. Examples of attenuation measurements. The transients and Fourier transform magnitudes for castor oil (a) and liver with metastasis (b) are shown. The solid lines in the attenuation plots were calculated using equation 2 as discussed in section IIc. The results for castor oil are in excellent agreement with points derived from the data of Fry and Dunn (12).

Reproduced with permission of the copyright owner. Further reproduction prohibited without permission.

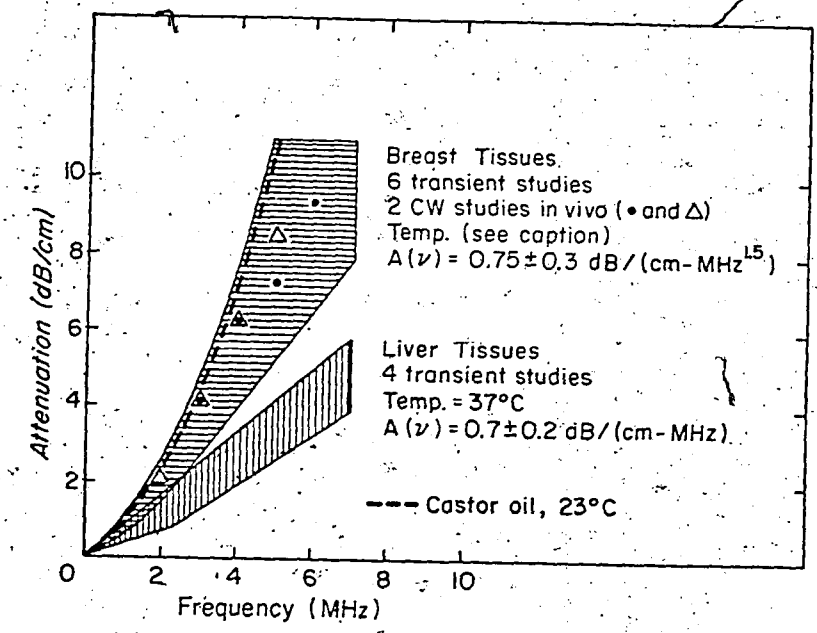

Figure 14. Summary of attenuation measurements. Three breast samples were processed at 25°C and three at 37°C. Little change in attenuation was observed when one breast sample was heated from 25°C to 37°C.

tissue. Chivers and Hill performed their measurements on fixed samples at a temperature of 19 ± 2°C whereas the present measurements were performed on fresh tissue at 37 ± 2°C. We have observed that attenuation in liver falls markedly with increasing temperature (14). Also, Goss et al (15) have shown that fixation increases the attenuation of liver tissue.

Information on attenuation in breast tissue is quite scarce. Calderon et al (16) performed measurements on fixed samples of normal, malignant and benign breast tissues using an interferometric technique. Their results showed normal

Reproduced with permission of the copyright owner. Further reproduction prohibited without permission.

breast to have an attenuation of 1.0 ± 0.5 dB/(cm - MHz). Kelly Fry et al (17) obtained similar results for a fixed sample of breast tissue using a transient technique. By comparison our studies of six transient measurements on fresh breast tissue, taken from women between the ages of 54 and 74, resulted in an attenuation coefficient of 0.75 ± 0.3 dB/(cm - $MHz^{1.5}$) (see Figure 14). The main difference is the exponent of the frequency dependence. Thus, attenuation in breast is similar to that of liver at low frequencies but increases much more rapidly at higher frequencies. This is an important factor to consider in the design of a breast scanning system. Preliminary in vivo experiments were performed to check the validity of the in vitro results. In these experiments a matched set of wideband transducers were placed in contact with opposite sides of the breast and used in the standard transmission configuration. The maximum amplitude of a 10 μs burst of ultrasound transmitted through the breast was compared to the amplitude transmitted through an equivalent distance of water to generate an attenuation coefficient. Figure 14 shows that the points from the in vivo study are in fairly good agreement with the results of the transient analysis.

The structure of human tissue is highly variable and many more samples would be required to fully characterize the attenuation of liver and breast. However, it is clear when comparing Figures 14 and 12 that the smaller the attenuation for a given tissue, the better the focussing properties of the ultrasound beam. This leads to several interesting questions. What is the connection between attenuation and defocussing? What relative amounts do the scattering and absorption components of attenuation contribute to the defocussing? How do the frequency responses of the various system components affect focussing?

The answers to the questions posed in the preceding paragraph were elucidated, in part, by experiments performed on castor oil. This liquid is particularly

Reproduced with permission of the copyright owner. Further reproduction prohibited without permission.

interesting since its total attenuation is similar to that of breast (Figure 14) but contains no component due to scattering. In the first experiment (Figure 15b) the wideband pulse was focussed through 4.3 cm of castor oil in the same manner that the tissue experiments were performed. The defocussing effect, as expected, is similar to that of breast (compare Figures 15b and 12). In Figure 15a, the effect of narrowing the bandwidth of the transmitted pulse is tested. Here a 10 μs burst of 3 MHz ultrasound is focussed through the castor oil. The result is compared to the earlier result for the same experiment in water. There is no apparent degradation due to the absorption of ultrasound. This indicates that the deterioration of focussing for the wideband case is due to the selective absorption of the high frequencies, leaving the lower frequencies to form the focal zone. As shown in equation 3, spreading of the beam results because the FWHM is inversely proportional to frequency. It is important to note that the overall bandwidth of the system and not just the bandwidth of the transmitted pulse governs the focussing characteristics. For example, consider the case of focussing the wideband pulse of Figure 5a in castor oil. If the output of the microphone amplifier is filtered with a bandpass of 2.95-3.05 MHz, we arrive back at the result for CW focussing in water (Figure 15c). Thus it is apparent that narrowing the receiver bandpass to a selected frequency range can be used to improve focussing in this simple system.

If this approach is applied to tissue the results vary. Figure 16a shows a comparison between wideband and narrow band pulses as they are focussed in brain tissue. Here, reducing the system bandwidth to a narrow region at 3 MHz, provides a significant improvement in focussing. However, the CW beam profiles for a sample of breast displayed such unusual features (Figure 16b) that it was impossible to plot a focussing curve. It appears that the tissue acts as a complicated diffracting medium, producing a distribution with many peaks and no

Reproduced with permission of the copyright owner. Further reproduction prohibited without permission.

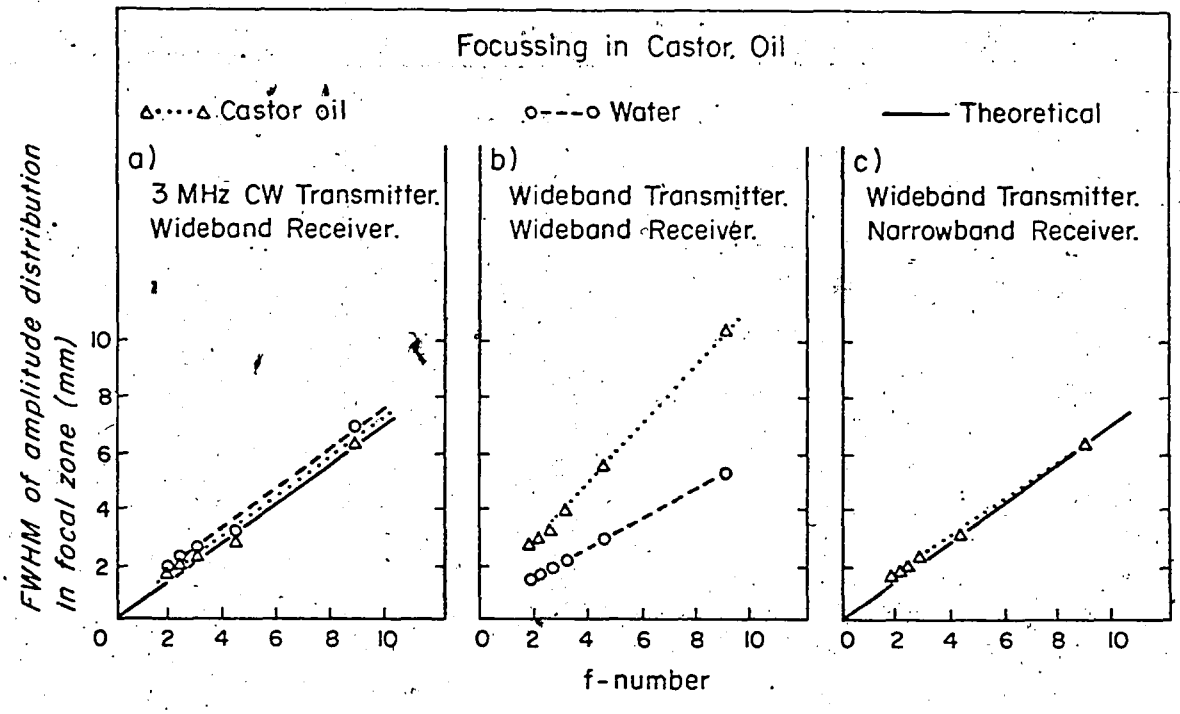

Figure 15. Focussing in an attenuating but non-scattering medium (4.3 cm castor oil). Temperature = 23°C. The focussing of CW ultrasound (a) is not affected by the absorption characteristics of castor oil. However the focussing of a wideband pulse (b) is severely affected (see Figure 5b for the pulse properties). Here the higher frequencies have been selectively absorbed leaving only the lower frequencies to form the focal zone. Consequently the beam is much wider in castor oil than in water. By filtering the wideband signal over the narrow range 2.95-3.05 MHz the focussing properties are once again independent of absorption characteristics (c). Defocussing due to absorption appears to be wholly dependent on the overall system bandwidth.

Reproduced with permission of the copyright owner. Further reproduction prohibited without permission.

Reproduced with permission of the copyright owner. Further reproduction prohibited without permission.

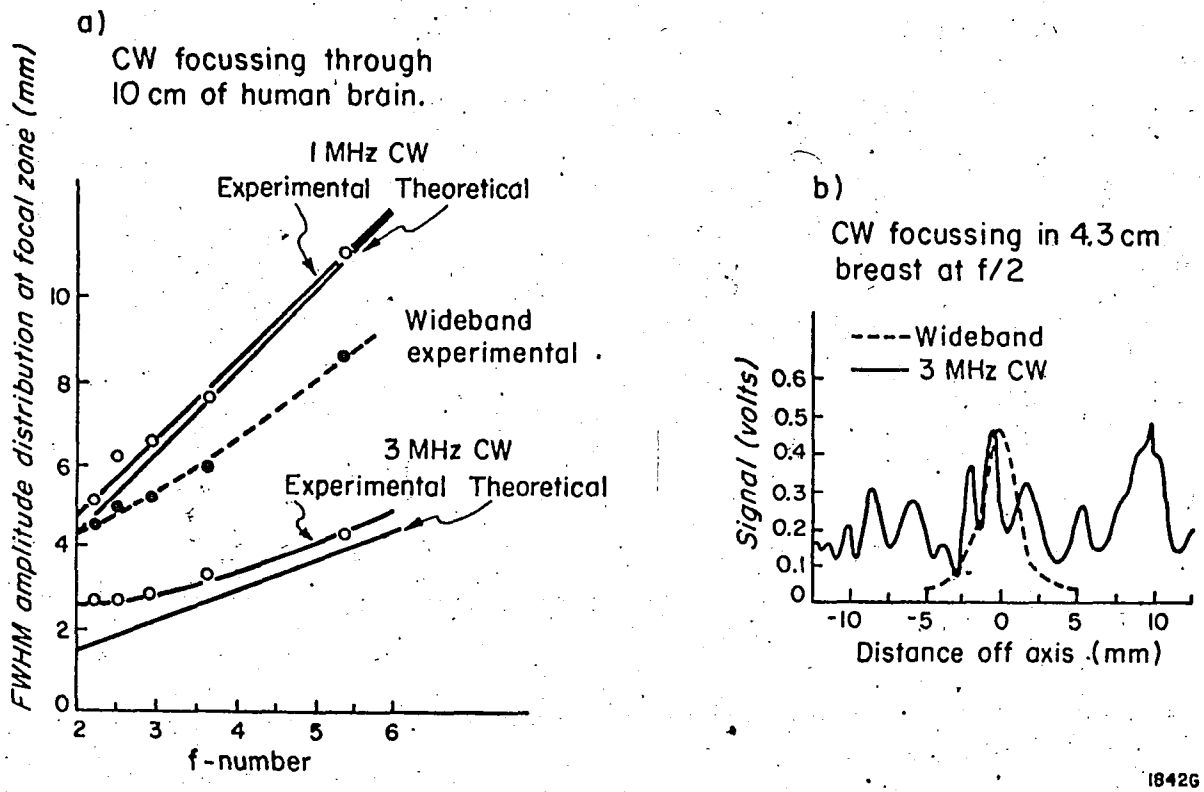

Figure 16. CW focussing in brain and breast. (a) Brain appears to support the focussing of continuous waves reasonably well. The reduction of the system bandwidth greatly improved the focussing properties in this case. (b) Breast on the other hand, had a disastrous effect on the CW beam. Note that the wideband pulse provided a much better focal distribution measured under exactly the same conditions.

real focus. By comparison, the wideband profile for the breast tissue, is also shown in Figure 16b. Notice that this profile demonstrates a reasonably well-defined focus. Presumably the observed differences between brain and breast are due to the structures of these tissues. Breast is quite heterogeneous with closely associated regions of fat, connective tissue, blood and glandular tissue. Perhaps the large refractive index variations of these constituents lead to a grating effect that bends ultrasound away from the true focus. This effect, as with interference phenomenon generally, would be highly dependent on the strong coherence associated with a narrow band source, and therefore it is probable that such effects would not be as evident in the wideband case. It is clear, however, that much additional work is required to understand this phenomenon.

IV. SUMMARY

A 50 mm diameter annular array with a simple liquid Freon lens has been used to investigate the focussing of ultrasound in human tissue. The performance of the transducer and lens was first tested in distilled water and good agreement was obtained with the theoretically predicted distribution at the focal plane over the frequency range 1-7 MHz. Subsequently the system was used to quantize focal distortion due to intervening human tissues. In liver tissue it was observed that focussing ability decreased linearly with increasing thickness (Figure 9). Since the linear plots for different f-numbers are parallel it appears that the rate of defocussing with increased tissue depth, is independent of f-number. The optimum f-number for focussing in liver and other homogeneous tissues is less than f/2. For breast, an heterogeneous and highly attenuating tissue, focussing ability is much reduced compared to liver but seems to improve linearly with decreasing f-number. Some breast samples have shown nonlinear focussing responses such as leveling off of the FWHM between f/3 and f/2 and

Reproduced with permission of the copyright owner. Further reproduction prohibited without permission.

anomalous focussing or defocussing at higher f-numbers. The optimum f-number for focussing in breast tissue may be between f/3 and f/2 or perhaps lower. It is apparent that lower f-numbers provide a more stable focus in tissue. This can be seen by comparing the scatter of the focussing data above and below f/3 in Figures 9, 11 and 12.

There appear to be two processes responsible for degradation of focussing in tissue: (i) spectral shift due to frequency-dependent attenuation; and (ii) phase distortion of the converging wavefront via refractive index variations in the tissue. Attenuation measurements on breast, liver and castor oil verified the former process. The results showed that the attenuation of liver was linear with frequency at 0.7 ± 0.2 dB/(cm - MHz) while attenuation in breast was nonlinear with frequency with a value of 0.75 ± 0.3 dB/(cm - $MHz^{1.5}$). Thus for a given bandwidth, the expected shift to lower frequencies and consequent reduction of focussing is more severe for breast than for liver. This is borne out in Figure 12.

Studies of focussing in castor oil, which has an attenuation similar to that of breast, indicate that under pulsed conditions, defocussing is caused mainly by the spectral shift effect (compare Figures 15b and 12). If the spectral shift is reduced to zero by narrowing the bandwidth of the system to zero (ie. CW conditions) there is no defocussing in castor oil (see Figures 15a and 15c). If the same experiment is performed for brain, focussing is much improved as the bandwidth is narrowed. However, for breast, the distribution in the focal zone is severely affected. Here it appears that refractive index variations and scattering effects in the tissue have deflected ultrasound off the axis at the focal zone. The selection of the optimum bandwidth for focussing in a given tissue is the object of future research.

Reproduced with permission of the copyright owner. Further reproduction prohibited without permission.

REFERENCES

1. Kossoff, G., Robinson, D.E. and Garrett, W.J. Ultrasonic visualization for medical diagnosis. J. Acoust. Soc. Am. 44: 1310-1318 (1968).

2. Dietz, D.R., Parks, S.I. and Linzer, M. Expanding aperture annular array. Ultrasonic Imaging 1: 56-75 (1979).

3. Melton, H.E. Electronic focal scanning for improved resolution in ultrasonic imaging. Ph.D. Thesis, 1971 (Duke University, Durham, North Carolina) (unpublished).

4. Burckhardt, C.B., Grandchamp, P.A. and Hoffman, H. Focussing ultrasound over a large depth with an annular transducer - an alternative method. IEEE Trans. Sonics and Ultrasonics SU 22: 11-15 (1975).

5. Macovski, A. and Norton, S.J. High resolution B-scan systems using a circular array. In: Acoustical Holography, Vol. 6, (ed. N. Booth), Plenum Press, New York. pp. 121-143 (1975).

6. Halliwell, M. and Mountford, R.A. Physical sources of registration errors in pulse echo ultrasonic imaging systems, I and II. Med. Biol. Engng. 11: 27-32 and 33-38 (1973).

7. Banjavic, R.A. Zagzebski, J.A., Madsen, E.K. and Jutila, R.E. Ultrasonic beam sensitivity profile changes in mammalian tissue. Ultrasound in Medicine. (ed. D.N. White and E.A. Lyons). AIUM and Plenum Press, pp. 515-518 (1978).

8. Halliwell, M. Ultrasonic beam distortion by normal female breast in vivo. Ultrasound in Medicine. (ed. D.N. White and E.A. Lyons). AIUM and Plenum Press, pp. 555-556 (1978).

9. Foster, F.S. and Hunt, J.W. The design and characterization of short pulse ultrasound transducers. Ultrasonics 16: 116-122 (1978).

10. Wells, P.N.T. Biomedical Ultrasonics. Academic Press, New York, p. 14 (1977).

Reproduced with permission of the copyright owner. Further reproduction prohibited without permission.

11. Heyman, J.S. Phase insensitive acoustoelectric transducer. J. Acoust. Soc. Am. 64: 243-249 (1978).

12. Fry, W.J. and Dunn, F. In: Physical Techniques in Biological Research. (ed. W.L. Nastuk). Academic Press, New York. p. 270 (1962).

13. Chivers, R.C. and Hill, C.R. Ultrasonic attenuation in human tissue. Ultrasound in Med. and Biol. 2: 25-32 (1975).

14. Foster, F.S. Personal communication (1978).

15. Goss, S.A., Johnston, R.K. and Dunn, F. Comprehensive compilation of empirical ultrasonic properties of mammalian tissues. J. Acoust. Soc. Am. 64: 423-427 (1-78).

16. Calderon, C., Vilkomerson, D., Mezrich, R., Etzold, K.F., Kingsley, B. and Haskin, M. Differences in the attenuation of ultrasound by normal, benign and malignant breast tissue. J. Clin. Ultrasound 4: 249-254 (1976).

17. Kelly Fry, E., Sanghvi, N.T. and Fry, F.J. Frequency dependent attenuation of malignant breast tumours studied by the fast Fourier transform technique. In: Ultrasonic Tissue Characterization. (ed. M. Linzer). National Bureau of Standards Special Publication 525, U.S. Government Printing Office, Washington D.C. pp. 89-95 (1978).

Reproduced with permission of the copyright owner. Further reproduction prohibited without permission.

CHAPTER 3

THE DEMONSTRATION SCANNER

Reproduced with permission of the copyright owner. Further reproduction prohibited without permission.

I. INTRODUCTION

The results of our focussing studies (Chapter 2) indicated that f-numbers in the region f/2 to f/3 were optimal for breast imaging. Such highly convergent beams have very low depth-of-field, as pointed out in Chapter 1, Figure 5. The simplest way to overcome this limitation is to divide the depth dimension into a number of zones as illustrated in Figure 1 and image each zone separately. The Demonstration Scanner was designed to provide a flexible proving ground for the zone focussing approach in high resolution imaging. Conceptually, the operation of the Demonstration Scanner is simple: a number of separate pulse-echo images are generated, each with the focal length of a Freon lens set at different depths in the tissue. By selecting information only from the focal zones and adding the images together, a high resolution scan with good depth-of-field, is synthesized.

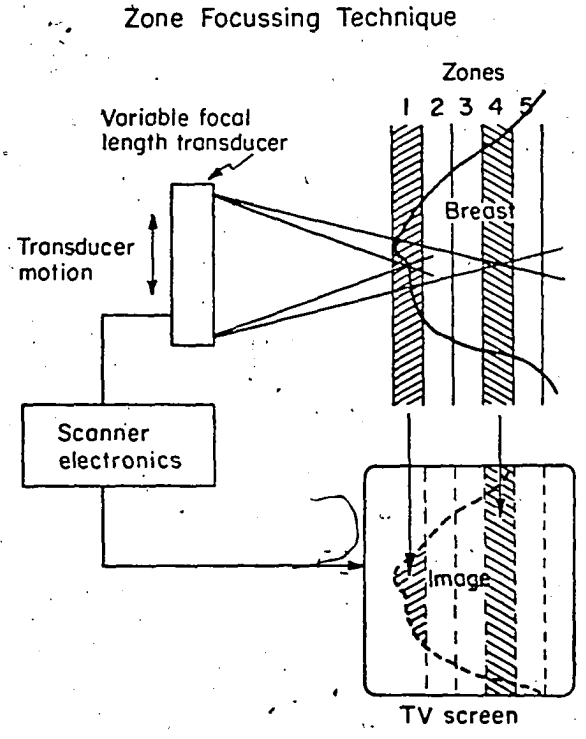

Figure 1. The zone focussing technique utilizes a variable focal length transducer to focus at different depths in tissue. Separate pulse-echo images are made at each depth and an electronic gate transfers the information from each focal region (zone) to the final image.

Reproduced with permission of the copyright owner. Further reproduction prohibited without permission.

In this Chapter, the design, construction and preliminary testing of the Demonstration Scanner are discussed. We look specifically at the resolution gains of low f-number imaging in phantoms and tissue and the selection of zone width. Each of these topics is of prime concern in the final design of our high resolution breast scanner.

II. GENERAL DESCRIPTION

A block diagram of the Demonstration Scanner is shown in Figure 2. It consists of:

a) a Freon focussed, 75 mm diameter transducer (AR2);

b) a Freon reservoir and pump to change the focal length;

c) an electronic gate to select information from the focal zone only; and

d) stepping motors and slides to move the transducer.

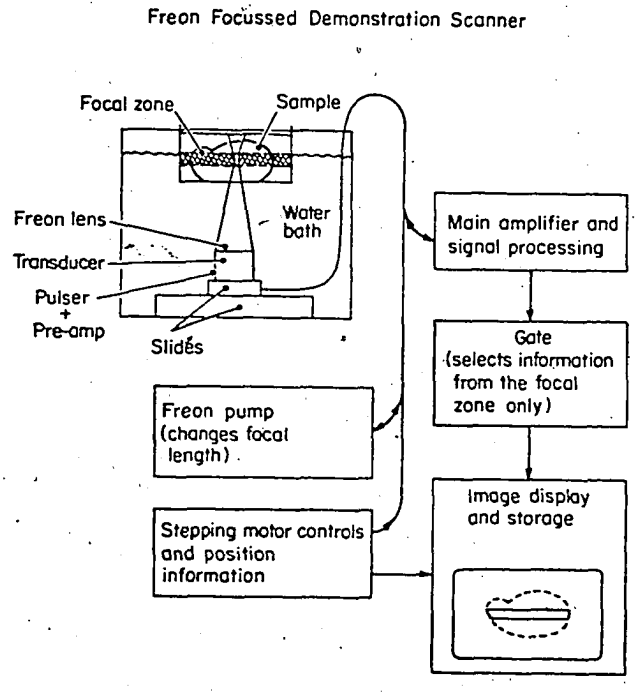

Figure 2. The Demonstration Scanner is a laboratory system to test the zone focussing approach for phantoms and in vitro tissue samples. A Freon lens is used to change the focal length of the transducer. For each selected zone the transducer makes one pass under the sample and a gate selects the focussed information for display and storage. The focal length is changed by means of a Freon pump and the process is repeated for the next zone until a complete image is formed.

Reproduced with permission of the copyright owner. Further reproduction prohibited without permission.

a) Transducer (AR2)

A cross-section of AR2 is shown in Figure 3. The active element, a 3.3 MHz, 75 mm diameter PZT5A disk divided into five annuli of equal area, is mounted on a lossy backing composed of tungsten dust in epoxy. To minimize stray inductance, each of the annuli has a co-axial input as illustrated in Figure 3. A 2 mm brass pipe is soldered to the back face of the annulus and a lead passed through both the pipe and a small hole in the crystal, is soldered to the front face. A coil is mounted very close to where the brass

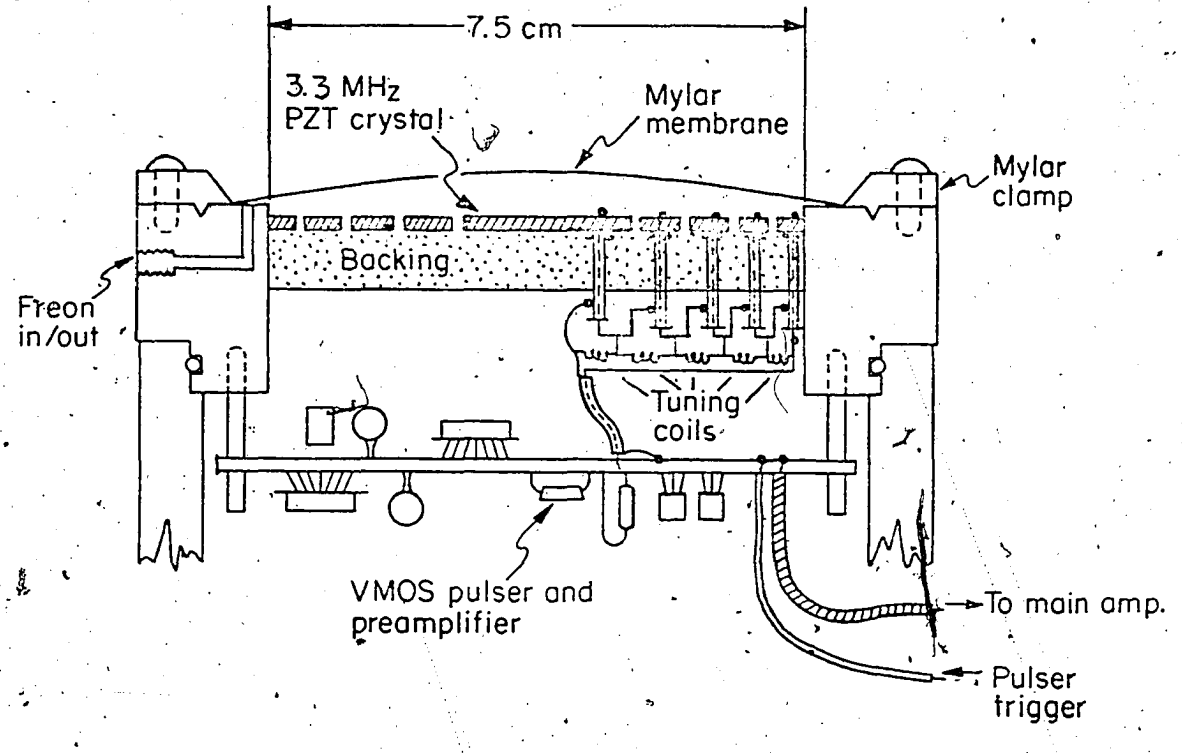

Figure 3. AR2, a 3.3 MHz, 7.5 cm diameter Freon focussed annular array.

pipe emerges, for the purpose of tuning the annulus to the proper frequency. Each of the tuned sections is then connected in series to match the impedance of the pulsing circuit. The use of series tuned sections is due to the low electrical impedance of PZT5A disks; a single 7.5 cm diameter disk would have resulted in an impedance mis-match of ~20 between the transducer and the pulser.

Reproduced with permission of the copyright owner. Further reproduction prohibited without permission.

Note that the division of the transducer into an annular array is not in any way connected to beam focussing. The sensitivity and efficiency of AR2 were maximized by (a) placing the pulser and preamplifier right in the transducer case, minimizing cable noise and loss, and (b) carefully matching the impedance of the pulser to the transducer. Experience has shown that this results in as much as a one hundred fold gain in the signal to noise ratio. Details of the impedance matching and front end (pulser-preamplifier) electronics are given in Appendix 1. Figure 4 shows photographs of AR2 (a) from the front, and (b) from the back, showing the pulser, preamplifier and tuning circuitry.

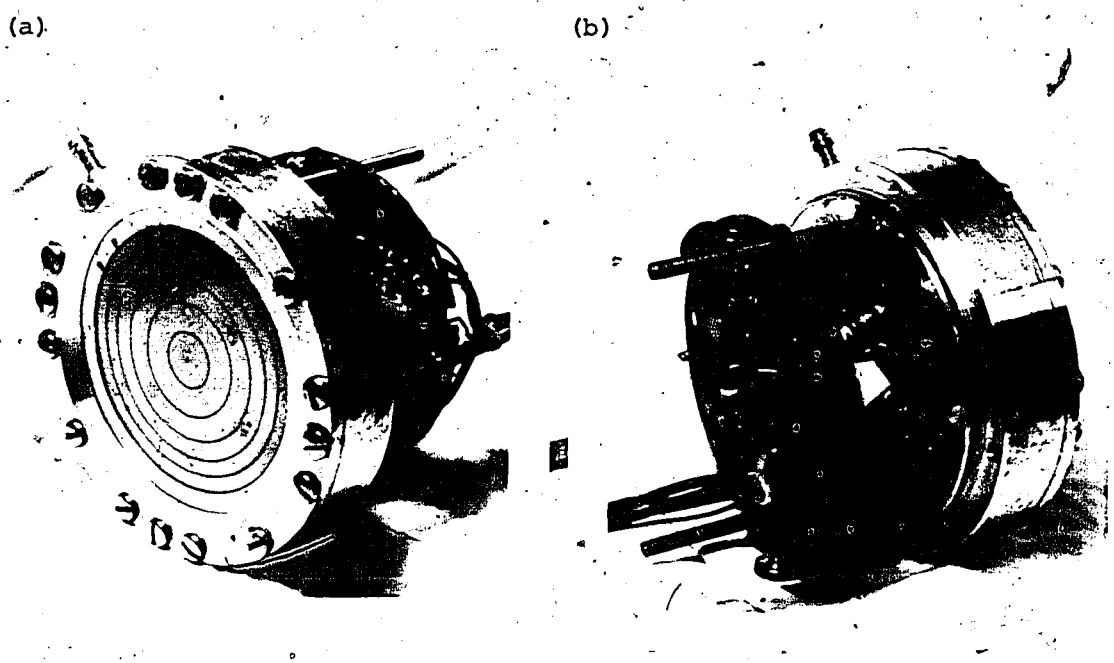

Figure 4. Photographs of AR2, (a) from the front showing the annular array, and (b) from the back showing the pulser and preamplifier.

Reproduced with permission of the copyright owner. Further reproduction prohibited without permission.

Pulse-Echo Response

The pulse-echo response of AR2 was measured with the arrangement shown in Figure 5. A two cycle 3.1 MHz centre frequency trigger signal was applied to the pulser and the echo from a plane Plexiglas interface at 16 cm was examined using an oscilloscope and spectrum analyzer. The peak to peak amplitude of the echo signal was 9.6 V as shown in Figure 5, while the noise was approximately 1.0 mV. The signal to noise ratio was therefore a reasonable 79 dB (nearly

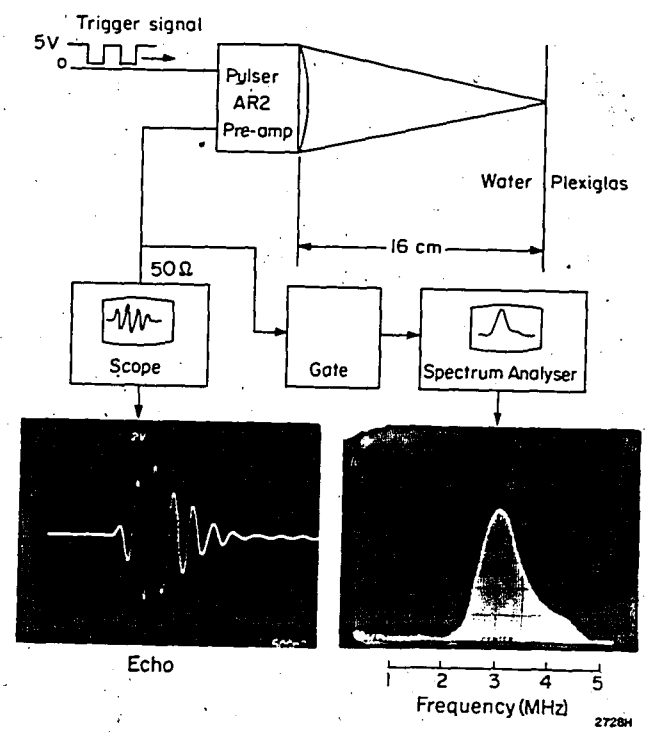

Figure 5. Pulse-echo response of AR2. The echo from a plane Plexiglas interface at 16 cm was observed with an oscilloscope and spectrum analyzer. The noise at the scope was approximately 1 mV.

Reproduced with permission of the copyright owner. Further reproduction prohibited without permission.

10,000 in amplitude). An estimate of the axial resolution may be obtained by measuring the time over which the echo signal remains above 10% of its maximum amplitude. For AR2 this time is about 2.0 μs, corresponding to a distance of 3.0 mm in tissue. Since the ultrasound must travel to, and return from a given interface, the axial resolution is approximately 3.0 mm/2 = 1.5 mm. The frequency content of the pulse exhibits a peak at 3.1 MHz and a shoulder at 4.3 MHz. The average frequency is about 3.3 MHz. Note that the spectrum cuts off rapidly below 2.5 MHz such that resolution degradation due to the spectral shift effect (Chapter 2, Figure 15) should be minimized.

b) Freon Focussing System

AR2 is focussed by a liquid Freon lens similar to that discussed in Chapter 2, Section II. Accurate reproducible focussing was achieved by means of a screw driven bellows which forced Freon in or out of AR2. The mechanism is illustrated in Figure 6. A stepping motor turns the screw at the rate of one turn per 400 steps and each turn results in a 1.0 mm displacement of the piston which compresses the Freon bellows. The number of steps, and hence the volume of Freon taken in or out of the lens, was controlled

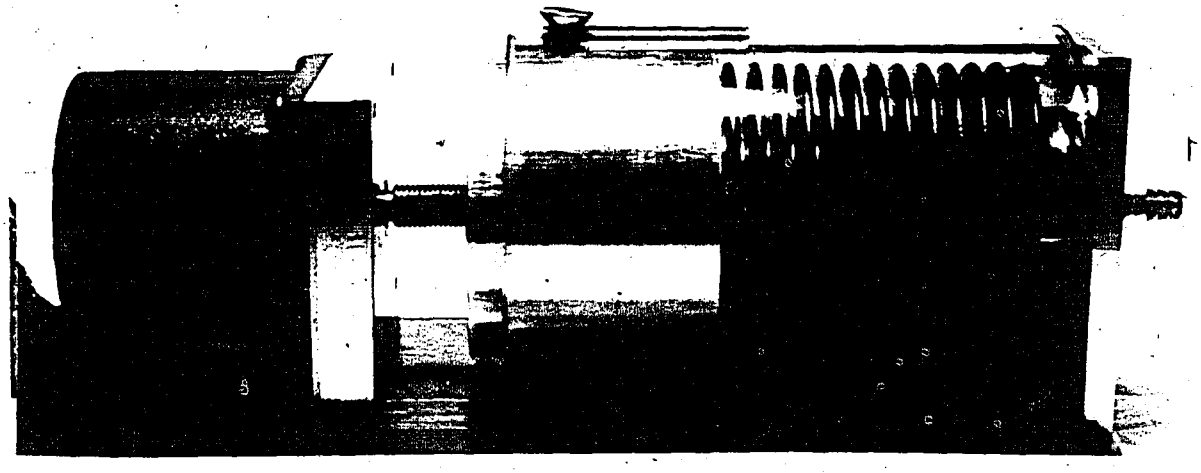

Figure 6. The Freon pump. Freon was confined in a brass bellows with a diameter of 5.0 cm and a stroke of 2.0 cm. A stepping motor drives a piston that compresses the bellows to force Freon into the lens of AR2.

Reproduced with permission of the copyright owner. Further reproduction prohibited without permission.

by digital electronics (Appendix A). The operator begins each experiment by maximizing the signal from a wire target at a focal length of 15 cm (f/2) by manual operation of the stepping motor. New focal lengths are selected by referring to the calibration curve given in Figure 7 and entering the required number of pulses via thumbwheel switches. For example, changing the focal length from 15 cm to 20 cm requires the number 530 to be entered.

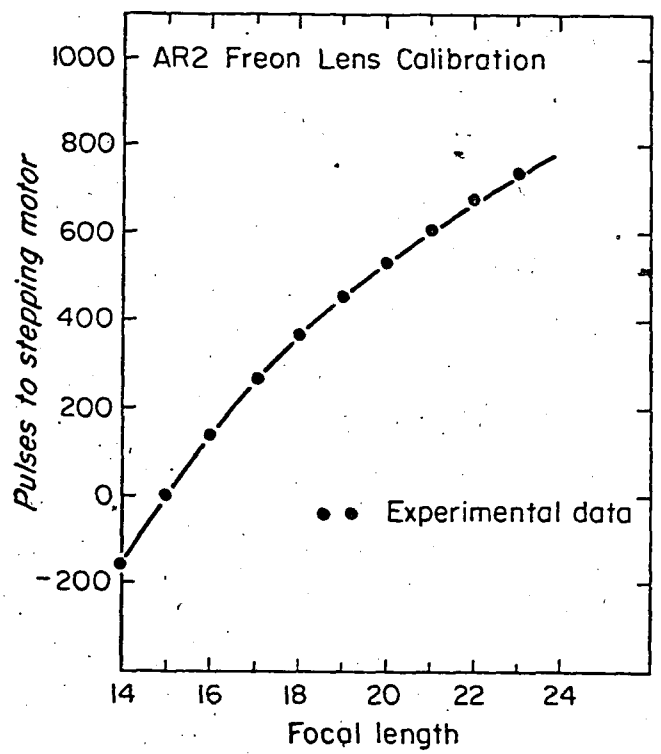

Figure 7. AR2 lens calibration. Once the lens is set at a focal length of 15 cm, new focal lengths are selected by reading the required number of pulses from the graph. This value is entered via thumbwheel switches on the electronics console. The exact number of pulses is counted electronically and sent to the Freon stepping motor..

The focussing of the Freon lens was tested in both transmission and pulse-echo modes. In transmission the lens was focussed at a particular depth and a 0.8 mm diameter microphone (see Chapter 2, Section IIb) was scanned across the focus. The output of the microphone was plotted as a function of position

Reproduced with permission of the copyright owner. Further reproduction prohibited without permission.

to generate a beam profile. In the pulse-echo case, the echo signal amplitude from a 2 mm diameter glass bead was used to generate the beam profile. The FWHM of the transmitted beam was plotted as a function of focal length in Figure 8. The transmission measurement was performed at 3.1 MHz CW and is compared to the result predicted by equation 3 in Chapter 2. Agreement is

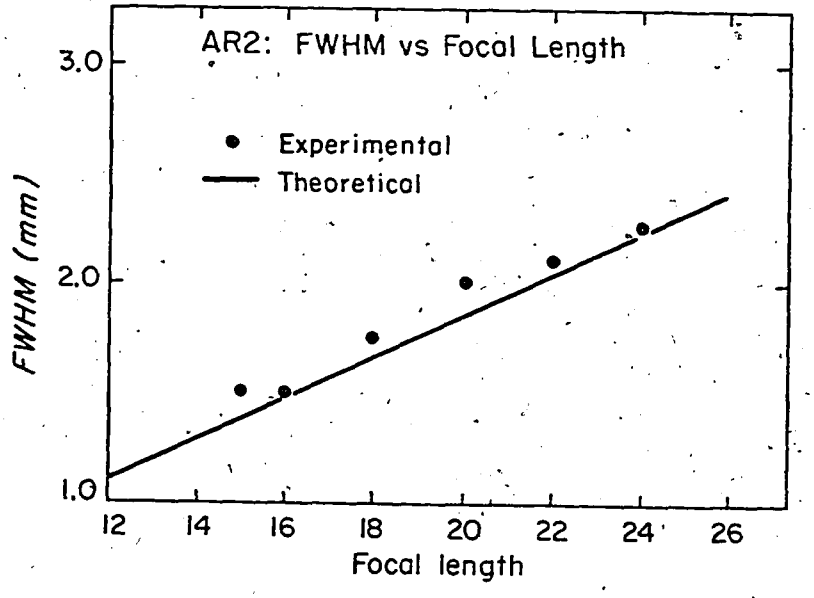

Figure 8. FWHM of the transmitted beam measured with an 0.8 mm diameter microphone.

reasonably good over the entire focussing range of AR2. In Figure 9, the pulse-echo profiles are plotted over the range 15 to 24 cm. Here, the beam is narrower than in the transmission case because focussing is also achieved in reception. The values of the FWHM vary from 1.05 mm at 15 cm to 1.6 mm at 24 cm.

Reproduced with permission of the copyright owner. Further reproduction prohibited without permission.

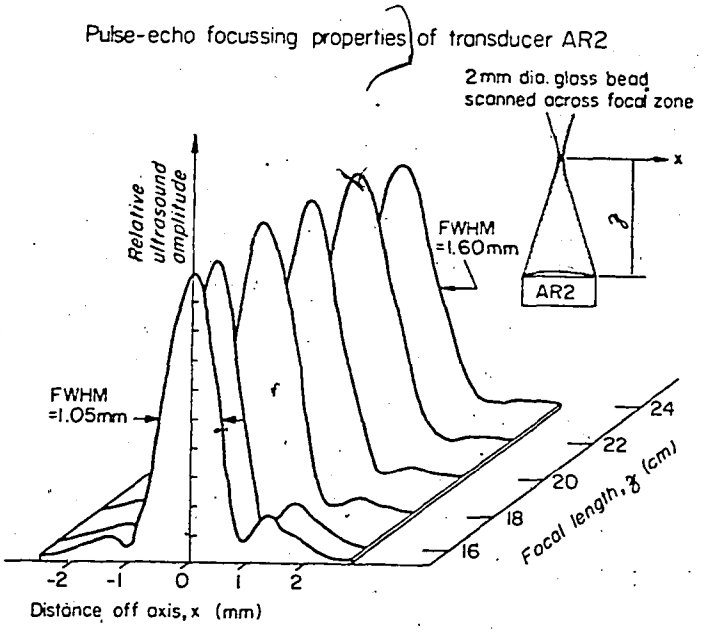

Figure 9. Pulse-echo beam profiles as a function of focal length. The echo FWHM runs from 1.05 mm at 15 cm to 1.6 mm at 24 cm.

c) Gating

The echoes coming from a particular zone are selectively displayed by means of an electronic gate that opens at a time corresponding to the beginning of the zone and closes at the end of the zone. The times at which the gate opens and closes are selected by consulting the graph of delay vs depth given in Figure 10. As an example, consider the case of a sample of breast tissue placed 15.0 cm from AR2. If we wish to display echoes in the range 4 to 6 cm deep in the tissue, the delays must be set to correspond to 19 and 21 cm respectively. Based on a velocity of 1500 m s^{-1} (water at 26°C) the gate must open at 263.0 µs and close at 290.0 µs as shown in Figure 10. This information is entered by the operator on thumbwheel switches. Details of the electronic control circuitry are given in Appendix A.

Unfortunately, the velocity of ultrasound in breast tissue is not a constant.

Reproduced with permission of the copyright owner. Further reproduction prohibited without permission.

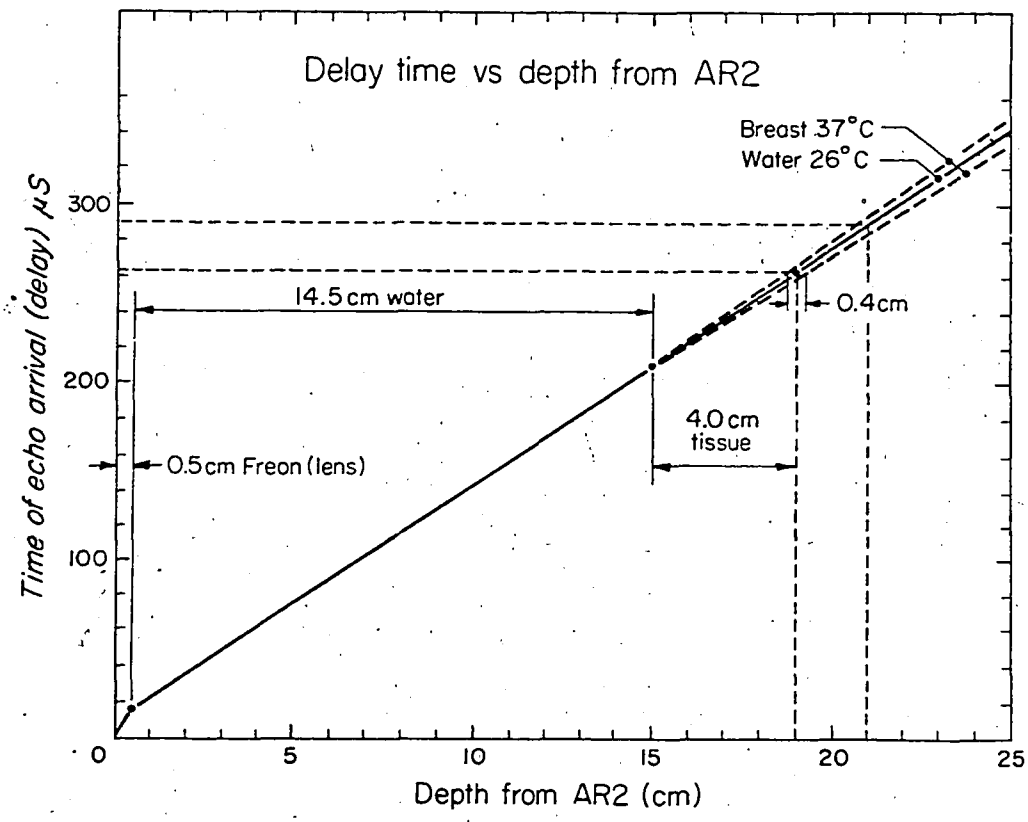

Figure 10. Delay vs depth calibration curve used to set the opening and closing times of the gate. Normal variations in the velocity of ultrasound in breast tissue cause uncertainty in the selection of delay time.

Reproduced with permission of the copyright owner. Further reproduction prohibited without permission.

Kossoff et al (1) have shown that the velocity of ultrasound in normal breast varies between 1430 and 1565 m s^{-1}. Therefore it is impossible to specify the exact delays necessary for a given sample. Figure 10 shows that the accuracy with which the depth can be specified is ±0.2 cm at a depth of 4.0 cm in the breast. This amounts to about 15% of the total depth-of-field as we will see later. The impact of this error on image quality has not yet been assessed.

d) Transducer Motion

To avoid misalignment between zones, an accurate reproducible means of translating the transducer was required. This was provided by a crossed arrangement of linear slide assemblies for x and y motions, driven by stepping motors as shown in Figure 11. The operator selects scan motions ranging from

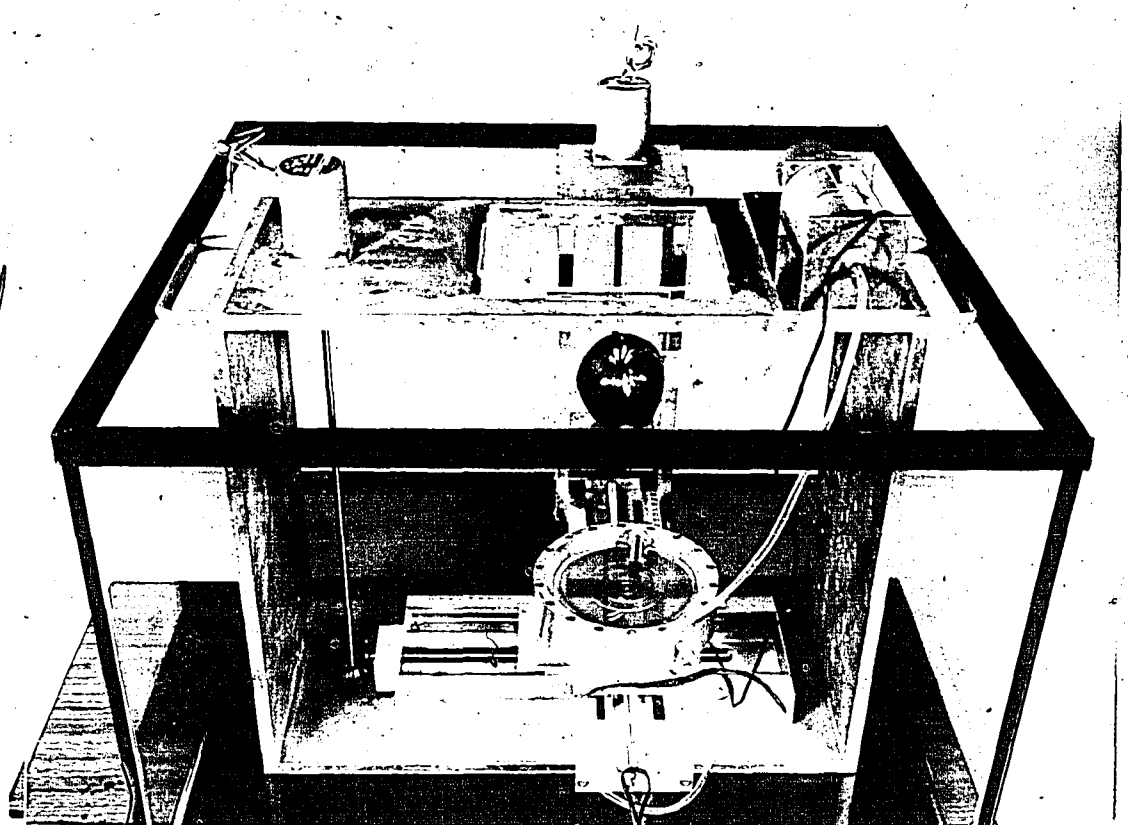

Figure 11. Demonstration scanner showing stepping motors and slide arrangement. Also shown are the Freon pump and sample holder.

Reproduced with permission of the copyright owner. Further reproduction prohibited without permission.

0.5 cm to 16 cm. On the display, the horizontal position is provided by an 8 bit digital to analogue convertor whose output is determined by a binary counter that counts the pulses going to the stepping motors. The display is automatically normalized so that the 256 lines cover the full width of the screen for each range.

III. RESULTS

a) Phantom Study

The zone focussing approach was first tested on a phantom consisting of an array of nylon strings separated by 2 cm. The first image, Figure 12a, was obtained with a state-of-the-art commercial scanner (Picker 80L/DI) at about f/5. Note the poor lateral resolution and depth-of-field. The Demonstration Scanner was interfaced to the signal processing and display circuitry developed by the electronics group for a breast scanner prototype described in Chapter 6. The image shown in Figure 12b was obtained with the Demonstration Scanner

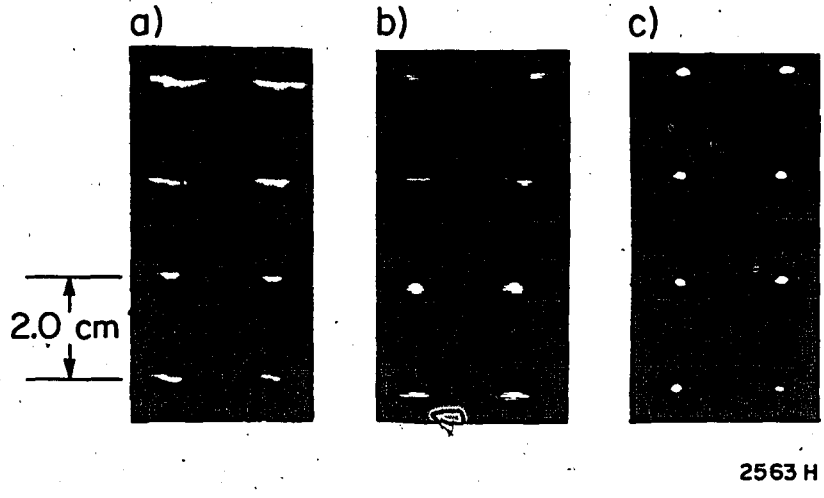

Figure 12. Images of a nylon string phantom by, (a) Picker 80L/DI state-of-the-art clinical scanner; (b) Demonstration Scanner without zone focussing; and (c) the Demonstration Scanner with zone focussing.

Reproduced with permission of the copyright owner. Further reproduction prohibited without permission.

focussed at the level of the second set of wires, a distance of 18.0 cm from the transducer (f/2.4). In the absence of zone focussing, the resolution is excellent at the focus but the depth-of-field is very poor. The best results are obtained by combining the low f-number lens with the zone focussing approach (Figure 12c). Here, four 2 cm wide zones are employed and the consequent improvement of resolution and depth-of-field is very pronounced.

b) Zone Width

The latter image is slightly misleading since the focus of each zone coincided with the levels of the nylon strings. In clinical imaging, the widths of the zones (ie. depth-of-field) must be chosen such that the resolution at the edge of the zone is reasonably close to that at the centre. A rule for determining the widths of the zones was developed experimentally. A wire phantom was imaged at various focal lengths. For each focal length, the phantom was moved to a number of positions, both in front and behind the true focus and measurements of its full width at one tenth maximum echo amplitude (FWTM) were made. The reason for choosing FWTM will be discussed shortly. The results of these measurements for focal lengths of (a) 15.0 cm, (b) 17.5 cm, (c) 20.0 cm, and (d) 22.5 cm are given in Figure 13. As an example consider the measurement at a focal length of 22.5 cm. The minimum FWTM, ℓ, occurs at 22.5 cm as expected and has a value of 2.4 mm. As the phantom is moved in front or behind 22.5 cm, the beam profiles become smeared out and the FWTM becomes larger, indicating a reduction in resolution. We adopted the empirical rule that the edges of the zone correspond to the positions at which the FWTM had increased to $\sqrt{2}$ times ℓ, the value at the true focus. Based on this rule, the 22.5 cm focal zone lies between 21.8 and 23.9 cms as indicated in Figure 13. Note that the depth-of-field is not symmetrical about the focus. In general

Reproduced with permission of the copyright owner. Further reproduction prohibited without permission.

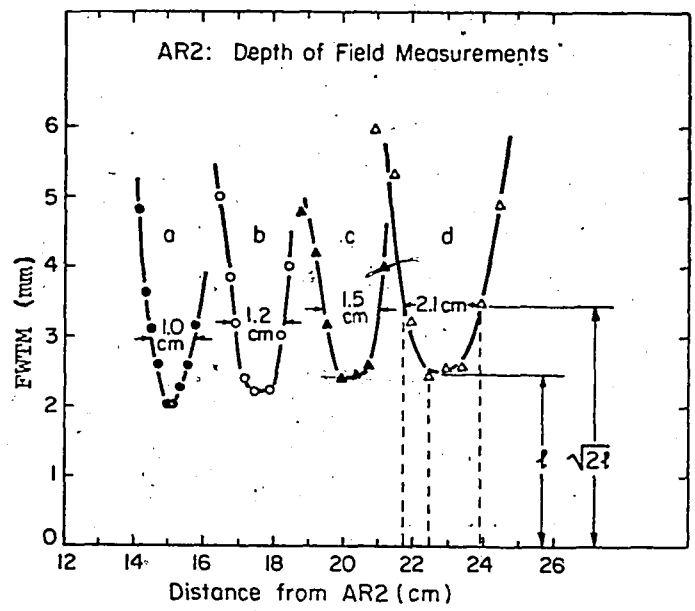

Figure 13. Depth-of-field measurements at (a) 15 cm, (b) 17.5 cm, (c) 20 cm and (d) 22.5 cm. Depth-of-field was defined as the distance over which the FWTM of the echo beam profile remained less than $\sqrt{2}$ times that measured at the focus.

1/3 of the total depth-of-field is directed towards the transducer and 2/3 is directed away. This is similar to the "one third in" rule (2) used by photographers to set focussing for scenes of great depth (the camera is focussed to a point one third into the scene). Figure 13 also shows a decrease in depth-of-field as the focal length is reduced. This is expected because the ultrasound beam converges more rapidly at the shorter focal lengths.

How well does the depth-of-field rule apply in practical imaging? This question is examined in Figure 14. Five wires with spacings of 5, 3, 2 and 1 mm were imaged at a number of depths with the focal length of the Demonstration Scanner set at 15.0 cm (f/2). At the focus (Figure 14b) excellent resolution is obtained, with the wires separated by 1 mm being just resolved. Based on the depth-of-field rule discussed previously the focal zone extends from 14.7 to 15.7 cm (see Figure 13a). Images of the wire phantom near the edges of the

Reproduced with permission of the copyright owner. Further reproduction prohibited without permission.

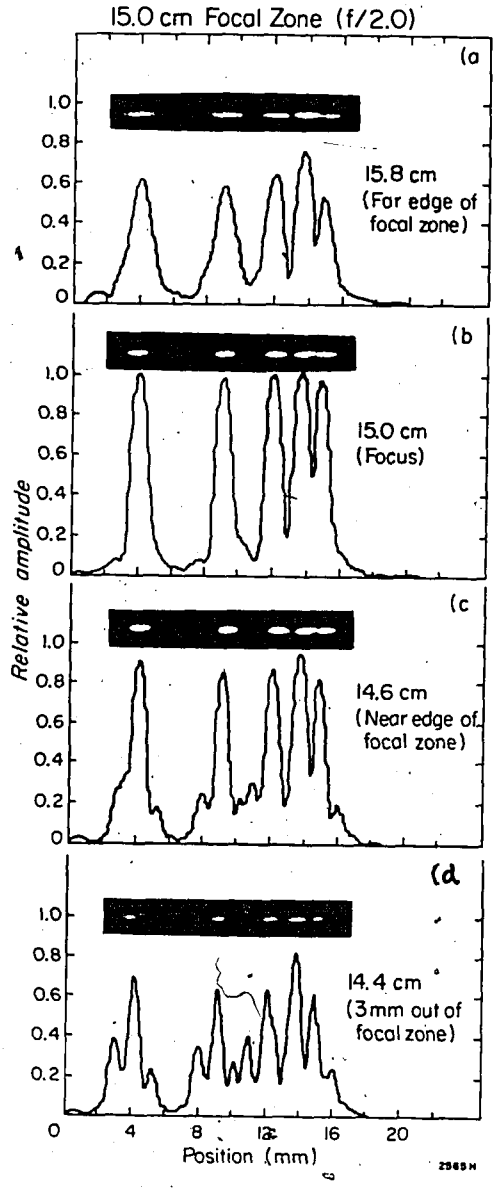

Figure 14. Images and echo profiles for the 15 cm (f/2) zone: (b) at the focus the resolution is excellent with the 1 mm wires reasonably well resolved; (a) and (c) at the edges of the focal zone, the resolution is slightly reduced and the side lobe levels are increasing; and (d) 3 mm outside the focal zone, as defined in the text, the image quality is severely reduced and spurious information appears between the wires.

Reproduced with permission of the copyright owner. Further reproduction prohibited without permission.

focal zone are shown in Figures 14a and 14c. In both cases the image of the wires is slightly poorer but it is still possible to resolve the 1.0 mm set. However, note in Figure 14c that secondary structure is just starting to appear between the wires. The plot of echo amplitude beneath this image shows that the FWHM of the echo distribution is unchanged while the base (10% level) is considerably widened. For this reason, the FWTM is used in the definition of depth-of-field instead of FWHM.

Depth-of-field is plotted as a function of f-number in Figure 15. The data is derived from the results given in Figure 13 and, in this form, may be applied to any ultrasound imaging system operating between f/2 and f/3.

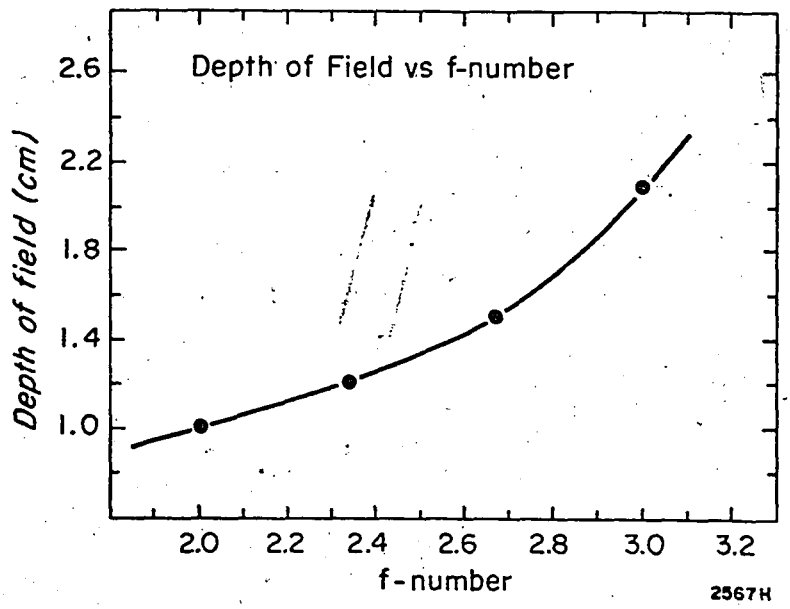

Figure 15. Depth-of-field vs f-number may be used to select zone widths for imaging systems operating between f/2 and f/3.

Reproduced with permission of the copyright owner. Further reproduction prohibited without permission.

c) Tissue Study

The ability of zone focussing to improve the quality of liver scans is examined in Figure 16. A bovine liver sample was cut fresh by the local butcher and placed immediately in saline. The sample plus saline was subsequently transferred to the sample container of the Demonstration Scanner and imaged at 23°C. The zone focussed image (Figure 16, top) was made using seven, 1 cm wide zones. The first zone had an f-number of 2 and the seventh zone had an f-number of 3. Seven zones were more than necessary, based on the former analysis of depth-of-field, but it was simpler to perform the scans using a constant zone width. For comparison an image obtained with a conventional f/5, 3.5 MHz, Aerotech transducer is given in the lower part of Figure 16. In this scan, the conventional transducer was mounted such that its central axis coincided with that of AR2 and its focus was 3 cm into the tissue. The same motion, signal

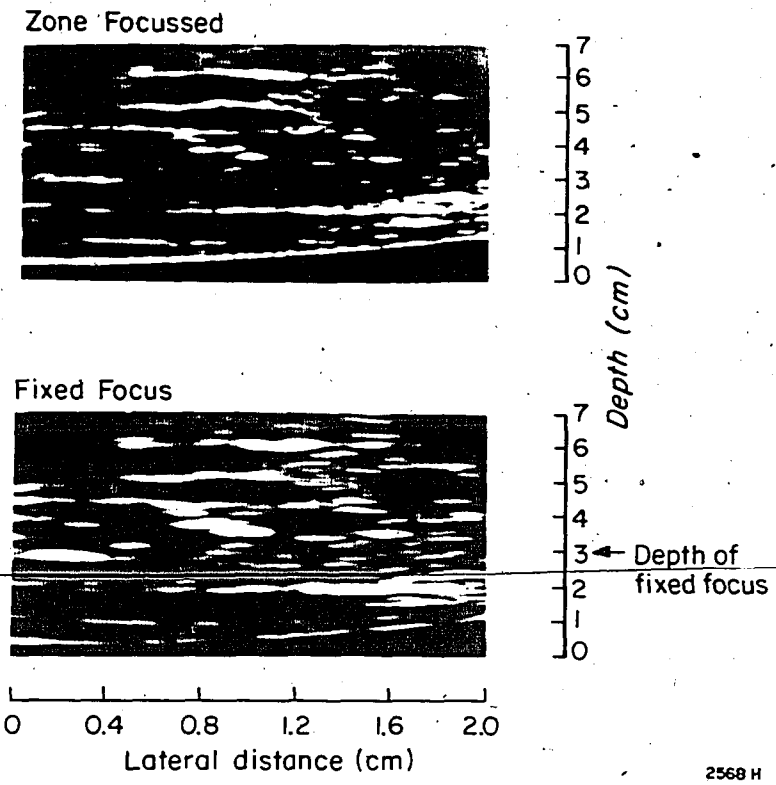

Figure 16. Images of bovine liver sample in vitro: (top) zone focussed image using seven 1 cm wide zones with f-numbers ranging from 2 to 3; and (bottom) the corresponding image obtained using a conventional fixed focus, f/5, 3.5 MHz transducer under exactly the same conditions. The low f-number zone focussing approach results in a two- to three-fold improvement in resolution. This is particularly evident at the structure labelled "a".

Reproduced with permission of the copyright owner. Further reproduction prohibited without permission.

processing and display electronics were used in both images. The liver sample had a smooth surface and some well defined vascular structure at a depth of 4 to 6 cm. The zone focussed image exhibits a two- to three-fold improvement in lateral resolution compared with the conventional image, based on the lateral dimensions of the textural structure and more prominent structures such as that at point "a". The improvement in resolution is due to both the zone focussing and lower f-number of AR2 compared to the conventional transducer. Note that there is no apparent discontinuity between zones.

IV. SUMMARY

A flexible testing system called the Demonstration Scanner was built to examine the effectiveness of the zone focussing approach in ultrasonic imaging. A 7.5 cm Freon focussed transducer was used to focus ultrasound over the range f/2 to f/3.3 (15-25 cm). The quality of the focus was tested in transmission using a 0.8 mm microphone scanned across the focal zone, and in echo mode using wire and glass bead phantoms. In each case the agreement with theory was good over the full range of f-numbers. Digital electronic circuits were designed to control the stepping motors which focussed the lens and moved the transducer. In operation the focal length and gating functions were determined using calibration curves and were entered via thumbwheel switches.

A rule for depth-of-field (zone length) was derived empirically and substantiated experimentally: the full width at one tenth maximum amplitude of the echo beam profile at a point inside the depth-of-field must be no more than $\sqrt{2}$ times that at the focus.

Reproduced with permission of the copyright owner. Further reproduction prohibited without permission.

Phantom and preliminary liver tissue studies indicated an improvement in resolution of between 2 and 3 over conventional scanning techniques. Studies on breast tissue are forthcoming.

Reproduced with permission of the copyright owner. Further reproduction prohibited without permission.

CHAPTER 3

REFERENCES

1. Kossoff, G., Kelly-Fry, E. and Jellins, J.: Average velocity of ultrasound in the human female breast. J. Acoust. Soc. Am. 53: 1730-1736 (1973).

2. Horder, A.: The Manual of Photography, Focal Press, New York, p. 109 (1971).

Reproduced with permission of the copyright owner. Further reproduction prohibited without permission.

CHAPTER 4

THE CYLINDRICAL TRANSDUCER SCATTER SCANNER

Submitted to
The Journal of the Acoustical Society of America

Reproduced with permission of the copyright owner. Further reproduction prohibited without permission.

I. INTRODUCTION

One of the most persistent and difficult problems in medical ultrasonographic imaging is the lack of resolution in the lateral directions (1,2). In the majority of clinical applications, transducers are gently focussed with diameters ranging from 10 to 20 mm. The selection of transducer diameter and focal length is a compromise between the smallest lateral beam width at the focus, and the greatest depth-of-field. As a result, an f-number (focal length/diameter) of approximately 5.0 is employed in most systems. The lateral resolution, as defined by the full width at half maximum of the ultrasound amplitude distribution (FWHM), varies directly with the f-number of the transducer, and λ, the wavelength of the ultrasound. The diffraction limit (3,4) at the focus is given by

$$\text{FWHM} = 1.41\lambda \ (\text{f-number}) \qquad (1)$$

For a typical transducer with a diameter of 19 mm, focal length of 95 mm, and an average frequency of 3.5 MHz (λ = 0.43 mm in water), the beam width varies from approximately 19 mm at its surface to 3.0 mm at the focus and again becomes large at distances greater than the focal length. The axial resolution, by contrast, remains relatively constant and is usually in the order of 1.0 mm. The lateral resolution is therefore approximately 3 to 10 times poorer than the axial resolution, depending on the position in the ultrasound field. One feasible means to improve lateral resolution is to lower the f-number of the transducer by increasing its diameter. Unfortunately, this approach yields an unacceptably shallow depth-of-field. Annular phased arrays (5) may be employed to overcome the latter problem but these devices require extensive electronics and may increase the length of time to generate an image.

Reproduced with permission of the copyright owner. Further reproduction prohibited without permission.

A unique and exceptionally simple method for maintaining good lateral resolution over a large depth of tissue has been investigated. This new technique is based on scattering at right angles from tissue. High spatial resolution and depth-of-field are obtained by a cylindrical transducer that generates a line focus. In this paper the physics of the cylindrical transducer and its application to a scatter imaging device are investigated. Particular attention is paid to the ultrasound field of the cylindrical transducer. As well a simple scanner has been constructed to image phantoms and in vitro tissue samples. The images from this device are very encouraging and suggest that this approach may eventually play a useful role in medical ultrasonography.

II. BASIC PRINCIPLES OF THE CYLINDRICAL TRANSDUCER SCATTER SCANNER

A schematic representation of the "Cylindrical Transducer Scatter Scanner" (6) is shown in Figure 1. Instead of using one transducer to both transmit and receive, as used in conventional pulse-echo ultrasonography, two separate transducers are employed. The first is a cylindrical transducer which generates a cylindrical ultrasound wave-front that converges to a line focus at the central axis of the cylinder. Scattering structures within the material, that lie on or near the line of focus, emit secondary ultrasound waves simultaneously with the arrival of the transmitted pulse. A second transducer, positioned colinear with the line focus, receives the scattered waves and converts them into electrical signals as a function of time. In the same way as a pulse-echo scanner, there is a direct relationship between the time of arrival, and the position of scatterer. Display is accomplished as in conventional pulse-echo imaging. Since the ultrasound beam is focussed

Reproduced with permission of the copyright owner. Further reproduction prohibited without permission.

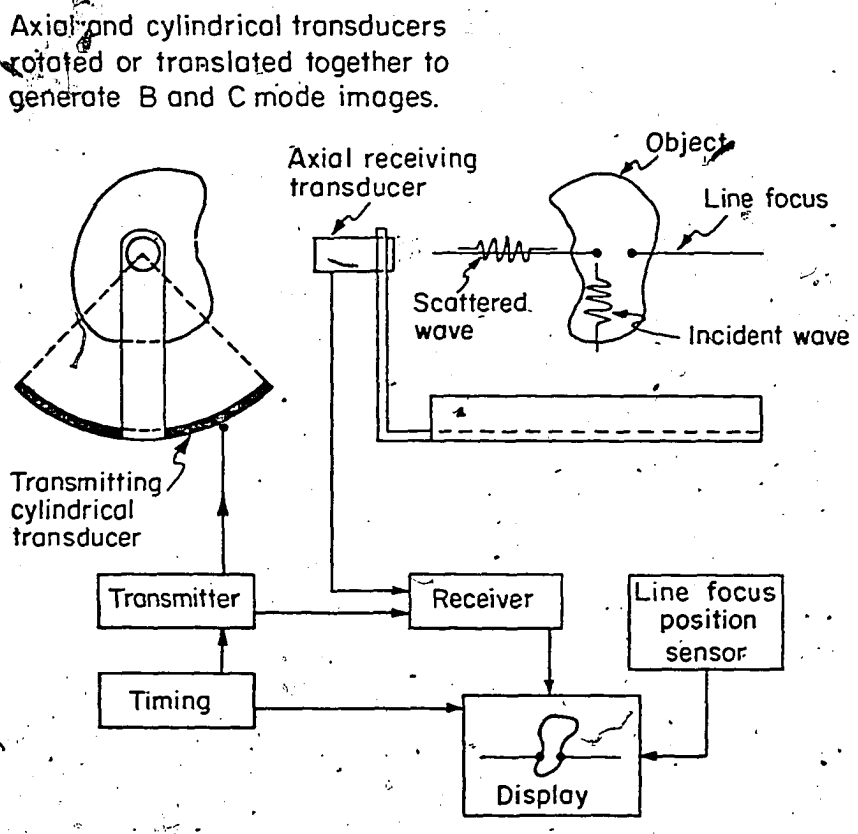

Figure 1. The cylindrical transducer transmits a pulse of ultrasound that converges to a line focus in the object to be imaged. A receiving transducer aimed along the line focus, detects some of the ultrasound scattered at an angle of 90° to the insonifying pulse. The receiver converts the scattered ultrasound into electrical signals for display. A tomographic image is generated by translating or rotating the two transducers as a unit, while appropriately displaying the scanner information.

Reproduced with permission of the copyright owner. Further reproduction prohibited without permission.

to the same extent at all points along the line focus, the depth-of-field problem inherent in pulse-echo imaging is eliminated.

Alternatively, the cylindrical transducer may be used as the receiver and the transducer aimed along the line of focus may be used as the transmitter. Due to the reciprocal nature of transduction (7), the focussing principle is basically the same as described previously.

From a physical viewpoint, the information contained in the image results from two general processes. Firstly, specular reflections at right angles to the insonifying pulse as shown in Figure 2a, result in relatively large signals which form the image highlights. The other component of image information is provided by 90° scattering as shown in Figure 2b. Here, a polar plot of ultrasound scattering *vs* angle (Waag *et al* (8)) for pig liver at 3 MHz is superimposed over the line focus. This plot shows that a significant fraction of the ultrasound is scattered at ±90°, more than is back-scattered (ie. at 180°). If this type of scattering profile is similar to that for human tissue, a large scatter signal should be obtained. Gray scale echography (9) has clearly demonstrated the clinical value of the back-scattered ultrasound and it is therefore quite likely that 90° scatter, with its larger amplitude, will also provide valuable information.

III. CYLINDRICAL TRANSDUCERS: PRACTICAL CONSIDERATIONS

The success of the scatter scanner depends critically on the angle, ϕ, subtended at the line focus by the cylinder. In general, it will be shown later that angles in excess of 100° are desirable. Thus, the use of cylindrical acoustic lenses would appear to be impractical, and it is necessary

Reproduced with permission of the copyright owner. Further reproduction prohibited without permission.

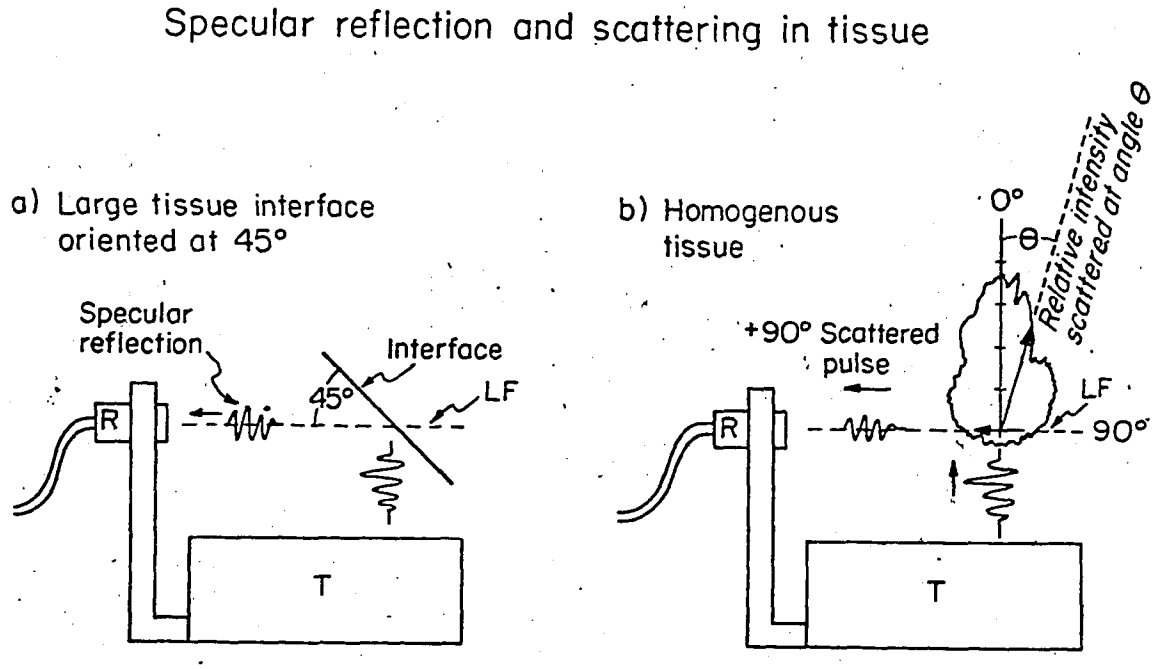

Figure 2. Two types of displayed information result from (a) specular reflection by large tissue interfaces oriented at 45° to the line focus, LF, of cylindrical transducer, T; and (b) scatter from homogeneous tissue. A polar plot of the angular scattering distribution from pigs liver at 3 3 MHz (Waag et al (8)) shows that considerably more ultrasound is scattered at 90° than is backscattered (180°).

Reproduced with permission of the copyright owner. Further reproduction prohibited without permission.

to employ a Piezoelectric material preformed into the shape of a cylinder. For piezoelectric ceramics such as PZT5[a], this is difficult but not impossible. A simpler approach is to use a piezoelectric plastic such as polyvinylidene difluoride (PVF_2) (10)[b], which easily conforms to the cylindrical backing. The important properties of both materials are listed in Table I. This data is derived from information provided by the manufacturers, with the exception of the dielectric constant for PVF_2 which was measured by Callerame et al (11). Unfortunately, the piezoelectric coefficients for thickness mode are not published for PVF_2. However, the shear coefficients do give an indication of the piezoelectric strengths of the two materials. Note that g_{31}, a piezoelectric coefficient important in reception, is much larger for PVF_2 than for PZT while the e_{31}, a piezoelectric coefficient important in transmission, is much lower for PVF_2 than for PZT. In general, we have found the PVF_2 to be ~20 dB less sensitive than PZT used under comparable loading conditions. The principle advantages of PVF_2 over PZT are its mechanical flexibility and low acoustical impedance.

Figure 3 shows a photograph of the PVF_2 cylinder used in the present study. Epoxy was used to bond the PVF_2 to a 120° section of aluminum pipe having a length of 8.0 cm and a radius of 4.0 cm. The aluminum backing served as the back electrode while the front electrode was formed by evaporating silver onto the PVF_2.

When PVF_2 is mounted on a high impedance material such as aluminum, it tends to resonate at a frequency such that the thickness of the PVF_2 is one quarter of the ultrasound wavelength. A resonant frequency of 16.7 MHz was measured experimentally for 30 μm thick PVF_2 mounted on aluminum. Swartz and Plummer (12) have applied the Mason model (13) to predict the voltage output/stress input vs frequency of the one quarter wave PVF_2 transducer. Their results show that the decline in sensitivity of these devices is only 6

Reproduced with permission of the copyright owner. Further reproduction prohibited without permission.

PHYSICAL CONSTANTS OF PVF_2 AND PZT5

Property	Unit	PVF_2	PZT5
Density	10^3 kg/m^3	1.8	7.75
Dielectric constant*	—	8.3 @ 3MHz	1700.
Velocity of sound	m/s	2000.	4350.
Impedance	10^6 Rayl	3.56	33.5
e_{31} } Piezoelectric constants	10^{-2} N/Vm	6.0	520.
g_{31} } Piezoelectric constants	10^{-3} Vm/N	174.0	10.7
Available thicknesses	10^{-6} m	9. and 30. only	100. - 100000.

Table I.

Reproduced with permission of the copyright owner. Further reproduction prohibited without permission.

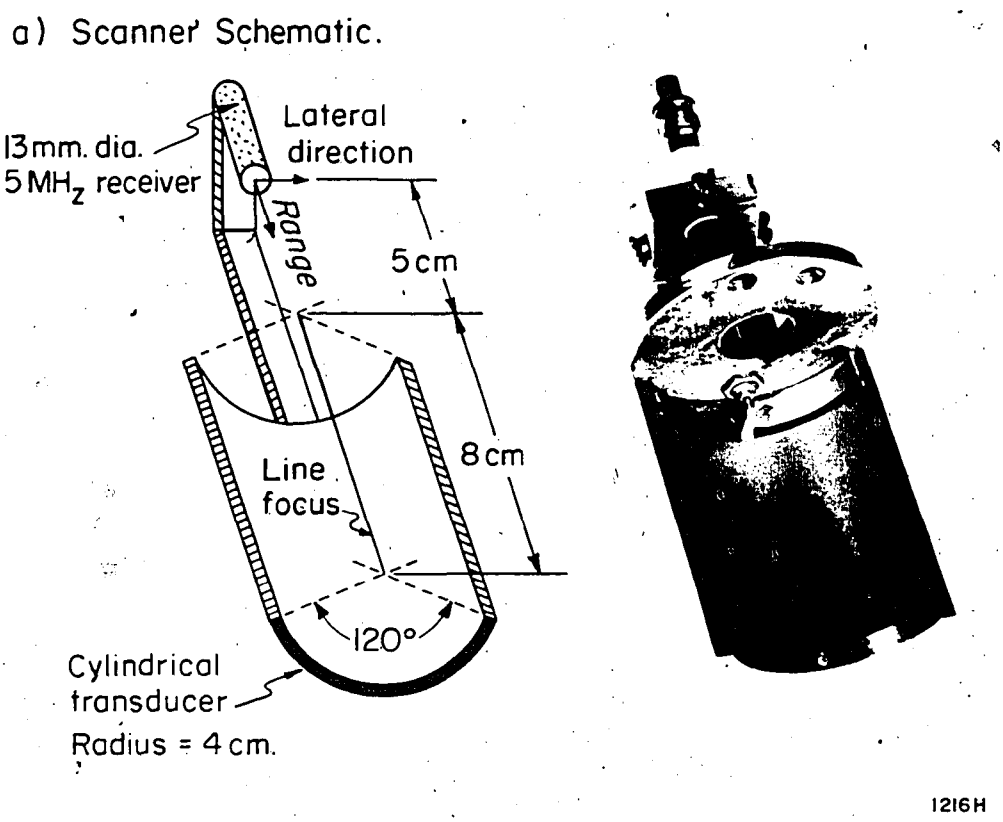

Figure 3. Schematic and photograph of CS1, a simple scatter scanner. The cylindrical transducer is a sheet of PVF_2 bonded to a cylindrical section of aluminum pipe.

Reproduced with permission of the copyright owner. Further reproduction prohibited without permission.

dB between zero and the PVF_2 resonant frequency. Thus, it is feasible to use PVF_2 transducers at frequencies more applicable to medical applications (1-10 MHz).

IV. ELECTRONICS AND MEASUREMENT TECHNIQUES

Gated radiofrequency (RF) bursts produced by a waveform generator (Wavetek Model 164, San Diego, California, U.S.A.) were amplified by a 50 Watt wideband RF amplifier (Electronic Navigation Industries, Model 240L, Rochester, New York, U.S.A.) and applied to the electrodes of the cylindrical transducer. Typically, frequencies between 0.5 and 5 MHz were employed with pulse amplitudes between 10 and 200 V. The pulse length was variable from one complete oscillation to continuous oscillation. A 5 MHz, 13 mm diameter, medium focussed transducer (Aerotech, Gamma Series, Lewistown, Pennsylvania, U.S.A.) was used to receive the scattered ultrasound. The receiver signal was amplified and processed as in conventional ultrasonography using electronics designed and built by the electronics group at the Ontario Cancer Institute.

Measurement of the ultrasound field of the cylindrical transducer was performed by scanning a microphone across the focal line and recording the signal amplitude as a function of position. The microphone consisted of a 0.8 mm diameter, 5.0 MHz disk of PZT5 mounted in the tip of an 18 gauge (0.85 mm inside diameter) hypodermic needle. A 22 gauge (0.64 mm) varnished copper wire was inserted through the hypodermic needle to make contact with the back face of the disk and conductive epoxy was used to make an electrical connection between the front face and the body of the needle. The bandpass was from 3.5 to 6 MHz (-6 dB points), although the microphone was useful down to a frequency of 0.5 MHz. The sensitivity of the microphone was measured as a function of angle at 1.4 MHz. In this test an angle of 0^o was defined when the hypodermic needle was perpendicular to the wave front generated by a distant transducer. A signal

Reproduced with permission of the copyright owner. Further reproduction prohibited without permission.

variation of ±4.3 dB was observed as the angle was changed from 0° to ±60°.

V. THE ULTRASOUND FIELD OF THE CYLINDRICAL TRANSDUCER

The time varying pressure at a point in the field of a cylindrical transducer may be expressed as a sum of contributions from elementary Huygens' sources on the surface of the transducer. The cylindrical transducer may be divided into 2 regions. The first is the central part of the cylinder, in which the field is similar to that which would be expected for an infinite cylinder. The second region comprises the area near the edge of the cylinder.

a) Central Region

The field of the infinite cylinder may be treated, with reasonable approximation, as a two-dimensional problem. The geometry for the calculations is shown in Figure 4. By slight modification of the conventional velocity potential approach (see Beyer and Letcher (14)), the complex CW (continuous wave) pressure at a field point, $p(r_1,\phi_1,t)$, may be represented by the following integral:

$$p(r_1,\phi_1,t) = \frac{K}{j} \int_{-\phi/2}^{\phi/2} \frac{e^{j2\pi\,(r/\lambda - \nu t)}}{r}\, r_2 d\phi_2 \qquad (2)$$

where K is a constant proportional to $1/\lambda$ and to the CW pressure at the surface of the transducer, r_2 is the radius of the cylinder, r is the distance from the field point to an elemental Huygens' source on the surface of the transducer, and ν is the frequency of ultrasound employed. The maximum pressure amplitude,

Reproduced with permission of the copyright owner. Further reproduction prohibited without permission.

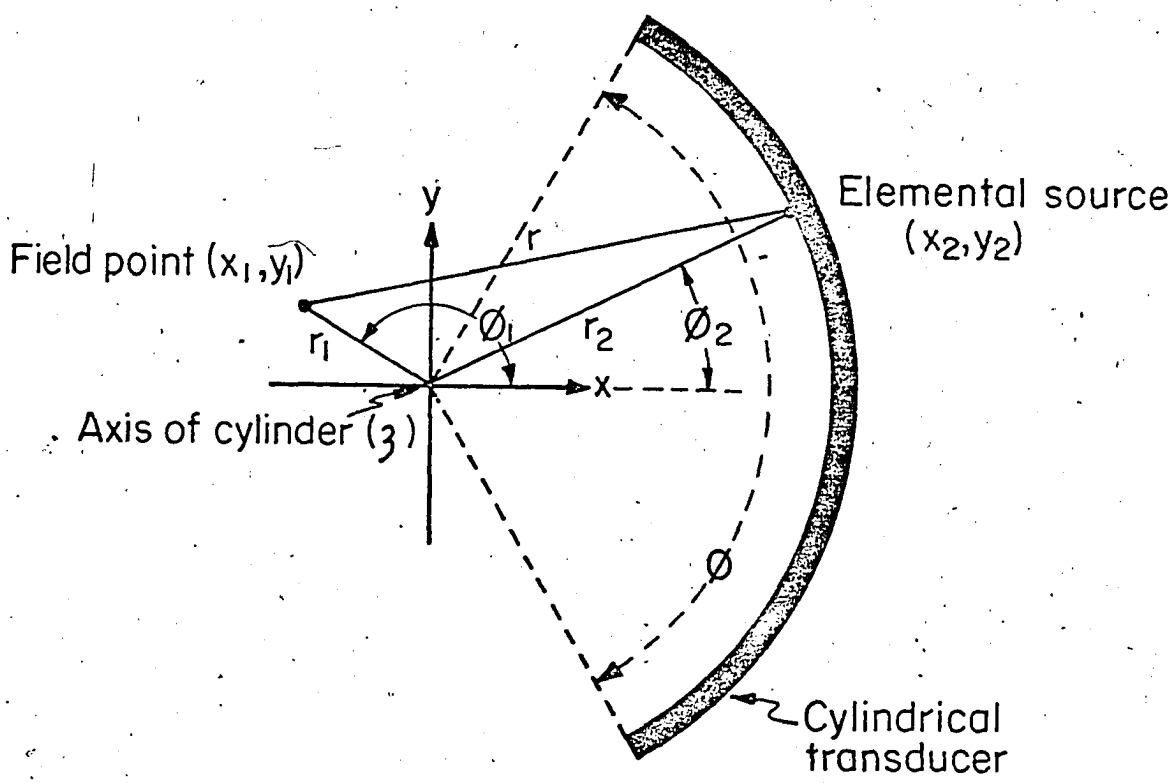

Figure 4. Geometry used in the ultrasound field calculations for cylindrical transducers.

Reproduced with permission of the copyright owner. Further reproduction prohibited without permission.

$P_{max}\ (r_1,\phi_1)$, may be calculated using the expression:

$$p_{max}\ (r_1,\phi_1) = Re_{max}\ \{p(r_1,\phi_1,t)\} \qquad (3)$$

The equation for r is:

$$r = \left[\{r_2\ \mathrm{Cos}\ (\phi_2) - r_1\ \mathrm{Cos}\ (\phi_1)\}^2 + \{r_2\ \mathrm{Sin}\ (\phi_2) - r_1\ \mathrm{Sin}\ (\phi_1)\}^2\right]^{\frac{1}{2}} \qquad (4)$$

If we restrict attention to points near the cylindrical axis ($r_1 << r$) the approximation, $r_2/r \approx 1$, may be applied to terms outside the exponential and equation 2 may be rewritten:

$$p(r_1,\phi_1,t) = \frac{K}{j}\int_{-\phi/2}^{\phi/2} e^{j2\pi\ (r/\lambda - \nu t)}\ d\phi_2 \qquad (5)$$

This equation is most easily treated by numerical computation, however analytic solutions exist for two interesting cases. The first of these is the distribution along the y axis ($\phi_1 = 90°$) for small angles ($\phi \lesssim 30°$) of the cylinder. The substitution of $r_1 = y$, into Equation 4 yields:

$$r = [r_2^2 + y^2 - 2r_2\ y\ \mathrm{Sin}\ (\phi_2)] = (r_2^2 + y^2)^{\frac{1}{2}}\left[1 - \frac{2r_2\ y\ \mathrm{Sin}\ (\phi_2)}{r_2^2 + y^2}\right]^{\frac{1}{2}}$$

in which the second term in the square bracket is $\ll 1$. Further reduction of this formula, using the binomial approximation, gives:

$$r = (r_2^2 + y^2)^{\frac{1}{2}} - r_2 y\ \mathrm{Sin}\ (\phi_2)/(r_2^2 + y^2)^{\frac{1}{2}}$$

and

Reproduced with permission of the copyright owner. Further reproduction prohibited without permission.

$$r = r_2 - y \text{ Sin } (\phi_2) \text{ for } y << r \qquad (6)$$

Substituting equation 6 into equation 5 results in

$$p(y,t) = \frac{K}{j} e^{j2\pi (r_2/\lambda - \nu t)} \int_{-\phi/2}^{\phi/2} e^{-j2\pi y \text{ Sin } (\phi_2)/\lambda} d\phi_2 \qquad (7)$$

If the angle of the cylinder is small, the approximation, Sin $(\phi_2) = \phi_2$, is valid and equation 7 becomes:

$$p(y,t) = \frac{K}{j} e^{j2\pi (r_2/\lambda - \nu t)} \int_{-\phi/2}^{\phi/2} e^{-j2\pi y \phi_2/\lambda} d\phi_2$$

$$= \frac{K}{j} \phi e^{j2\pi (r_2/\lambda - \nu t)} \text{ Sinc } (y \phi/\lambda) \qquad (8)$$

where Sinc is defined by the expression Sinc(x) = Sin $(\pi x)/(\pi x)$. The final expression for maximum pressure amplitude is then obtained by substituting equation 8 into equation 3:

$$p_{max}(y) = Re_{max} \{p(y,t)\} = K \phi \text{ Sinc } (y \phi/\lambda) \qquad (9)$$

For small cylinder angles the ultrasound distribution (equation 9), as might be expected, is exactly the Fraunhofer distribution for an infinite slit of angular width ϕ (3).

Another case, in which numerical integration can be avoided, is that of a complete cylinder ($\phi = 2\pi$). Since ϕ_2 is no longer small, equation 7 must be integrated directly. The complex pressure becomes

$$p(y,t) = \frac{2\pi K}{j} e^{j2\pi (r_2/\lambda - \nu t)} J_o (2\pi y/\lambda)$$

Reproduced with permission of the copyright owner. Further reproduction prohibited without permission.

where J_o is the zeroth order Bessel function.

Application of equation 3 results in:

$$p_{max}(y) = 2\pi K J_o (2\pi y/\lambda) \qquad (10)$$

Figure 5 shows the shapes of the ultrasound distributions predicted by equations 9 and 10. Equation 9 is examined for $\phi = 30^o$ and compared to the result obtained by numerical computation of equation 5. Similarly equation 10 is applied to a cylinder of 360°. In both cases the numerical results are in excellent agreement with the theoretical equations. Figure 5 demonstrates that as the cylindrical angle is increased, the width of the main and side lobes are reduced but the height of the side lobes is increased relative to the main lobe.

The full width at half maximum (FWHM) of the main lobe was computed numerically as a function of ϕ in both the x and y directions (see Figure 6). The cylindrical beam converges along the x axis to the focus and diverges thereafter. Thus, the ultrasound distribution along the x axis depends on two factors: the physical convergence of the beam and diffraction effects. Figure 6 shows that the x beamwidth is, as expected, larger and more dependent on the angle of convergence than the y beamwidth. Also when the cylinder completely encircles the line focus ($\phi = 360°$) the x and y beamwidths are exactly equal. By employing angles greater than 100° it is possible to obtain submillimeter beamwidths along the length of the cylinder using a modest frequency of 5 MHz.

The first experimental cylindrical transducer was shown in Figure 3, and had an angle, ϕ, of 120°. A theoretical and experimental study of its beam distribution in both the x and y directions are shown in Figure 7. The theoretical distribution of ultrasound amplitude in the y direction is

Reproduced with permission of the copyright owner. Further reproduction prohibited without permission.

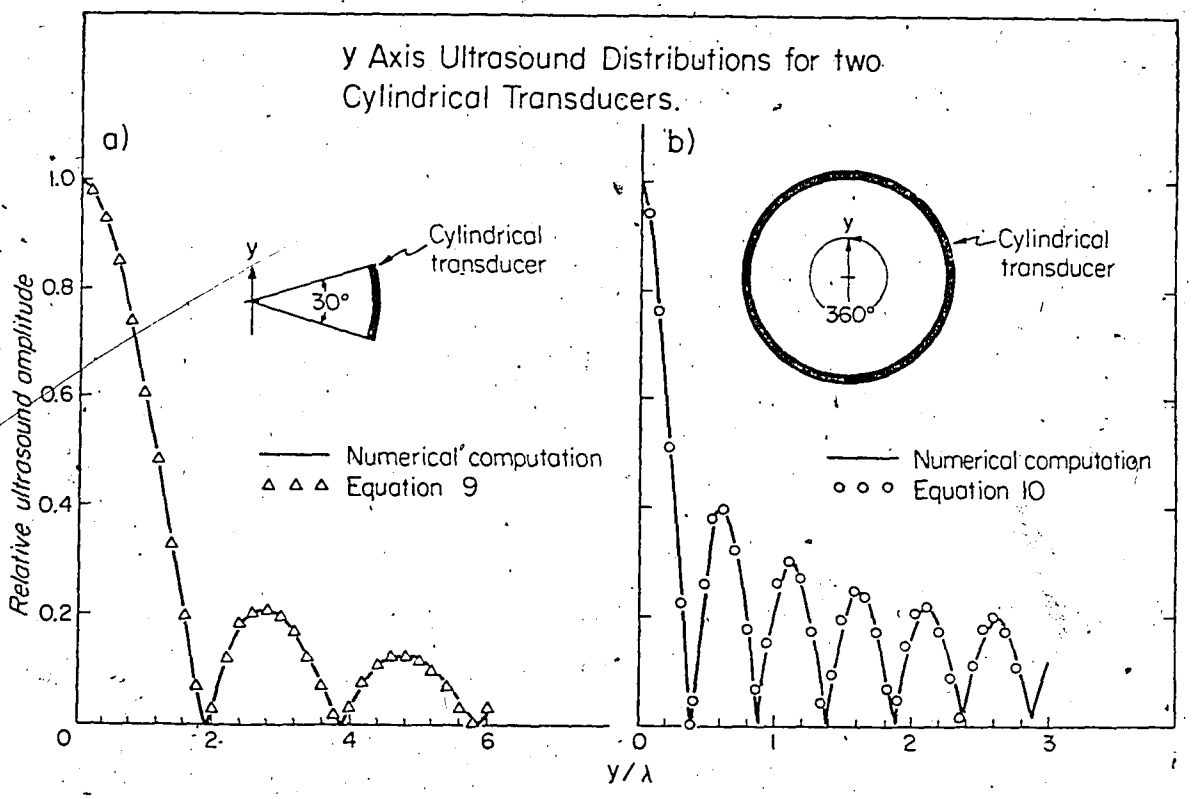

Figure 5. Comparison of numerical analysis and analytical solutions with approximations. At small angles (a) the y distribution reduces to Fraunhofer diffraction by an infinite slit of angular width ϕ. At large angles (b) the distribution is proportional to the zeroth order Bessel function.

Reproduced with permission of the copyright owner. Further reproduction prohibited without permission.

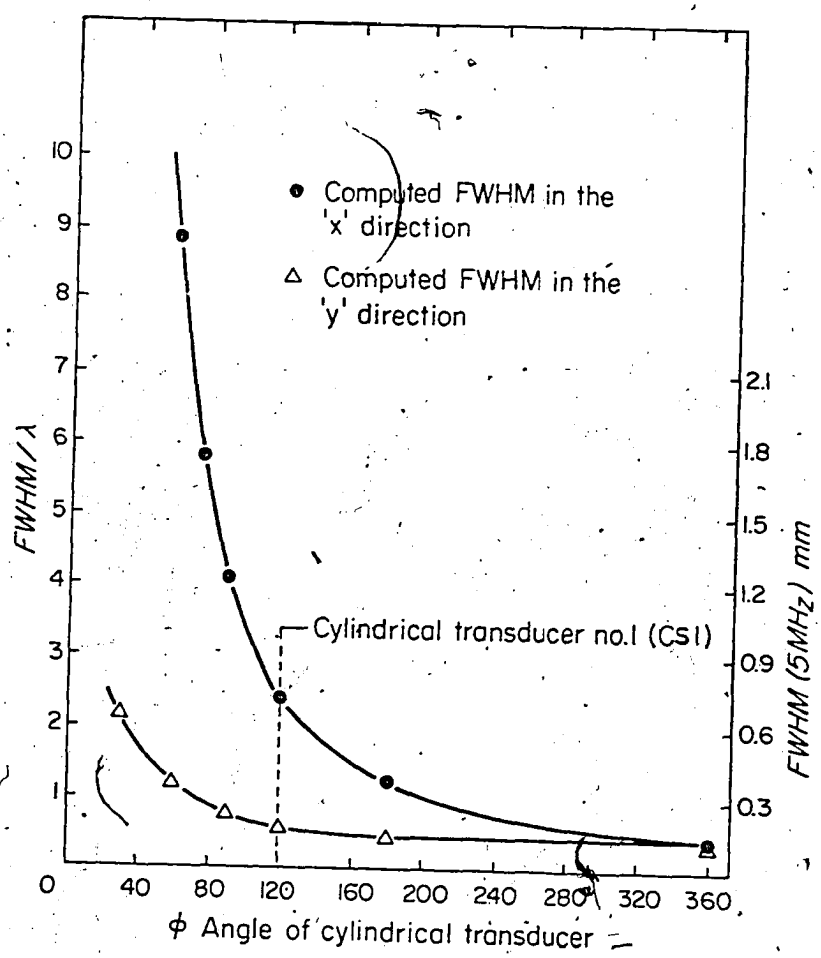

Figure 6. Computed beam widths as a function of transducer angle. The distribution in the x direction is more dependent on transducer angle than is the y distribution. This is largely due to the physical convergence of the beam. An angle of 120° was chosen for CS1.

Reproduced with permission of the copyright owner. Further reproduction prohibited without permission.

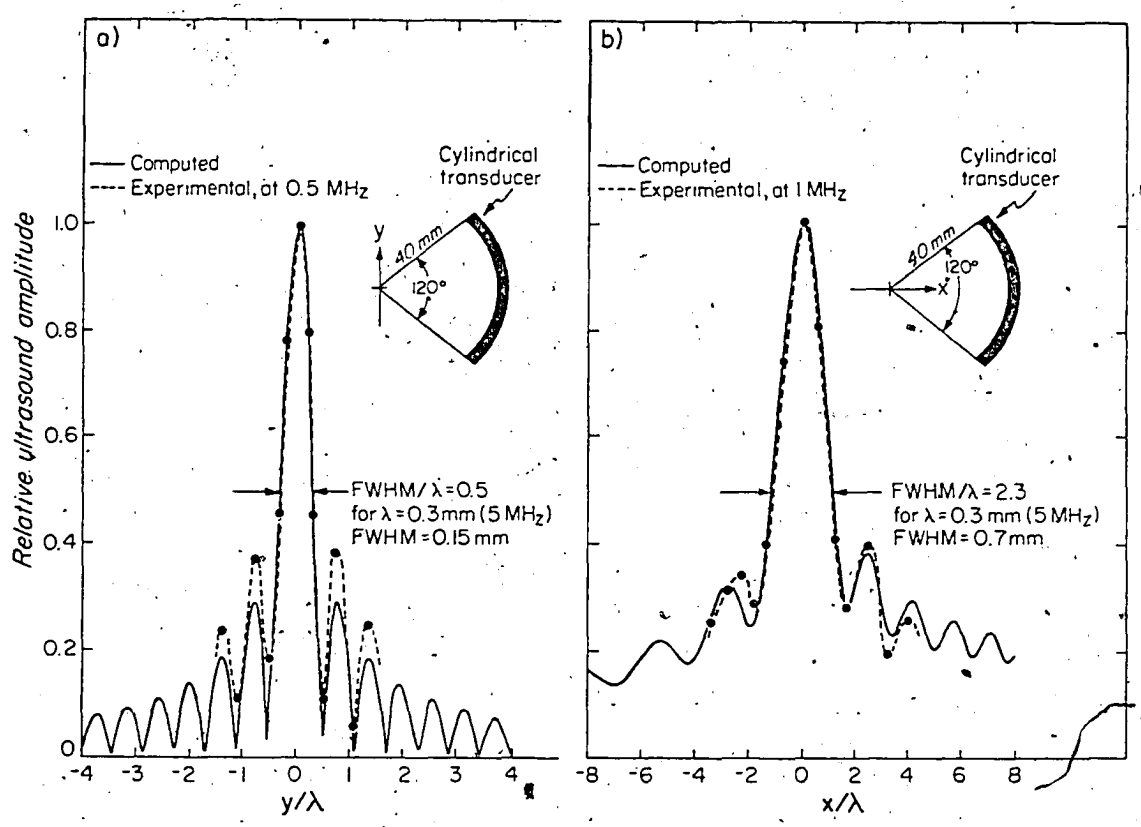

Figure 7. Computed continuous wave ultrasound distributions in the y (a) and x (b) directions for a 120° cylindrical transducer. Experimental distributions were obtained for CS1 by scanning a 0.8 mm diameter piezoelectric microphone in the appropriate direction and recording the CW amplitude of the signal. These measurements were performed at relatively low frequencies to minimize innacuracies due to the angular response of the microphone. The theoretical FWHM at 5 MHz is 0.15 mm in the y direction and 0.7 mm in the x direction.

Reproduced with permission of the copyright owner. Further reproduction prohibited without permission.

represented by the solid line in Figure 7a. The results are normalized to the wavelength in this graph but a feeling for the sharpness of this focus can be obtained by computing the FWHM for λ = 0.3 mm (5 MHz). At this wavelength, the theoretical FWHM is 0.15 mm, ie. 0.5 λ. Experimentally, it is difficult to verify a distribution this sharp, however it was possible to verify the theoretical predictions at lower frequencies. The points shown in Figure 7a were measured at 0.5 MHz by monitoring the output of the 0.8 mm diameter microphone (see Section III) at various points on the y axis. The experimental measurement agrees very well with theory, except that the side lobes appear approximately 25% higher than predicted. This discrepancy may be due to the size and angular response of the microphone or to imperfections in the physical construction of the cylindrical transducer. Cylinder imperfections may have a severe effect on the distributions at higher frequencies. Figure 7b shows a wavelength normalized plot of the amplitude distribution along the x axis. As expected, this distribution is considerably wider than that in the y direction. At 5.0 MHz the theoretical FWHM is 0.7 mm. The general shape of the distribution was verified at a low frequency, (1 MHz) by scanning a microphone along the x axis and recording the signal amplitude. The low frequency results are shown as the solid points in Figure 7b and are in excellent agreement with the theoretical predictions. Note that these experimental and theoretical assessments are carried out for a CW source. When the transmitted pulse is short, the side lobes are somewhat reduced.

Figure 8 shows a perspective plot of the beam as it approaches and passes through the focus. Here, the convergence of the 120° cylindrical beam and the basic difference between the x and y directions are very clearly illustrated. Notice that the x profile is actually a measure of the depth of field of the line focus.

Reproduced with permission of the copyright owner. Further reproduction prohibited without permission.

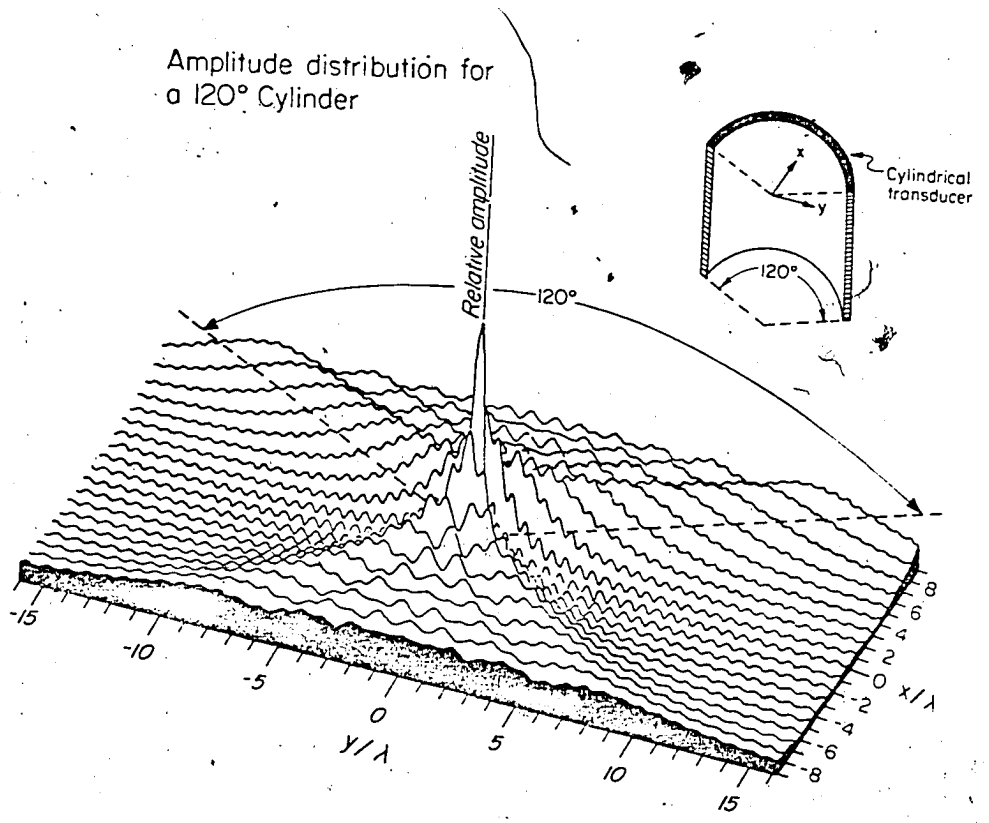

Figure 8. Perspective plot showing the ultrasound distribution in the x-y plane of a 120° cylinder.

Reproduced with permission of the copyright owner. Further reproduction prohibited without permission.

b) Edge Field

The fringing or edge field of the cylindrical transducer determines the useful distance over which imaging can be performed. An examination of the ultrasound amplitude along the cylindrical axis, z, shows that the field oscillates with increasing amplitude towards the edge followed by a rapid monotonic decrease to zero. Figure 9 shows the experimentally observed fringing field for CS1 at a CW frequency of 1.35 MHz. The measurements were performed with the 0.8 mm diameter microphone described earlier.

Theoretically, the symmetry of the cylinder reduces this problem to the Fresnel distribution of waves diffracted by a long narrow slit. The cylinder can be visualized as a superposition of these long slits arranged to be a constant distance from the points of observation. The results of numerical computations (Figure 9) were in excellent agreement with optical data (see, for example, Jenkins and White (15)) and also agreed very well with the experimental data.

The distance, s, between the last axial maximum and the point at which the ultrasound amplitude drops to one half its equilibrium value in the centre of the cylinder, is given by the formula

$$s = 1.2\ (r_2\ \lambda/2)^{\frac{1}{2}} \qquad (11)$$

(based on equation 8p, p. 188, Jenkins and White (15)). At 1.35 MHz and r_2 = 4.0 cm, s = 0.57 cm which is in excellent agreement with the numerical and experimental value evident in Figure 9. At 5 MHz, s is reduced to a value of 0.30 cm, indicating that the resolution of CS1 would only be degraded over about the last 0.5 cm at each end of the cylinder. This prediction is supported by imaging data to be given later in this paper.

Reproduced with permission of the copyright owner. Further reproduction prohibited without permission.

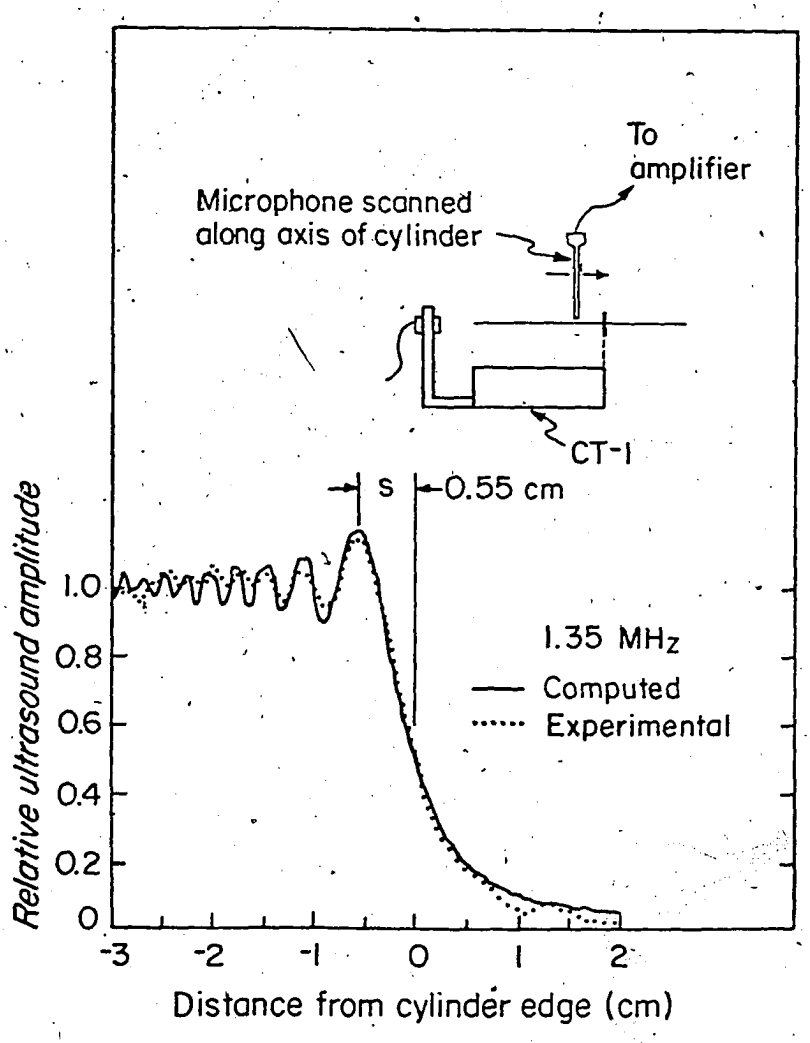

Figure 9. Comparison of experimental and theoretical axial ultrasound fields at the edge of a 120°, 1.35 MHz cylindrical transducer.

Reproduced with permission of the copyright owner. Further reproduction prohibited without permission.

VI. A SIMPLE SCATTER SCANNER FOR B AND C MODE IMAGING

The fabrication and dimensions of CS1, were given previously in Section III (Figure 3). The performance of this scanner was evaluated by replacing the microphone used in the field measurements with a small scattering object. In the first test, the system response to a point scatterer (point spread function) was evaluated along the cylinder as demonstrated in Figure 10. A 2 mm diameter glass bead was scanned across the line focus in the y direction while monitoring the output of the receiver. This experiment was performed at points 5 mm from each end of the cylinder (Figures 10a and 10c) and in the middle of the cylinder (Figure 10b). The results show the excellent resolution and depth-of-field expected in this direction. The overall response of the system is related to the product of the transmitting and receiving beam patterns and it can be seen that the point spread at position b is slightly narrower than at a and c. This appears to be due to the focussing of the receiver such that the narrowest point in its beam pattern coincides roughly with the position b. Edge effects of the cylindrical beam pattern may accentuate this phenomenon.

CS1 was coupled to the input of a conventional pulse-echo imaging system developed here at the Ontario Cancer Institute. After the received signal was detected and processed, as in conventional systems, the information was stored in an analog scan convertor (Hughes Co., Oceanside, Calif.) and displayed on a video screen. The position information was obtained from a potentiometer on the motorized assembly that translated the object being imaged. A phantom consisting of an irregular array of glass beads spaced over a depth of 6 cm was imaged in the y-z plane. A short burst of RF (centred at a 4 MHz) excited the cylindrical transducer. Figure 11a shows the resultant scan using the scatter scanner as described, and Figure 11b shows the control scan obtained by employing the receiver alone in the conventional pulse-echo mode under exactly the same conditions.

Reproduced with permission of the copyright owner. Further reproduction prohibited without permission.

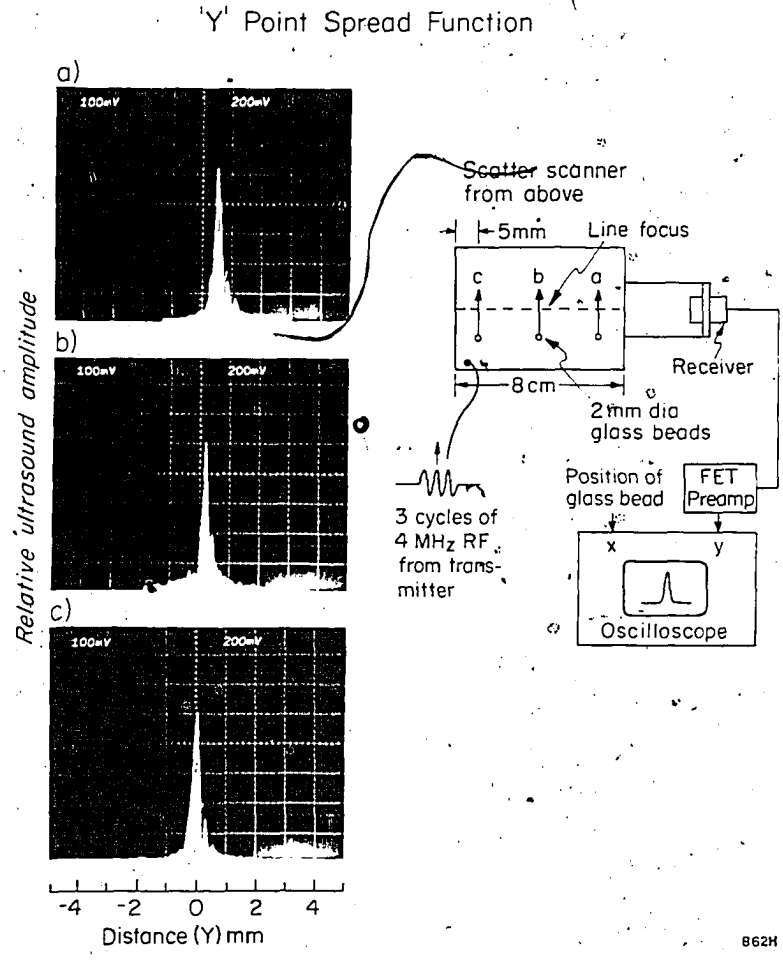

Figure 10. y point spread function as a function of position in the cylindrical beam. Measurements (a) and (c), performed 5 mm from the edges of the cylinder, are similar to the measurement made at the centre, (b). Edge field effects are minimal.

Reproduced with permission of the copyright owner. Further reproduction prohibited without permission.

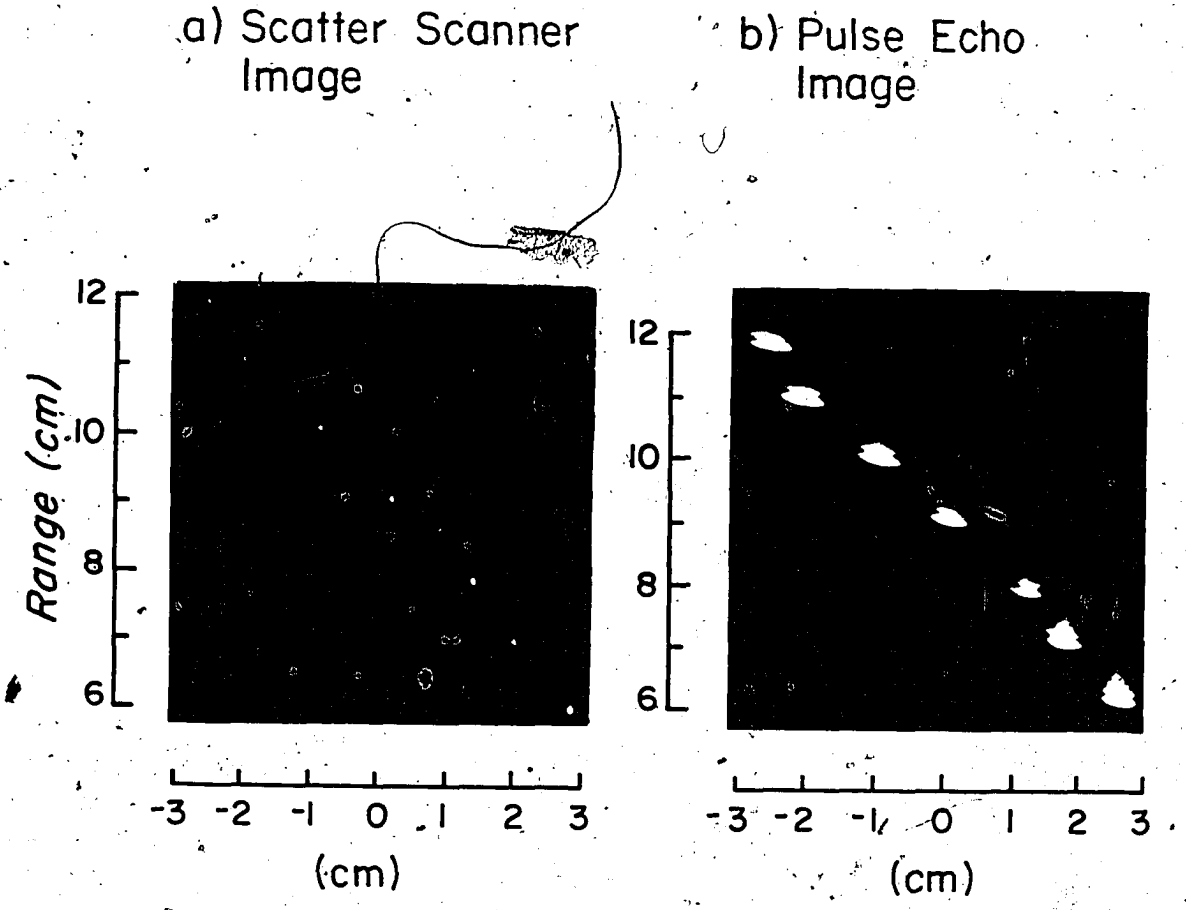

Figure 11. Comparison of scatter scanner and pulse-echo images for an irregular array of 2 mm diameter glass beads scanned in the y direction to produce an image in the y-z plane. The resolution and depth-of-field shown in the scatter image are significantly improved compared to that of the pulse-echo image.

Reproduced with permission of the copyright owner. Further reproduction prohibited without permission.

The scatter scan displays excellent lateral resolution (∿1 mm) throughout the full 6 cm depth of the phantom where as the pulse-echo image shows range dependent resolution varying from ∿4 mm at a range of 8 cm, to ∿10 mm at a range of 12 cm.

Tissue imaging poses several additional problems. Firstly, the tissue itself degrades the focus of the beam to an extent depending on the depth and type of tissue being imaged (4). Secondly, the comparatively wide distribution of ultrasound in the x direction could lead to some unusual artifacts. Figure 12 shows the first image of tissue obtained with the scatter scanner. A 2.5 cm thick slab of bovine liver containing a large blood vessel was scanned past the cylinder in the y direction such that the line focus was approximately in the middle of the sample. In general, the scatter-scan demonstrates 3 to 5 times better lateral resolution than the pulse-echo scan using the same system and geometry. Point 'a' in Figure 12 represents tissue structure as poorly resolved streaks in the pulse-echo image but as resolvable spots in the scatter image. Points 'c' and 'd' represent the blood vessel and right side of the sample respectively. The shape of the blood vessel is distorted due to the means by which the sample was supported above the scanner. Point 'b' represents structure that shows up well in the scatter scan but poorly in the pulse-echo scan. It is clear that both the pulse-echo and scatter scanner techniques incorporate different information into the final image. The diagnostic usefulness of the scatter-scan information has yet to be evaluated, but appears very promising.

VII. SUMMARY AND CONCLUSIONS

A new ultrasound imaging technique has been devised to overcome the depth-

Reproduced with permission of the copyright owner. Further reproduction prohibited without permission.

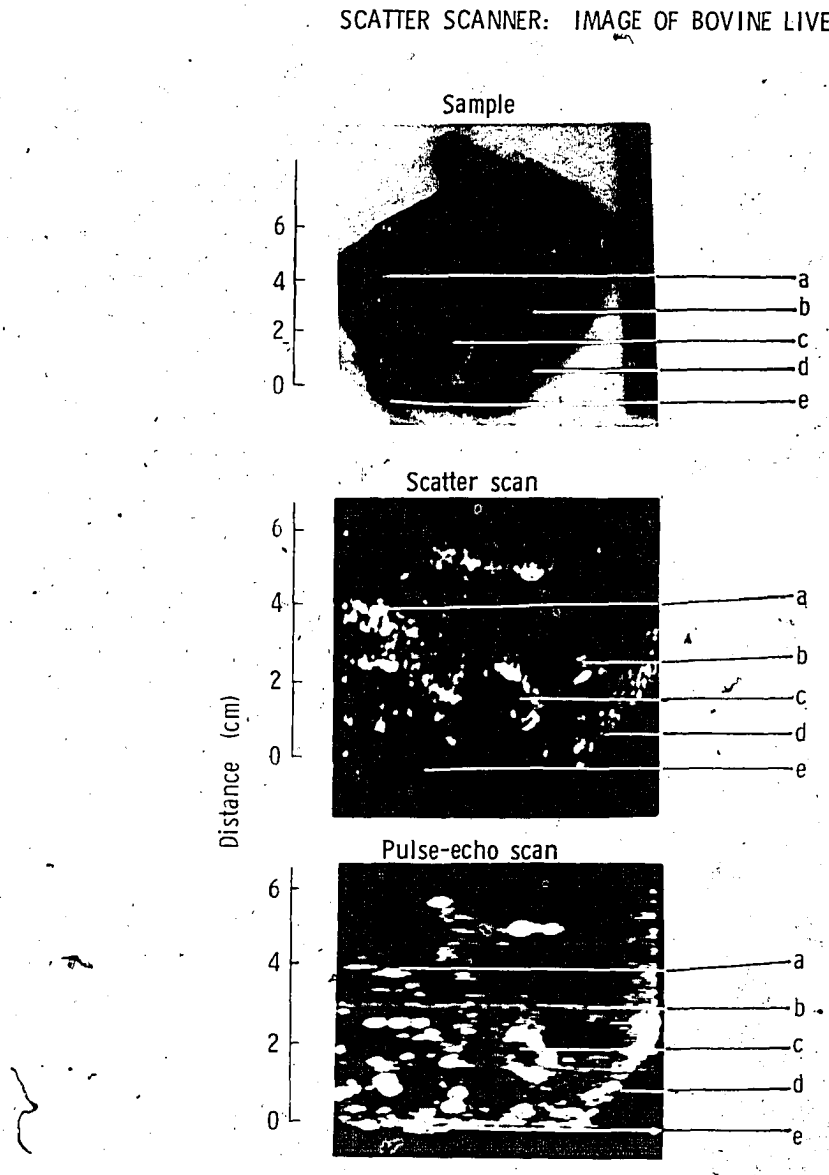

Figure 12. Comparative images of bovine liver in vitro. (a) Structure poorly resolved in pulse-echo image but highly resolved in scatter image. (b) Structure observed only in scatter image. (c) Blood vessel. (d) Right side of sample. (e) Front of sample observed only in pulse-echo image.

Reproduced with permission of the copyright owner. Further reproduction prohibited without permission.

of-field problem inherent in pulse-echo imaging. The new approach relies on a cylindrical transducer to project a line of focussed ultrasound into the tissue to be imaged. A receiver co-axial with the line focus receives the ultrasound scattered by tissue structures intersecting the line, and converts this information into an image. Hence, the device is referred to as a scatter scanner. This approach is particularly useful because highly focussed information is obtained over virtually the full length of the cylinder without sacrificing the simplicity or speed of the pulse-echo technique.

The success of the scatter scanner depends critically on the focussing properties of the cylindrical transducer. The ultrasound distribution across the focal line was examined theoretically and experimentally in two directions: x, along the line joining the centre of the cylinder and the line focus, and y, the transverse direction (see Figure 7). Both directions give distinctly different results. In the x direction, diffraction effects are superimposed on the physical convergence of the beam and the beam is comparatively wide, eg. at 5 MHz the theoretical FWHM is 0.7 mm for a 120° cylinder. In the y direction diffractive effects prevail and the beam is exceptionally sharp with a theoretical FWHM of 0.15 mm for a 120° cylinder for a 5 MHz source. Theoretical studies of beamwidth vs transducer angle showed that it was desirable to employ cylinders with angles greater than 100° since the x beamwidth increases very rapidly at angles less than this. At 1.35 MHz, experimental and theoretical investigations of the fringing field indicated that the field is only degraded in the last few millimeters at each end of the cylinder.

An experimental scatter scanner with a 120° PVF_2 cylindrical transmitter was constructed and tested. Scans of a simple phantom, consisting of an array of 2.0 mm diameter glass beads, showed nearly an order of magnitude improvement in resolution and depth-of-field, compared with the pulse-echo

Reproduced with permission of the copyright owner. Further reproduction prohibited without permission.

technique. A scan of bovine liver, *in vitro*, also demonstrated significant improvement in image quality. In general, the application of the scatter scanner concept to clinical imaging problems looks exceptionally promising.

Reproduced with permission of the copyright owner. Further reproduction prohibited without permission.

CHAPTER 4

REFERENCES

1. Kossoff, G., Robinson, D.E. and Garrett, W.J. "Ultrasonic two-dimensional visualization for medical diagnosis". J. Acoust. Soc. Am. 44: 1310-1318 (1968).

2. Wells, P.N.T. Biomedical Ultrasonics (Academic Press, New York, 1977) Chapter 2, pp 37-42.

3. Goodman, J.W. Introduction to Fourier Optics (McGraw-Hill, Toronto, 1968) p. 65.

4. Foster, F.S. and Hunt, J.W. "Transmission of ultrasound beams through human tissue: focussing and attenuation studies". Ultrasound in Med. and Biol. (in press).

5. Dietz, D.R., Parks, S.I. and Linzer, M. "Expanding aperture annular array". Ultrasonic Imaging 1: 56-75 (1979).

6. Foster, F.S. Canadian patent applied for 26th April 1979.

7. Freedman, A. "Sound field of plane or gently curved pulsed radiators". J. Acoust. Soc. Am. 48: 221-227 (1970).

8. Waag, R.C., Lee, P.P.K., Lerner, R.M., Hunter, L.P., Gramiac, R. and Schenk, E.A. "Angle scan and frequency-swept ultrasound scattering characterization of tissue". Proc. 2nd Int. Conf. Ultrasonic Tissue Characterization, National Bureau of Standards (1977).

9. Kossoff, G., Garrett, W.J., Carpenter, D.A., Jellins, J. and Dadd, M.J. "Principles and classification of soft tissues by gray scale echography". Ultrasound in Med. and Biol. 2: 89-105 (1976).

10. Murayama, N., Nakamura, K., Obera, H. and Segawa, M. "The strong piezoelectricity in poly vinylidene fluoride (PVDF)". Ultrasonics 14: 15-23 (1976).

11. Callerame, J., Tancrell, R.H. and Wilson, D.T. "Comparison of ceramic and polymer transducers for medical imaging". IEEE Ultrasonics Symposium Proc., IEEE Cat. No. 78CH 1334-ISU (1978).

Reproduced with permission of the copyright owner. Further reproduction prohibited without permission.

12. Swartz, R.G. and Plummer, J.D. "Monolithic silicon PVF_2 piezoelectric arrays for ultrasonic imaging". Proc. 8th Int. Symp. on Acoustical Imaging (Plenum Press, New York, 1979).

13. Auld, B.A. Acoustic Fields and Waves in Solids. Vol. I (J. Wiley and Sons, New York, 1973).

14. Beyer, R.T. and Letcher, S.V. Physical Ultrasonics (Academic Press, New York, 1969) p. 14.

15. Jenkins, F.A. and White, H.E. Fundamentals of Physical Optics (McGraw-Hill, New York, 1937) p. 194.

Reproduced with permission of the copyright owner. Further reproduction prohibited without permission.

CHAPTER 5

FUTURE OF THE CYLINDRICAL SCANNER

Reproduced with permission of the copyright owner. Further reproduction prohibited without permission.

In the previous chapter, the initial characterization of the Cylindrical Transducer Scatter Scanner was performed. This new imaging approach offers distinct advantages in the areas of resolution and depth-of-field compared with conventional pulse-echo imaging. The use of the cylindrical scanner to image different organs of the human body is restricted by the size and mechanical motions of the cylindrical assembly. Fortunately, the breast is a readily accessible organ, making it an ideal target for scatter imaging. The application of this approach to other organs may be possible using a new conical geometry discussed in this chapter. The future efforts to develop clinically useful scatter imaging technology will be directed in the following areas: (i) the physics of image formation; (ii) the investigation and development of low frequency (3-5 MHz) flexible piezoelectrics; and (iii) the construction of practical prototypes.

I. PHYSICS

(a) Scattering in Breast Tissue

The cylindrical scanner relies on 90° scatter from tissue to form an image. In the case of breast tissue, virtually nothing is known about the scattering characteristics of the component tissues (fat, glandular, structural, etc.). Also, it is not known if there are any differences in the scattering properties of normal and abnormal breast tissues. Waag and co-workers (1) have developed a versatile ultrasound scattering spectrometer and with it, have extensively characterized scattering in liver tissue. Similar studies on breast tissue could provide valuable information for the design of new cylindrical scanners. Measurements of the angular and frequency dependence of scatter in normal and pathological tissue might show specific differences that could be exploited to aid diagnosis. One particularly interesting case would be the study of the scattering properties of calcium deposits in the breast, since these are often associated with malignancies. In addition to characterizing the scattering properties, we would like to establish whether or not a 90° scatter image provides information that is not available in a back scatter image or vice versa. Considerable work is needed to understand the physical basis of images generated by the cylindrical scanner.

Reproduced with permission of the copyright owner. Further reproduction prohibited without permission.

(b) Artefact Reduction

In all imaging with the cylindrical scanner we assume that the ultrasound is scattered by structures on the line focus. This is not rigorously correct, since all scattering points having the same time of flight from transmitter to receiver will make some contribution to the image. The amount of this contribution depends on the ultrasound distributions from the cylindrical (see Chapter 4, Figure 8) and axial transducers, as well as the strength of the scatterer and the total attenuation along the path connecting the receiver scatter point and transmitter. Figure 1 illustrates the contributions from three such points.

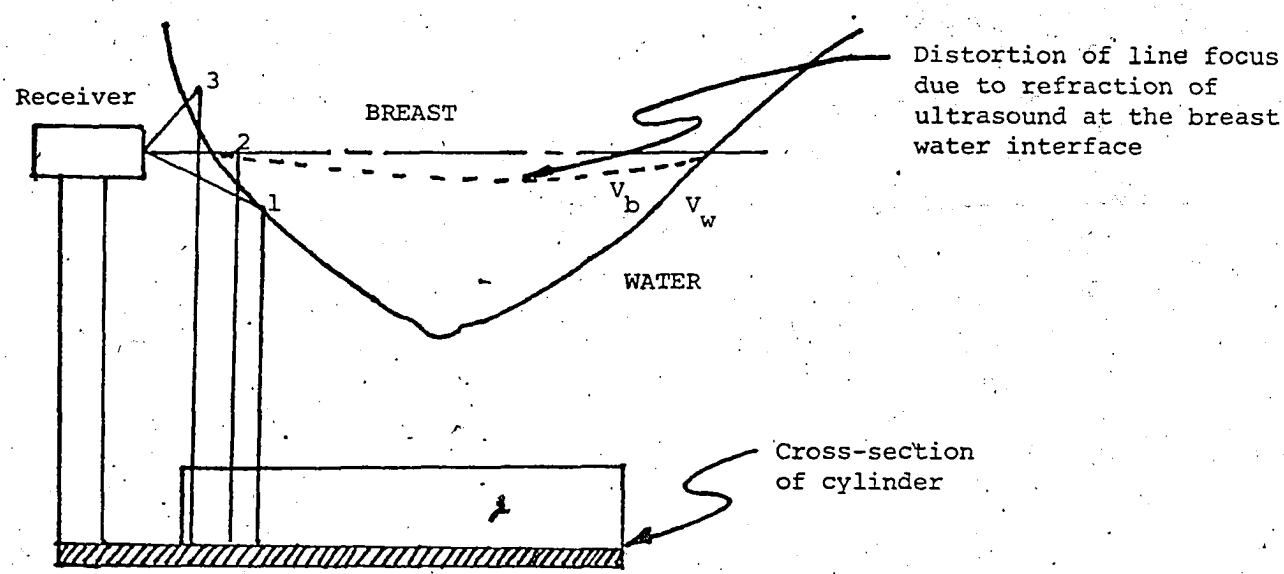

Figure 1. Cylindrical scanner artefacts. Points 1, 2 and 3 each have the same time of flight from the cylinder to the receiver. The specular reflector at 1, although off the line focus, may generate a larger signal than that from point 2. The difference in velocity of ultrasound between breast tissue, V_b, and water, V_w, may distort the line focus causing misalignment with the axial receiver.

The first scattering point is at the skin and is angled such as to direct the pulse towards the receiver by specular reflection. In this case, the scattered pulse is large, the attenuation is low, and in spite of the fact that the scattering point is well away from the line focus, a significant signal might be received and would appear in the image as an artefact. The signal from a scattering point on the line focus has been attenuated by the intervening tissue.

Reproduced with permission of the copyright owner. Further reproduction prohibited without permission.

If the strength of the scatterer is small, its signal could easily be overwhelmed by that from point 1. The contribution from point 3 would likely be small since it is well off-axis and does not reflect specularly towards the receiver. The problem of off-axis artefacts will be assessed experimentally using phantoms and biological specimens.

One possible technique to reduce off-axis artefacts is to improve the directivity of the axial transducer. This could be accomplished by means of linear or annular arrays.

The geometry and acoustical properties of the tissue degrade the quality of the line focus in much the same manner as discussed for large aperture spherically focussed transducers (Chapter 2). The techniques described in Chapter 2 will be used to assess this effect on cylindrically focussed beams. The cylindrical scanner is also subject to refractive distortion of the line focus due to differences in sound velocity between the breast and surrounding water. This effect, as illustrated in Figure 1, causes misalignment of the axial receiving transducer. It may be necessary to match the velocity in the breast to that in the surrounding medium for best results.

(c) New Geometrics

The 120° cylindrical scanner such as that discussed in Chapter 4 suffers from a relatively large beamwidth in the x direction (Chapter 4, Figure 7. Ideally a 360° cylinder should be employed to maximize resolution in both directions, but this is clumsy and difficult to implement because it requires that the object be physically inside the cylinder. One way around this problem is to change the shape of the transducer to that of a cone. In this manner it is possible to project the line focus away from the transducer as illustrated in Figure 2. The conical transducer is analogous to the optical element called an axicon (2) which brings a parallel beam of light to a line focus. Recently

Reproduced with permission of the copyright owner. Further reproduction prohibited without permission.

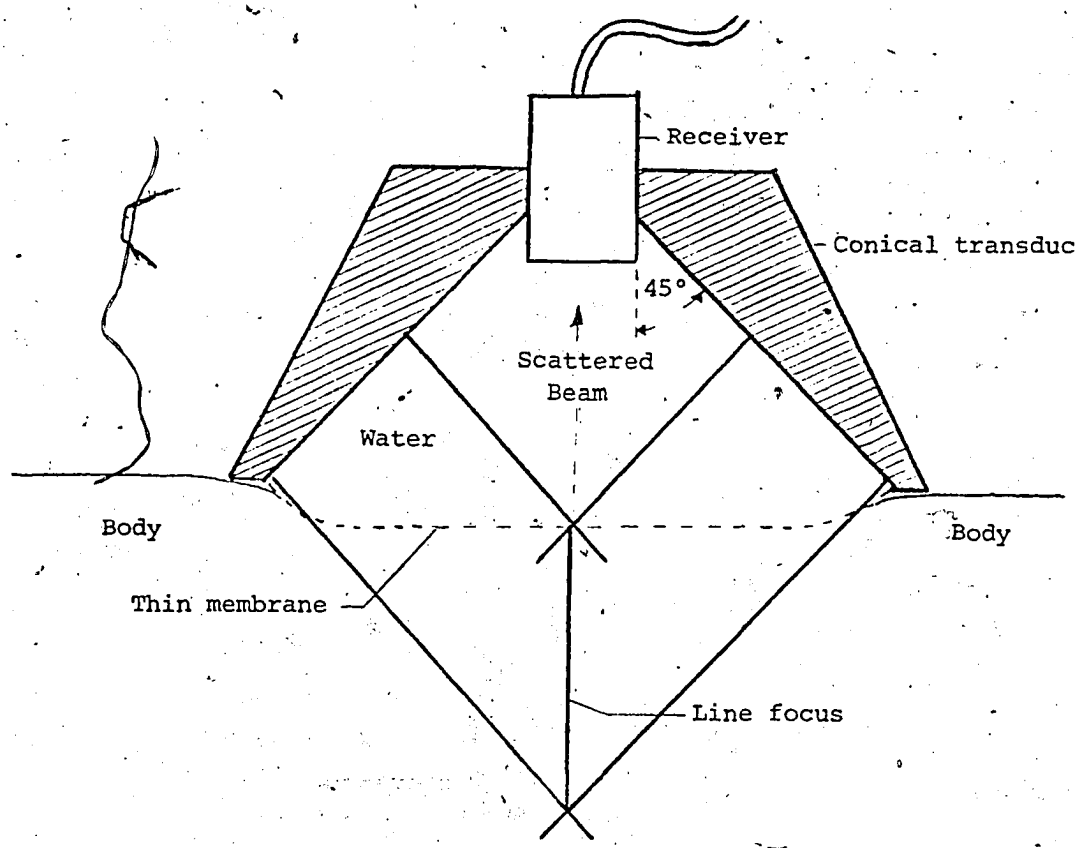

Figure 2. Conical Scanner. The line focus of the cone is projected away from the transducer and into the tissue. This enables the device to be used in much the same fashion as a conventional transducer but with greatly improved resolution and depth-of-field.

Burckhardt (3) attempted to exploit this principle to improve the resolution and depth-of-field of ultrasound images. His results for a 10° cone were encouraging but have not been followed up, largely because of the complexity of the transducer used to generate the conical beam. The advent of flexible piezoelectrics such as PVF_2 allow us to go directly to large (45-60°) angle cones in the scatter scanner configuration. This should enable resolution in the order of 0.5λ to 1.0λ to be achieved. Such an approach may be applicable to many areas of ultrasound imaging such as breast, thyroid, liver, etc. Computer simulations and in vitro tests will be used to predict the optimum cone angle for breast imaging. One of the major advantages of the cone is that it could be used in a system similar to the Breast III scanner, a high resolution, zone focussed device described in the next chapter.

Reproduced with permission of the copyright owner. Further reproduction prohibited without permission.

II. TRANSDUCER MATERIALS

Probably the single most important factor leading to the invention and swift development of the first cylindrical scanner was the piezoelectric plastic PVF_2. The properties of this flexible piezoelectric were discussed briefly in Chapter 4, Section III. The performance of the cylindrical scanner could be greatly enhanced by.

1. improving the sensitivity of PVF_2;
2. reducing the frequency of the commercially available PVF_2 from 17 MHz to about 5 MHz; and
3. improving our relationship with the Japanese manufacturers of PVF_2.

With respect to sensitivity, Miyata and co-workers (4) claim to have improved PVF_2 sensitivity by a factor of 3 using high pressure annealing. Their process is being commercially manufactured by Mitsubishi Petrochemical Co. (5). A sample of this material is expected shortly. Several Japanese companies, including Mitsubishi and Sumitomo Bakelite (6) are attempting to make PZT-PVF_2 composites in the hope that the high piezoelectric coefficient of PZT will increase the sensitivity of their product. This work is still very experimental.

Thus far, only Toray Co. (7) has reported on lowering the frequency of PVF_2 into the diagnostic range. They claim to have made 6 MHz PVF_2 and demonstrated very convincing images of biological samples made with a simple PVF_2 transducer.

The reluctance of the Japanese companies to sell or donate their materials to researchers is rapidly becoming a big problem. Most of the companies wish to supply only the finished transducers. While we continue our efforts to extract new PVF_2 and composite materials from the Japanese we should embark on a small development program of our own. There is nothing magic about making

Reproduced with permission of the copyright owner. Further reproduction prohibited without permission.

PVF_2 piezoelectric. The raw polymer must be stretched to form the correct crystal structure, and then polarized by placing a large electric field across the stretched material. The purpose of the electric field is to line up the polar moments of the otherwise randomly oriented crystal domains. Figure 3 shows a comparison between PVF_2 made here, using the crudest of techniques, and that manufactured by Kreha Corp. (8). Our starting point was raw PVF_2, 100 μm in thickness, supplied by Miyata (4). A 3 cm by 3 cm piece of this material was

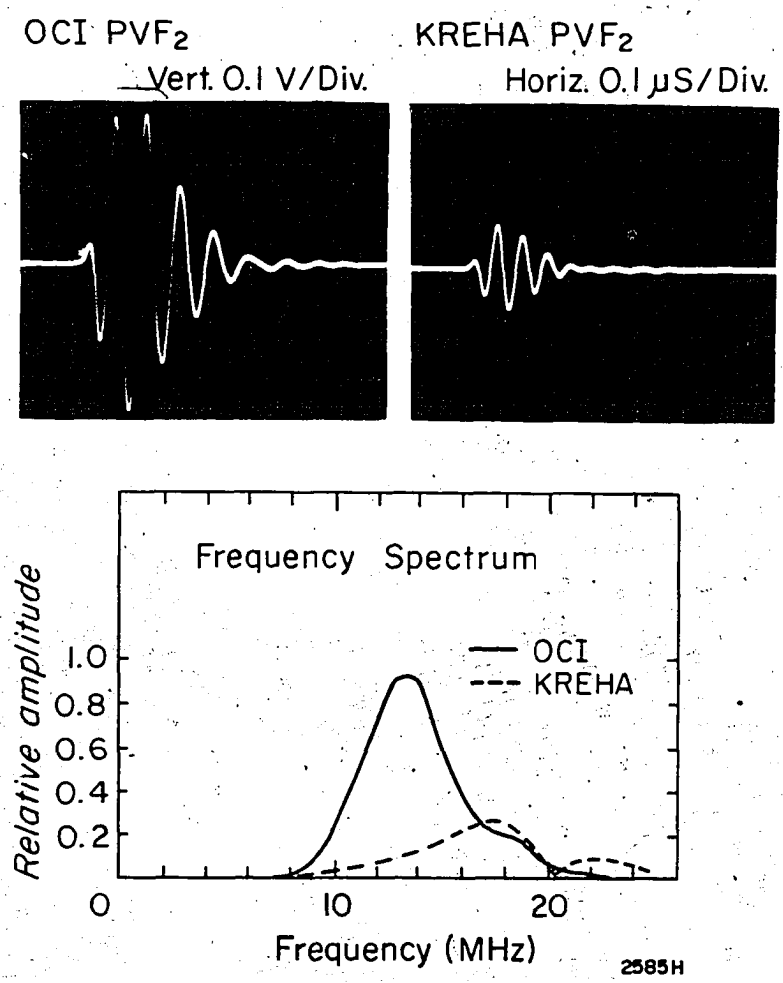

Figure 3. Comparison of PVF_2 made at OCI and that made commercially by Kreha Corporation.

Reproduced with permission of the copyright owner. Further reproduction prohibited without permission.

stretched in one dimension to 9 cm at 75°C. Polarization was accomplished by sandwiching a small sample of the stretched film between two pieces of circuit board and applying a 2.0 kV potential for 2 hours at 130 ± 10°C. The temperatures used in this procedure are those suggested by Miyata (4). The performance of the "home made" and commercial piezoelectrics was evaluated by mounting a 13 mm diameter sample of each on a 3.0 cm thick aluminium block. After silver electrodes were evaporated on to each sample, an Aerotech[a] UTA-3 transducer analyzer was used to examine the echo from the opposite side of the test block. Surprisingly, the echo strength of the "home made" PVF_2 was a factor of three greater than that of the commercial material (Figure 3). An analysis of the frequency content of each echo is also given in Figure 3. Note that the maximum sensitivities occur at 13 and 17 MHz for the OCI and commercial PVF_2's respectively. This analysis is by no means rigorous but it does indicate that, with a little effort, we could make our own high sensitivity PVF_2. Also it may be possible to develop a low frequency PVF_2 which would be invaluable to the cylindrical scanner project.

III. PROTOTYPE CYLINDRICAL SCANNERS

The cylindrical scanner described in Chapter 4 (CS1) had a number of drawbacks that made it unsuitable for application to in vivo imaging. Firstly, its size prohibited the scanning of objects more than 8 cm long or 3 cm deep. Secondly, the scanner was stationary and the object was moved, and lastly the noise characteristics of the electronics were poor. A new prototype (CS2) is presently being developed with the hope that it could be applied to breast imaging. A schematic drawing of CS2 is shown in Figure 4. The cylindrical angle, ϕ, has been maintained at 120° since the theoretical analysis carried

---

[a] Aerotech Corp., P.O. Box 350, Lewistown, PA 17044

Reproduced with permission of the copyright owner. Further reproduction prohibited without permission.

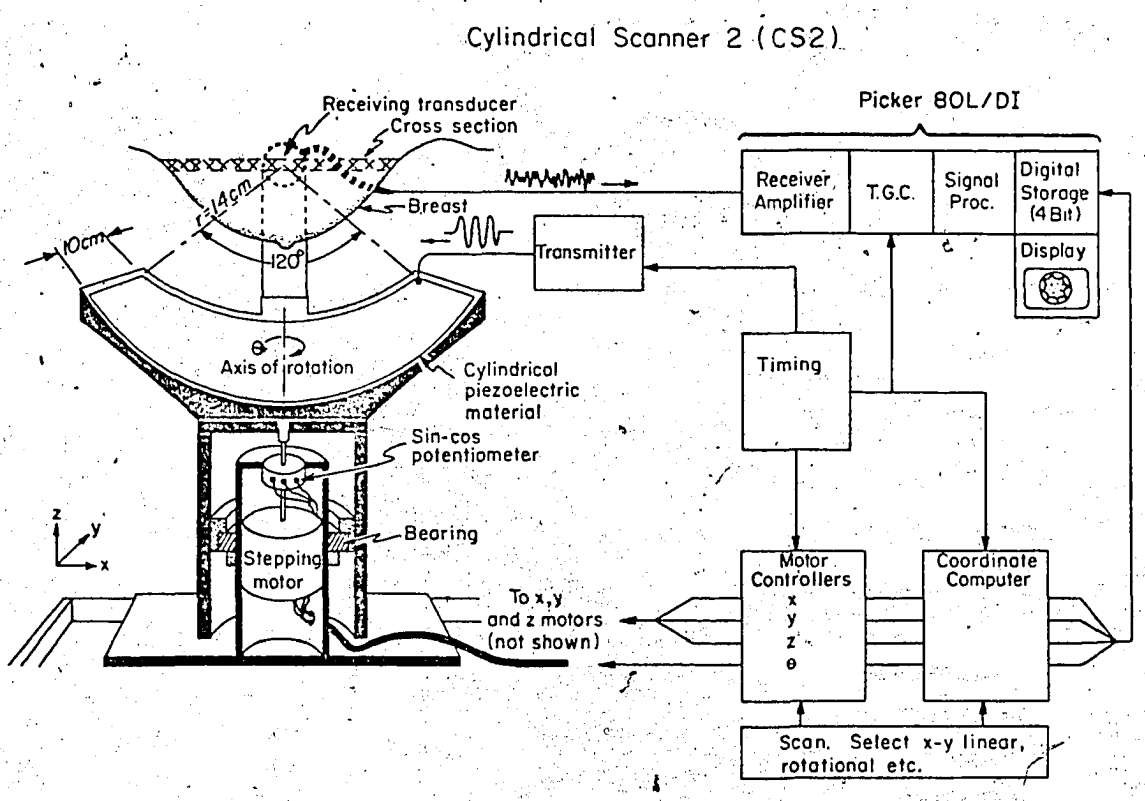

Figure 4. Proposed arrangement for breast imaging. Rotational and linear scans are provided. Signal processing and display are performed by a commercial system (Picker 80L/DI).

out in Chapter 4 indicated that 120° was a reasonable compromise between physical clumsiness and resolution. The size of the cylinder was increased to 20 cm in length with a 14 cm radius of curvature. This should enable the imaging of breasts as thick as 8 to 10 cm. In addition to linear scanning of the breast, a rotational mode will be added to take advantage of the natural symmetry of the breast. Figure 4 shows a section through CS2 demonstrating the preliminary configuration of the cylinder support and rotational bearing. A sin-cos potentiometer, in line with the motor, monitors the angular position, θ, of the cylinder.

The receiving transducer (19 mm diameter, 3.5 MHz, f/5), receiver amplifier, time-gain control (TGC), signal processing, digital memory and display systems,

Reproduced with permission of the copyright owner. Further reproduction prohibited without permission.

will be supplied by Picker Corporation in the form of an 80L/DI scanner console. From our experience, the 80L/DI has excellent signal handling and noise characteristics. This allows us to concentrate our efforts on the mechanics and electronic control of the cylindrical scanner. The additional electronics consist of a master timing circuit, motor controllers for the x, y z and θ motions, a coordinate computer to constantly inform the digital memory where information is to be stored, and a scan select circuit to determine what type of motion the scanner is to execute.

Recently the cylindrical transducer for CS2 was fabricated. The piezoelectric surface was formed by gluing three 10 cm by 20 cm sheets of Kreha PVF_2 to the surface of the machined cylinder using epoxy (Dow Versamid 125 + D.E.H. 331 hardener at 60°C). Excess epoxy was squeezed out using a photographic roller and silver electrodes were applied as described in Chapter 4. As an initial test, this transducer was mounted on the translational stage of the demonstration scanner (Chapter 3, Section IId). Simple linear scans were made possible by using existing electronics designed for the demonstration and breast scanners. The first images obtained with this version of CS2, were of porcine kidney in vitro. Figure 5a illustrates the geometry in which the scans were made. In Figure 5b, a transverse scan at level 1 in the kidney is compared to the corresponding histological section taken from the sample. The sample shows three distinct kidney tissues which are, from the outside in: cortex, medulla and calix. The cortex, a fairly homogeneous tissue, is represented in the scatter scan as low level signals of uniform texture whereas the calix appears to generate the high level scatter observed in the centre of the image. Unfortunately, the scattering properties of the cortex do not appear to differ appreciably from those of the medulla and it is not possible to identify this tissue. The presence of some high level scatter in the cortex that does not seem to correspond to any

Reproduced with permission of the copyright owner. Further reproduction prohibited without permission.

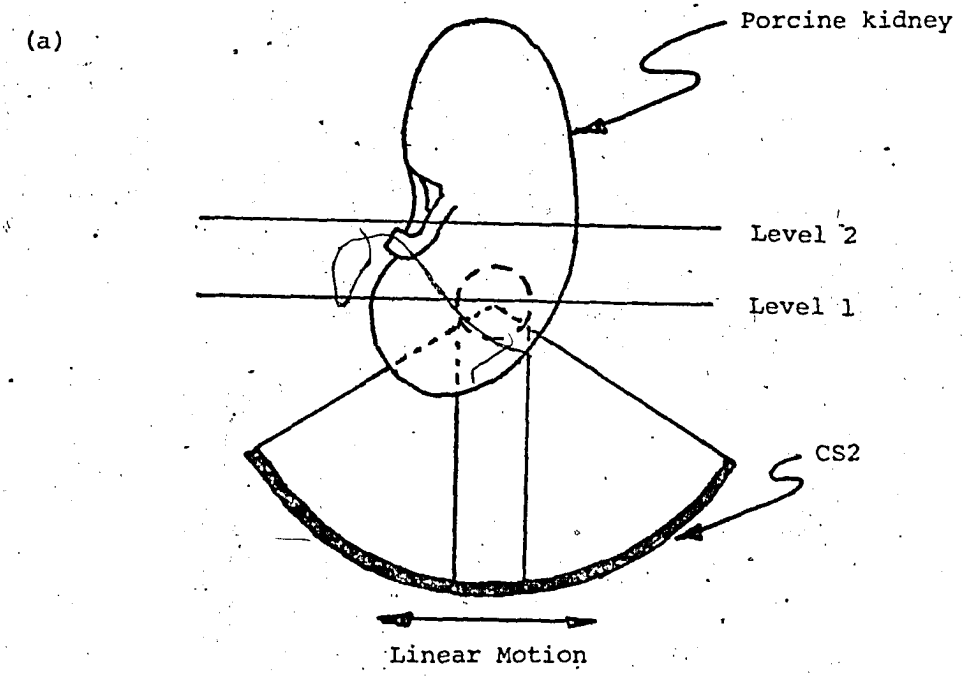

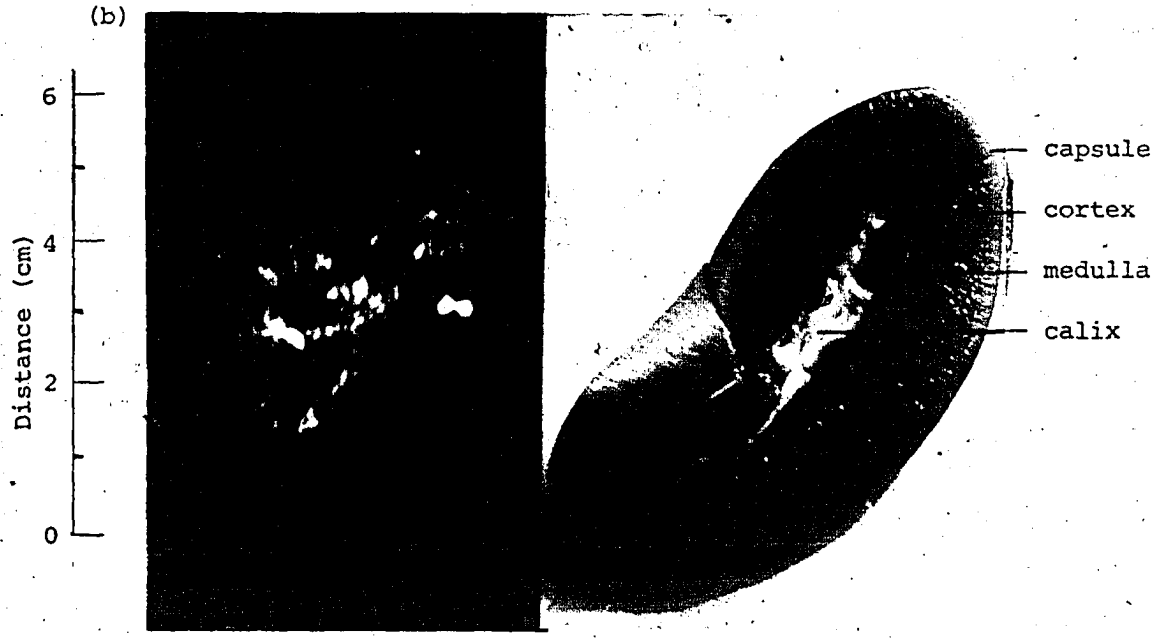

Figure 5. (a) Scan geometry for porcine kidney images. (b) Scatter image and histological section at level 1.

Reproduced with permission of the copyright owner. Further reproduction prohibited without permission.

structure, is suspicious. Perhaps the sample was not cut at the correct level in the kidney or the signals are artefacts. The cause and extent of artefacts in scatter images must be carefully investigated, as indicated previously. Another transverse scan near the centre of the kidney (level 2 in Figure 5) is given in Figure 6. In general, the scatter images possess a unique and startling quality compared with conventional ultrasound images. The texture of the tissue is very fine with little evidence of the lateral streaking common in pulse-echo images. As well, the resolution appears uniformly good across the entire image indicating the large depth-of-field expected of this imaging technique.

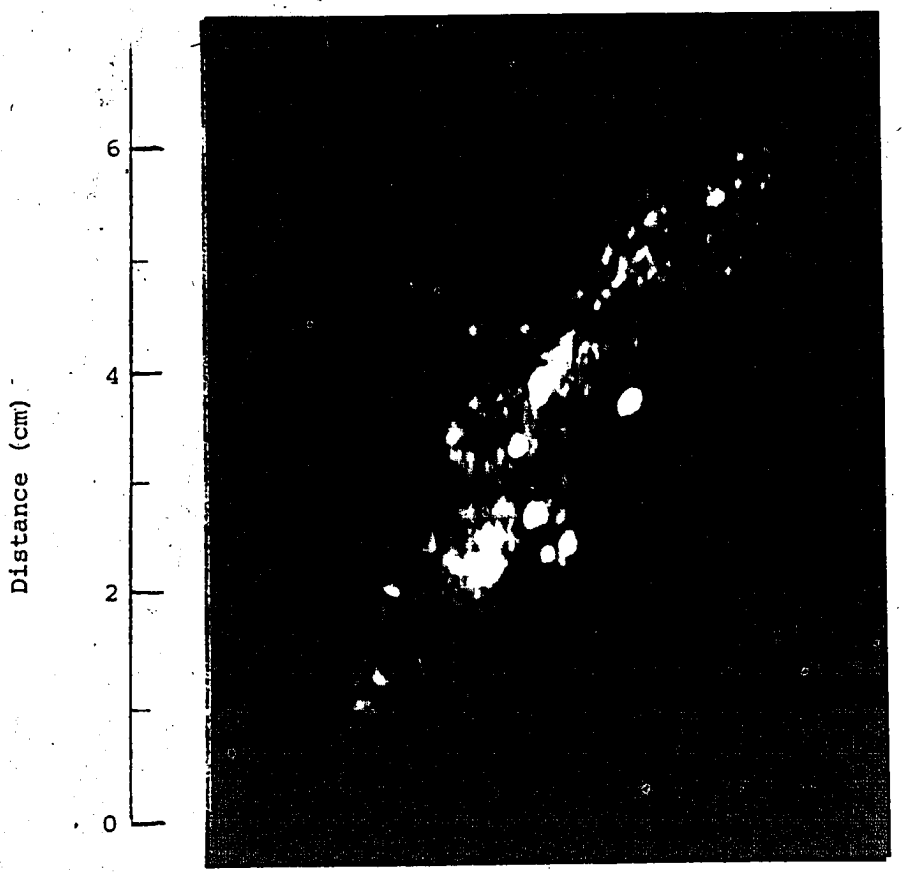

Figure 6. Scatter image of kidney at level 2 (see Figure 5). This is similar to the expected geometry for breast scanning. Note the fine texture of the tissue and excellent resolution.

Reproduced with permission of the copyright owner. Further reproduction prohibited without permission.

IV. SUMMARY

A flow chart of the projected course of the scatter scanner project over the next 20 months is given in Figure 7. The main thrust of the physics program is to investigate scattering in breast tissue *in vitro* as a function of angle, frequency, tissue type and condition. As well the cause and extent of artefacts in the scatter images will be examined and hopefully minimized by means of receiver arrays. New flexible piezoelectrics will be tested and an attempt will be made to fabricate 3 to 5 MHz PVF_2. *In vivo* tests of a large cylindrical scanner will begin as soon as possible after the arrival of the Picker 80L/DI console, using a modified version of the demonstration scanner. Based on the results of the latter scanner a clinical prototype (CS2, Figure 4) will be designed and constructed. Concurrent with the above programs work will commence on a conical scanner (Figure 2). Should this device prove more effective than the cylindrical geometry the C in CS2 may end up standing for conical instead of cylindrical.

Reproduced with permission of the copyright owner. Further reproduction prohibited without permission.

Reproduced with permission of the copyright owner. Further reproduction prohibited without permission.

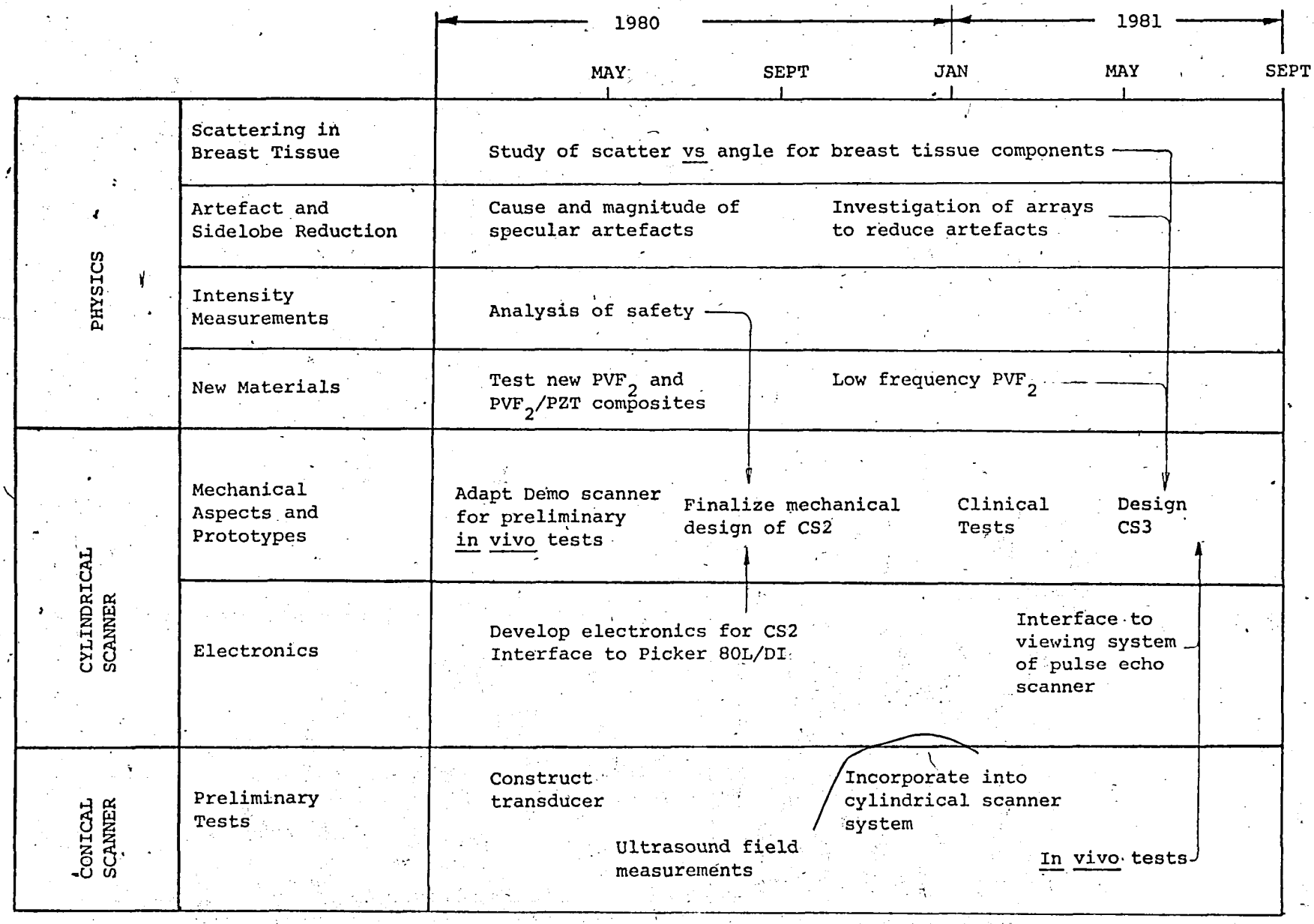

Figure 7. Scatter scanner project over the next 20 months.

CHAPTER 5

REFERENCES

1. Waag, R.C., Lee, P.P.K., Lerner, R.M., Hunter, L.P., Gramiak, R. and Schenk, E.A.: Angle scan and frequency swept ultrasonic scattering characterization of tissue. In: Ultrasonic Tissue Characterization II (ed. Melvin Linzer). National Bureau of Standards Special Publication 525, 1979.

2. McLeod, J.H.: The Axicon: a new type of apical element. J. Opt. Soc. Am. 44: 592-597 (1954).

3. Burckhardt, C.B., Hoffmann, H. and Grandchamp, P.A.: Ultrasound Axicon: a device for focussing over a large depth. J. Acoust. Soc. Am. 54: 1628-1630 (1973).

4. Miyata, A.: Personal communication, Faculty of Technology, Tokyo University of Agriculture and Technology, Koganei, Tokyo 184, Japan.

5. Ohtaki, T.: Personal communication, Fine Chemicals Division, Mitsubishi Petrochemical Co., 5-2 Marunouchi, Chiyoda-ku, Tokyo 100, Japan.

6. Uchida, Y.: Personal communication, Central Research, Sumitomo Bakelite Co., 495 Akiba-cho, Totsuka-ku, Yokohama, Japan.

7. Terada, K.: Personal communication, Health Care Products Department, Toray Industries Inc., 2 Nihonbashi-Muromachi-Chome, Chuo-ku, Tokyo 103, Japan.

8. Kreha Corporation, 1-8 Nihonbashi, Horidome-Cho, Chuo-ku, Tokyo, Japan.

Reproduced with permission of the copyright owner. Further reproduction prohibited without permission.

CHAPTER 6

CLINICAL PULSE-ECHO PROTOTYPES

Reproduced with permission of the copyright owner. Further reproduction prohibited without permission.

The clinical utility of any imaging system depends critically on its mechanical design. In the case of breast cancer, where the disease has an especially high emotional impact on the patient, it is essential to emphasize comfort and safety in the scanner design. While our investigations of focussing and depth-of-field were being carried out, two prototypes were designed and built, to help establish the optimum scanning procedure. The principal objective was to provide a clean and comfortable means of coupling the instrument to the breast with sufficient flexibility to scan each of the four quadrants - especially the upper outer quadrant and axilla. As illustrated in Figure 1, this latter region is the site of nearly 50% of all primary breast carcinomas (1). Conventional transducers were used and emphasis was not placed on resolution.

Figure 1. Distribution of primary breast cancers in the human female breast.

Reproduced with permission of the copyright owner. Further reproduction prohibited without permission.

I. SCANNING APPROACH

There are two schools of thought on how an ultrasound examination of the breast should be carried out. In one, the woman lies in the prone position and lowers her breasts into an open water bath. This approach is favoured by Jellins, Kossoff et al (2) and Life Instruments Inc., manufacturers of the commercial system shown in Figure 2a. The Japanese on the other hand (3), prefer the woman in the supine position as shown in Figure 2b. In the latter system, ultrasound is coupled nto the breast by means of a water bag lowered from above the patient. Table I summarizes the pros and cons of each approach. Compression of the breast is a necessary by-product of the supine approach, since the weight of the water bag rests on the breast. This tends to flatten the breast and extend structures in the lateral directions. It is difficult to say whether this distortion enhances or obstructs diagnosis. Indeed, the reported accuracies in each case are very close (2,3). However, by compressing the breast, much less penetration is required, a factor that allows the use of higher frequencies than possible in the prone approach. This in turn may lead to improved lateral resolution. Oblique interfaces may adversely effect focussing and pulse length, leading to a general degradation of resolution. The supine approach minimizes such effects by flattening the breast. Another problem associated with the prone approach is breast movement. Jellins (4) noted that this was a significant problem in his recently developed rapid scanning system, caused by the motion of the transducer in the water bath. The nipple artefact is an acoustic shadow caused by the attenuation and sound propagation characteristics of the nipple, which differ from those of the surrounding tissue. The nipple artefact tends to be more pronounced in the uncompressed breast than in the compressed breast (5). The prone approach does allow dimpling to be observed in the image but this is not a major advantage since this is easily

Reproduced with permission of the copyright owner. Further reproduction prohibited without permission.

TABLE I

	SUPINE	PRONE
Compression	yes	no
Depth of penetration required	3-7 cm	5-12 cm
Maximum oblique interface (linear scan)	20-30°	up to 60° (see Figure 2)
Breast movement	fixed	rapid movement of the transducer causes breast movement
Nipple artefact	reduced	can be severe
Dimpling	not visible	visible
Comfort and acceptability	good	fair
Accessibility to the breast for physical examination and observation	good	poor

Reproduced with permission of the copyright owner. Further reproduction prohibited without permission.

(a)

(b)

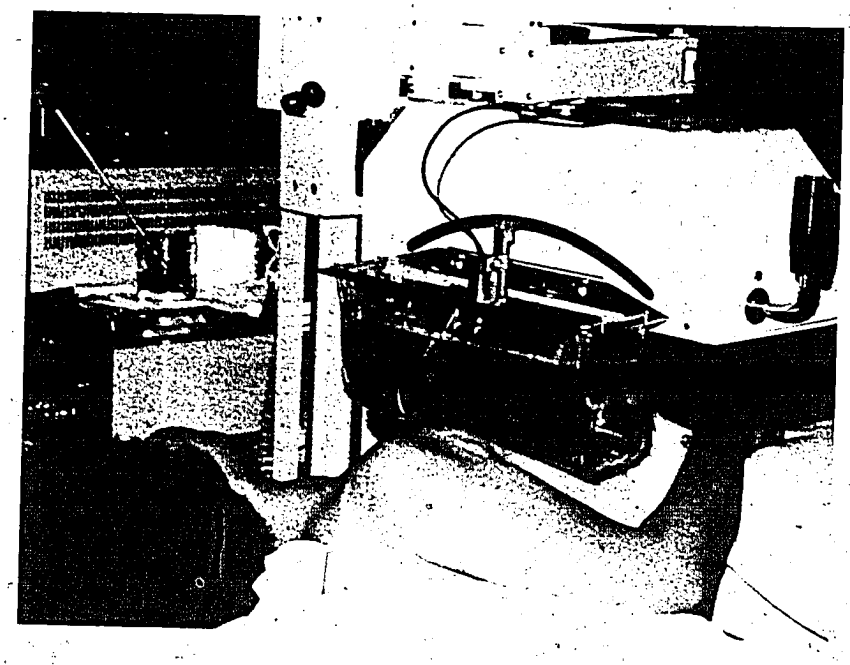

Figure 2. Scanning approaches. (a) Prone (Life Instruments, Boulder, Colorado); and (b) supine (Hitachi Inc., Tokyo, Japan).

Reproduced with permission of the copyright owner. Further reproduction prohibited without permission.

detected by physical examination. A number of volunteers who subjected themselves to both approaches unanimously selected the supine position as more comfortable and more acceptable to women, compared to the prone position. From the clinician's point of view, the breast is much more accessible for physical examination and observation when the patient is supine. Overall, it appears that the supine position offers distinct advantages that make it the method of choice.

II. BREAST II

The first clinical prototype, Breast II, had a balanced scanning head as shown in Figure 3, covered by a thin and very flexible silicone membrane. A large central bearing allowed complete 360° rotation of the scanning assembly while another bearing (not shown), controlled the tilt. This versitility allowed good contact to be made with all parts of the breast including the axilla. The transducer (Aerotech 19 mm ∿f/5) is positioned on a central shaft approximately 10.0 cm from the membrane and is capable of executing sector (±40°) or linear (±8 cm) motions. These are provided by geared low voltage D.C. motors mounted in the cylindrical housing behind the scanning head. Also in this housing are the transducer pulser, preamplifier, and position sensing electronics. A separate electronics console, designed and built here by the members of the electronics group, provides the control signals for the motors, amplification and signal processing of echo signals. An analog scan convertor (Hughes Co., Oceanside, Calif.) stores the image which is subsequently displayed on a television monitor.

Figure 4 shows the preferred scanning approach at present, in which the patient is lying supine. The ultrasound head is positioned above the patient, then lowered onto the breast. Excellent acoustic contact is obtained

Reproduced with permission of the copyright owner. Further reproduction prohibited without permission.

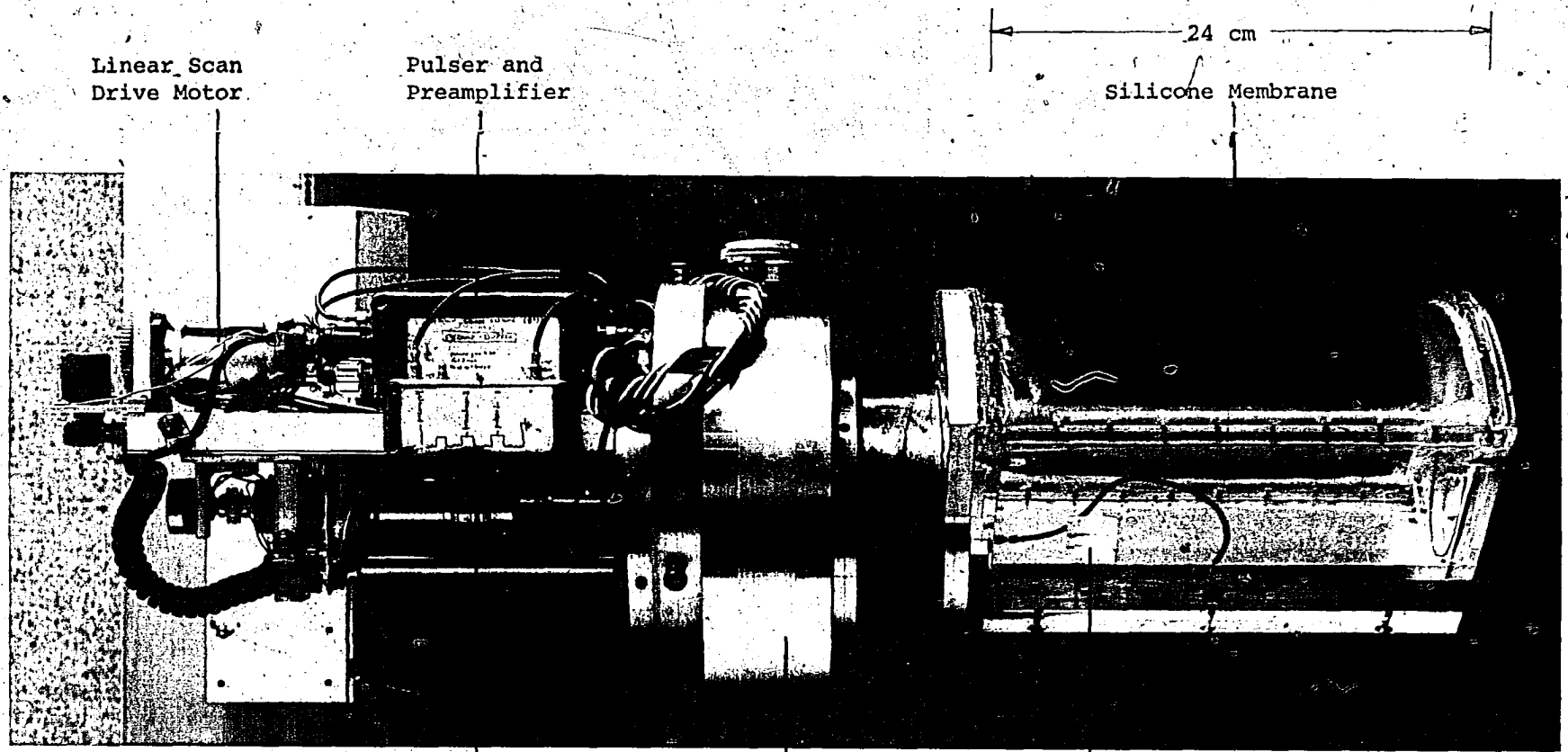

Figure 3. Breast II scanner.

Reproduced with permission of the copyright owner. Further reproduction prohibited without permission.

Figure 4. Breast II in use. The flexible scanning head is placed above the patient, then lowered onto the breast as shown. Electronics console and display system are shown in the background.

Reproduced with permission of the copyright owner. Further reproduction prohibited without permission.

by using a special low-viscosity gel (Echo Gel/Echo Labs., Lewistown, Penn.) between the membrane of the head, and the breast. Figure 5 shows an early image taken with this breast scanner, and a drawing of normal breast anatomy. The marginal fat lobules and Cooper's ligaments are well defined and the glandular tissue shows a uniformly echoic pattern broken by the shadow of the nipple.

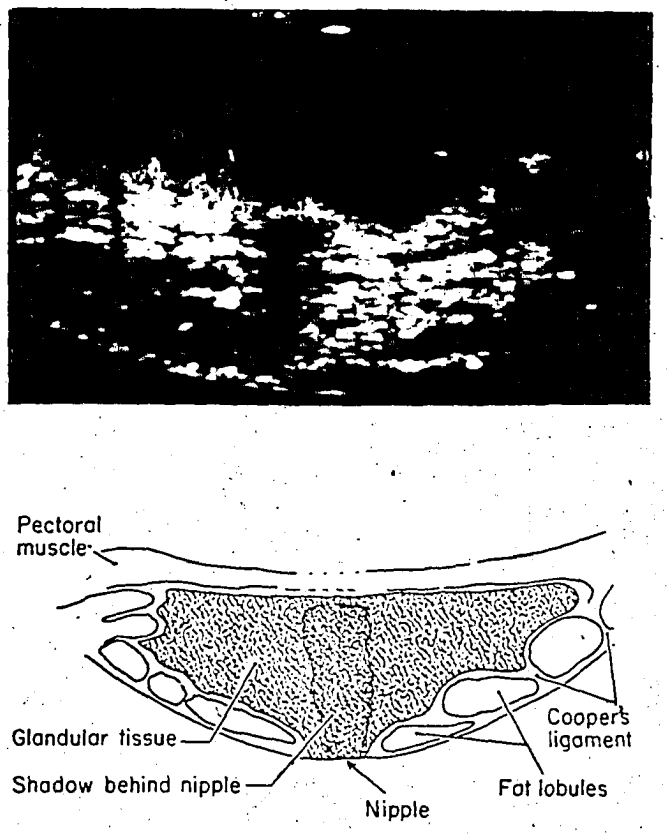

Figure 5. Ultrasound scan of normal breast.

Reproduced with permission of the copyright owner. Further reproduction prohibited without permission.

Behind this lie the pectoral and other retro-mammary muscles which send back fairly high level echoes. In Figure 6 a case of mammary dysplasia is examined using xeroradiography and ultrasound. The xeroradiogram displays a coarse pebbly appearance often associated with this disease, however it is not possible to distinguish whether the proliferating pockets of tissue are cystic or solid. In the ultrasonogram, which represents one slice near the level of the nipple, the normal layer of fat is visible but also a number of anechoic regions are present in the normally uniform glandular tissue. These regions are likely

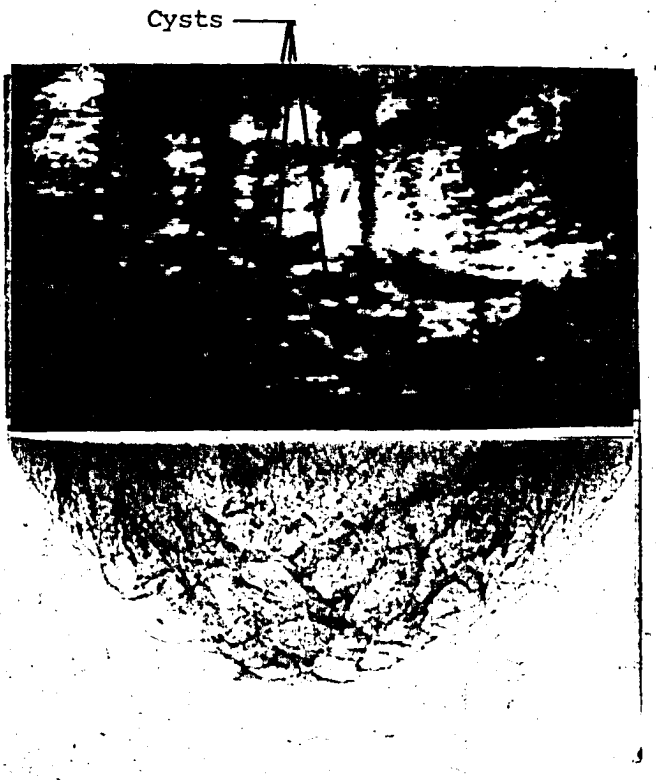

Figure 6. Ultrasound scan and xeroradiogram of patient with mammary dysplasia.

Reproduced with permission of the copyright owner. Further reproduction prohibited without permission.

cystic, based on the high degree of enhancement behind each.

The use of the closed water bag and the supine position affords some advantage over the open system used by the Japanese: the water tends to be displaced rather than have its full weight press on the breast. This also provides increased coverage of the breast and is very comfortable for the patient.

Linear scans such as those shown in Figures 5 and 6 were much better than scans obtained in the radial mode. The radial scans suffered severe reduction in quality near the edges where the angle between the transducer beam and the breast surface became extreme.

III. FUTURE WORK

While Breast II is being tested clinically, a new prototype, Breast III, is being built. The objective in Breast III is to incorporate the zone focussing concept into an enlarged, fully automated breast scanning system. The shape of the scanning head has been redesigned by John Hunt, to accommodate the bulkier transducer and also to make good contact with a larger portion of the breast. Once the scanner is positioned on the breast, scanning will proceed under microprocessor control until the entire breast has been imaged. It should not be necessary to reposition the scanner. Figure 7 shows the general arrangement planned. The transducer will execute linear motion across the breast in either of the two directions shown. The number and separation of slices imaged will be selected on the electronics console, while vital functions such as start, stop, gain and time gain control will be provided on the scanning head assembly. The images will be stored on video tape or in a special digital device which can play the images back

Reproduced with permission of the copyright owner. Further reproduction prohibited without permission.

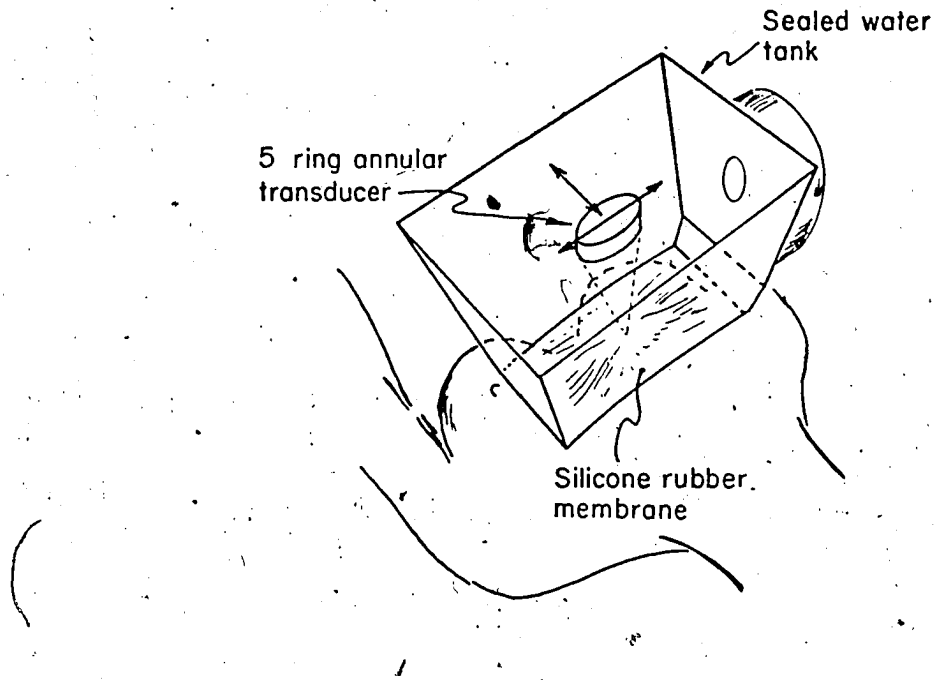

Figure 7. Scanning approach used in Breast III. The zone focussed transducer executes linear motions in both the directions indicated. The bottom of the water tank is curved to conform to the body.

in rapid succession to stimulate a 3-dimensional effect. The final means by which the radiologist will view and evaluate the images is presently a very open question. Much effort is needed in this area.

In Breast III a 3.5 MHz, 3.8 cm diameter, five ring annular array transducer will be employed. This transducer has a fixed focus at 10.0 cm (f/2.6) and will be electronically focussed in five zones between 7.5 and 15.0 cm. The electronic zone focussing approach is being developed by Marcel Arditi in conjunction with the electronics group and is elucidated in Figure 8. It is faster, and more reliable than the Freon approach described in Chapter 3 but is more complicated electronically and more susceptible to noise problems. In the electronic approach each of the five annuli (only four are shown in Figure 8), has a separate pulser and preamplifier. The beam is focussed to a particular zone by delaying the

Reproduced with permission of the copyright owner. Further reproduction prohibited without permission.

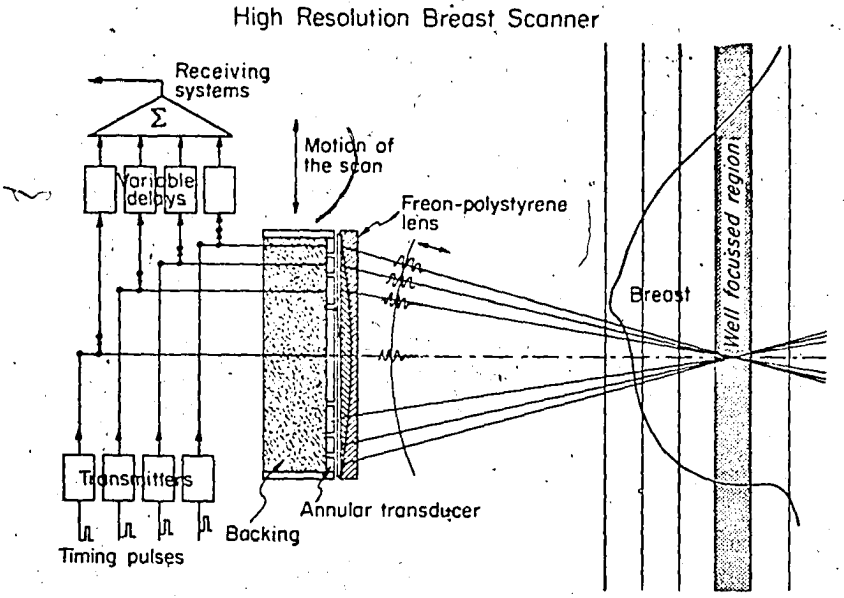

Figure 8. Electronic zone focussing system. Separate transmitters and receivers are used for each annulus of the transducer. Transmit pulses are delayed to focus the beam in front or, or behind the normal fixed focus, while received signals are delayed to synthesize focussing in reception. A five ring system will be used in Breast III.

triggers to the individual pulsers in such a way to cause the transmission of a spherical wavefront whose centre is approximately one-third into the zone (see Chapter 3, Section III). Echoes from the zone are received by each annuli, amplified separately, delayed and summed to synthesize focussing in reception. Since there are five zones, a completely focussed line requires 5 pulses. The time required per line is then 5 times 226 μs = 1.33 ms (based on a maximum penetration of 20 cm). A 512 line image could be generated in a little more than half a second. Due to mechanical constraints, Breast III will perform scans in ∿4 seconds and allowing (1) second between scans, would perform an entire examination (∿100 scans) in about 8 minutes.

Reproduced with permission of the copyright owner. Further reproduction prohibited without permission.

IV. SUMMARY AND CONCLUSIONS

Two prototype breast scanners have been described. The first prototype was developed using a very flexible silicone membrane over a sealed water container in a geometry that allowed excellent contact with any portion of the breast. Based on the comments of our volunteers, this approach was rated as the most comfortable and acceptable means of scanning the breast. Simple linear scanning was found to produce good images of normal and pathological breast tissue while radial scans proved less acceptable. Based on the results of the latter prototype and earlier focussing studies, a third prototype is now under construction. This high resolution system will employ zone focussing over the range f/2-f/4 and will perform automated rectilinear visualization of the entire breast. We are confident that Breast III will have a significant impact on the detection, localization and evaluation of small tumours of the breast.

Reproduced with permission of the copyright owner. Further reproduction prohibited without permission.

CHAPTER 7

CONCLUSIONS

Reproduced with permission of the copyright owner. Further reproduction prohibited without permission.

The purpose of our research in the past few years has been to develop new ultrasonic imaging techniques for the early detection of breast cancer. Most of the emphasis has been placed on the improvement of lateral resolution throughout the image. Studies of the physics of ultrasound interactions in breast tissue led us to conclude that an f-number of 2 to 3 and a frequency of 3.5 to 4 MHz were optimal for breast imaging. The immediate effect of using such low f-numbers was loss of depth-of-field. We explored the use of zone focussing to overcome this problem. With a Demonstration Scanner using a variable focal length liquid Freon lens, we found that excellent resolution could be obtained over a 10 cm depth, by dividing the image into seven well-focussed zones. The use of the Freon lens was slow and clumsy but an electronic version of this approach, developed by Marcel Arditi, is presently nearing completion. This version will eventually be installed in our clinical prototype, Breast III.

A new imaging device called the Cylindrical Transducer Scatter Scanner, offers the possibility of obtaining both extremely high resolution and large depth-of-field, without sacrificing the simplicity of the imaging process. This approach relies on ultrasound scattered at 90° to form the image. It is possible that the scattered ultrasound may contain information that is unavailable in conventional pulse-echo imaging. Scattering angles other than 90° may be achieved using conical geometries. Future investigations of scatter as a function of angle in in vitro tissue samples may identify scattering angles that are optimal for the detection of particular pathologies such as micro-calcification in breast tissue.

In October of 1979 the "First International Congress on the Ultrasonic Examination of the Breast" was held at Philadelphia in the United States. The question most asked by the delegates was whether or not ultrasound was ready for mass screening. At present, the concensus of opinion says no. Whether or

Reproduced with permission of the copyright owner. Further reproduction prohibited without permission.

not the developments described in this thesis will alter this circumstance depends on how well these ideas are incorporated into clinical scanning systems. A number of companies have approached us concerning the development of the zone focussing and cylindrical scanner ideas.

There is a justifiable hesitation on the part of the radiological community in accepting ultrasound before it can be statistically shown that it is at least as good as, if not better, than mammography and xeroradiography. However, assuming that properly controlled double blind trials do eventually prove the efficacy of ultrasound, what might its role in breast cancer management be? The most important application would be as a screening tool. An analysis of the cost vs benefit of breast cancer screening programs is beyond the scope of this thesis. However, if the substantial mortality reductions found in the Health Insurance Plan of New York screening trial prove to be generally true for all age groups, it is quite likely that women themselves would financially support a safe, effective screening program.

Ultrasound may also have an important role in the general clinical management of breast cancer patients. The effectiveness of ultrasound in the differential diagnosis of breast disease is rapidly improving. In the vast majority of breast examinations the condition is benign, but often, in instances of clinical uncertainty, biopsies or surgical removal of suspicious lumps are performed. It is possible that the addition of ultrasound to the tools available to the clinician would significantly reduce the number of such procedures. This would be especially valuable in the repeated assessment of young women with benign disease or lumpy breasts which are difficult to evaluate mammographically.

Reproduced with permission of the copyright owner. Further reproduction prohibited without permission.

Many of the ideas and developments described in this thesis may find eventual applications in areas of diagnostic ultrasound other than breast imaging. In particular the cylindrical and conical scanners may prove valuable in areas such as thyroid, liver, and vascular imaging. It has even been suggested that the ultrasound beam from a low frequency (0.5-1.0 MHz) conical scanner could penetrate the skull and give reasonable resolution of structures in the brain. The development of these applications into useful clinical tools provides a challenging objective for future research.

Reproduced with permission of the copyright owner. Further reproduction prohibited without permission.

APPENDIX 1

DEMONSTRATION SCANNER DETAILS

Reproduced with permission of the copyright owner. Further reproduction prohibited without permission.

A general description of the Demonstration Scanner was given in Chapter 3. In this Appendix, a more detailed description of the transducer and electronic circuits is provided. Figure 1 shows a block diagram of the equipment. The Demonstration Scanner is divided into three main sections: (i) the scanner mechanism, including motors, Freon pump and transducer (AR2); (ii) an electronics console that controls motor functions and gating; and (iii) an electronics console from the Breast II prototype, that performs signal processing and image display. The lower case letters in Figure 1 indicate the areas which will be discussed in greater depth.

a) Electrical Characteristics of AR2

In order to achieve maximum sensitivity and signal to noise ratio (S/N), the electrical impedance of the transducer must be matched to that of the pulser and receiver. The electrical impedance of AR2 was measured using the simple circuit shown in Figure 2. Here, a Wavetek signal generator drives a circuit consisting of a large resistance, R_L, in series with the comparatively low impedance of the transducer. If we assume R_L is much larger than the transducer impedance, a simple analysis of the circuit yields:

$$R = \frac{V_2}{V_1} R_L \cos \phi \qquad (1)$$

$$X = \frac{V_2}{V_1} R_L \sin \phi \qquad (2)$$

where R and X are the resistive and reactive components of the transducer impedance respectively, V_2 is the voltage across the transducer, V_1 is the voltage across R_L and ϕ is the phase shift between V_1 and V_2. With the five tuned annuli connected in series, the resistive and reactive components of AR2 were measured between 2.0 and 5.0 MHz. The results are plotted as discreet points in Figure 3.

Reproduced with permission of the copyright owner. Further reproduction prohibited without permission.

Reproduced with permission of the copyright owner. Further reproduction prohibited without permission.

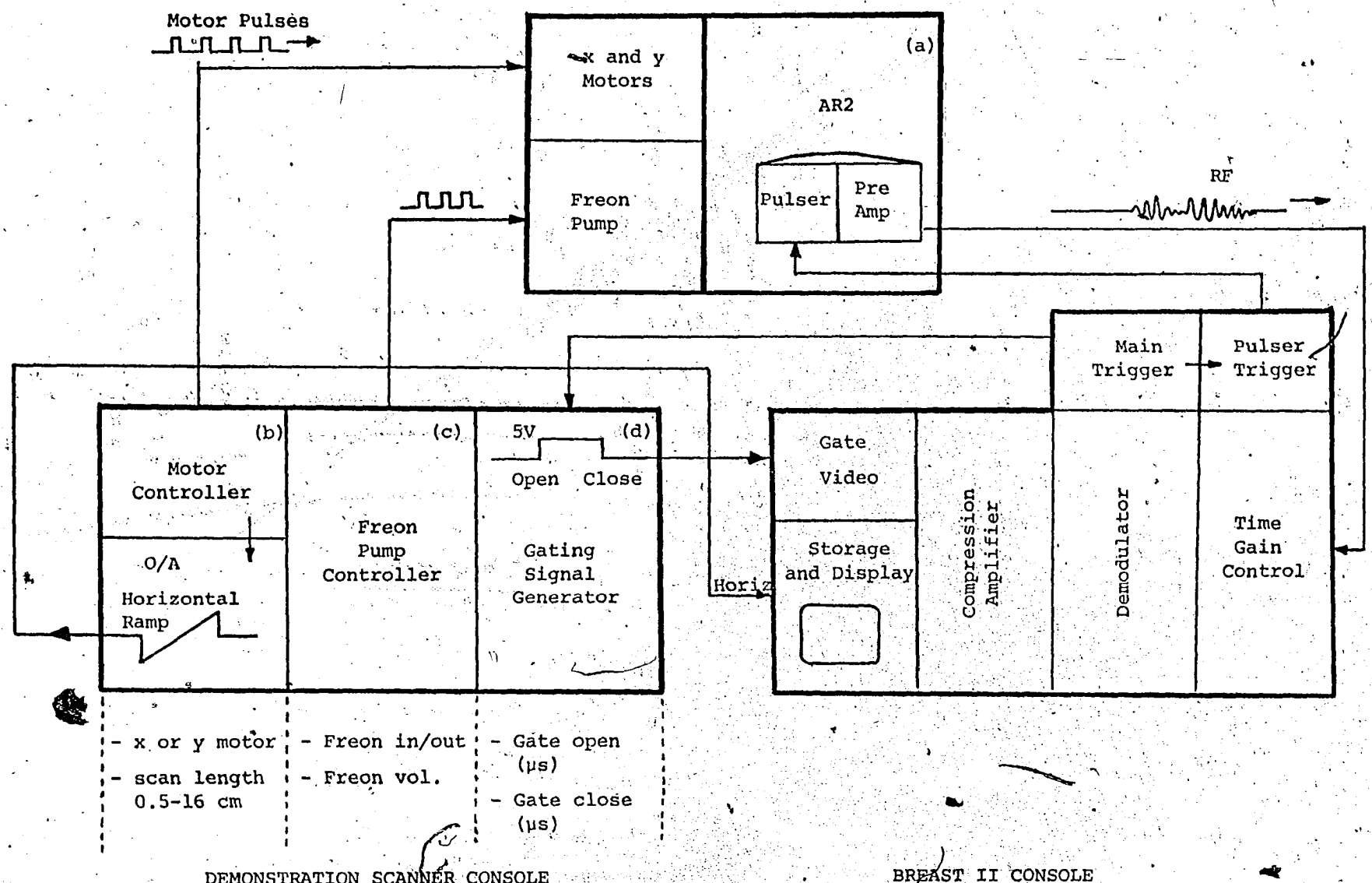

Figure 1. Block diagram of Demonstration Scanner electronics.

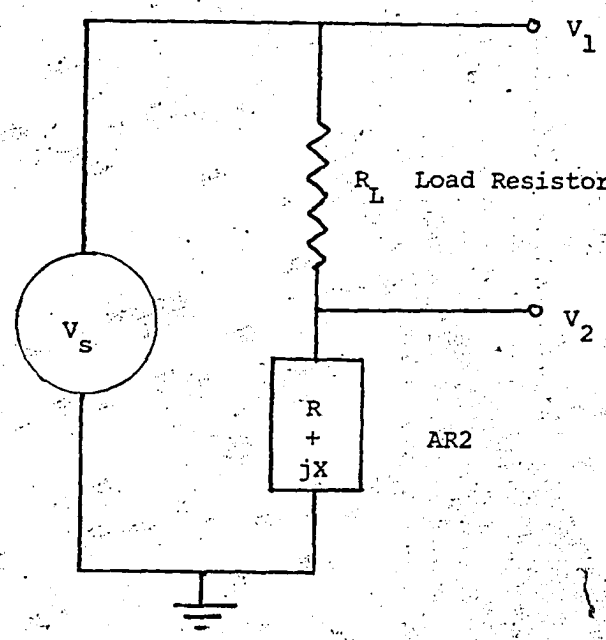

Figure 2. Circuit used to measure transducer impedance. $R_L >> R + jX$.

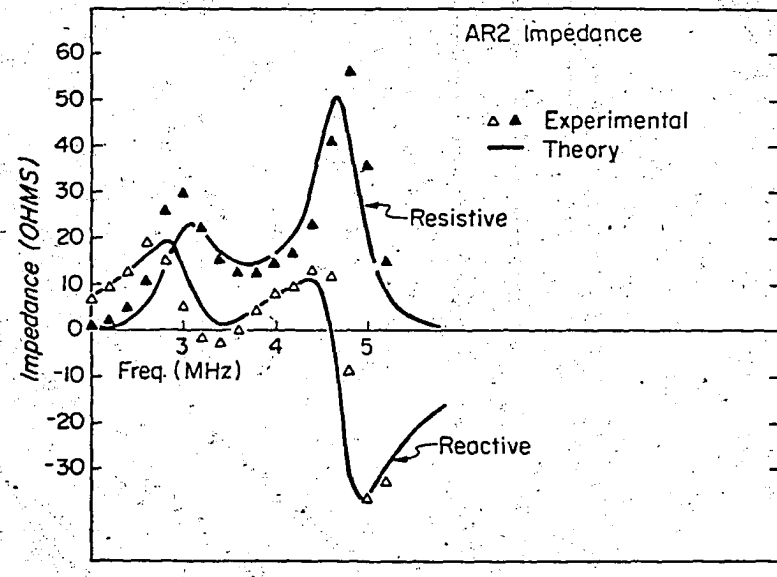

Figure 3. Theoretical and experimental electrical impedance of AR2 vs frequency.

Reproduced with permission of the copyright owner. Further reproduction prohibited without permission.

The theoretical impedance (solid lines), based on the Krimholtz transducer model (1), are also plotted and are in good agreement with the experimental results. The reactive impedance is very low in the frequency range 3.2-3.6 MHz indicating that the device is "tuned" in this region. Here, the total impedance is mainly resistive, ranging from 12 Ω to 22 Ω.

Circuits for the pulser and preamplifier that are built in to AR2 are given in Figure 4. These circuits were designed by the electronics group and expertly fabricated by Simon Backer. The pulser consists of two stages. The first accepts a TTL level pulse burst such as that shown in the circuit. This signal is buffered by the two input transistors and connected to a 2.5:1 step up transformer. The voltage swing at the output of the transformer is ∿12-15 V. A VMOS FET forms the second stage. VMOS was chosen for its fast response time and low output impedance (∿5Ω). When the voltage at the VMOS gate exceeds +10 V the VMOS switches on and the output is brought rapidly to -40 V where it remains until either the voltage at the gate drops below +10 V or the charge in the 1 μF Capacitor is exhausted. In essence, the pulser generates a -40 V low impedance replica of the TTL input. The measured output impedance of the pulser was 8.0 Ω which is reasonably close to the impedance of AR2 at 3.6 MHz (12.0Ω). (see Figure 3).

Echo signals from AR2 are matched to the preamplifier by a 3:1 step up transformer. The 3:1 transformer ratio was selected experimentally to optimize the S/N of the received signals. The input of the preamplifier is protected from the pulser by two 20 V zener diodes. Three parallel FET's formed a current driver for the low noise LH0032 operational amplifier. The voltage gain of the preamplifier is 10.0 and the noise at the output is 1.0 mV.

Reproduced with permission of the copyright owner. Further reproduction prohibited without permission.

Reproduced with permission of the copyright owner. Further reproduction prohibited without permission.

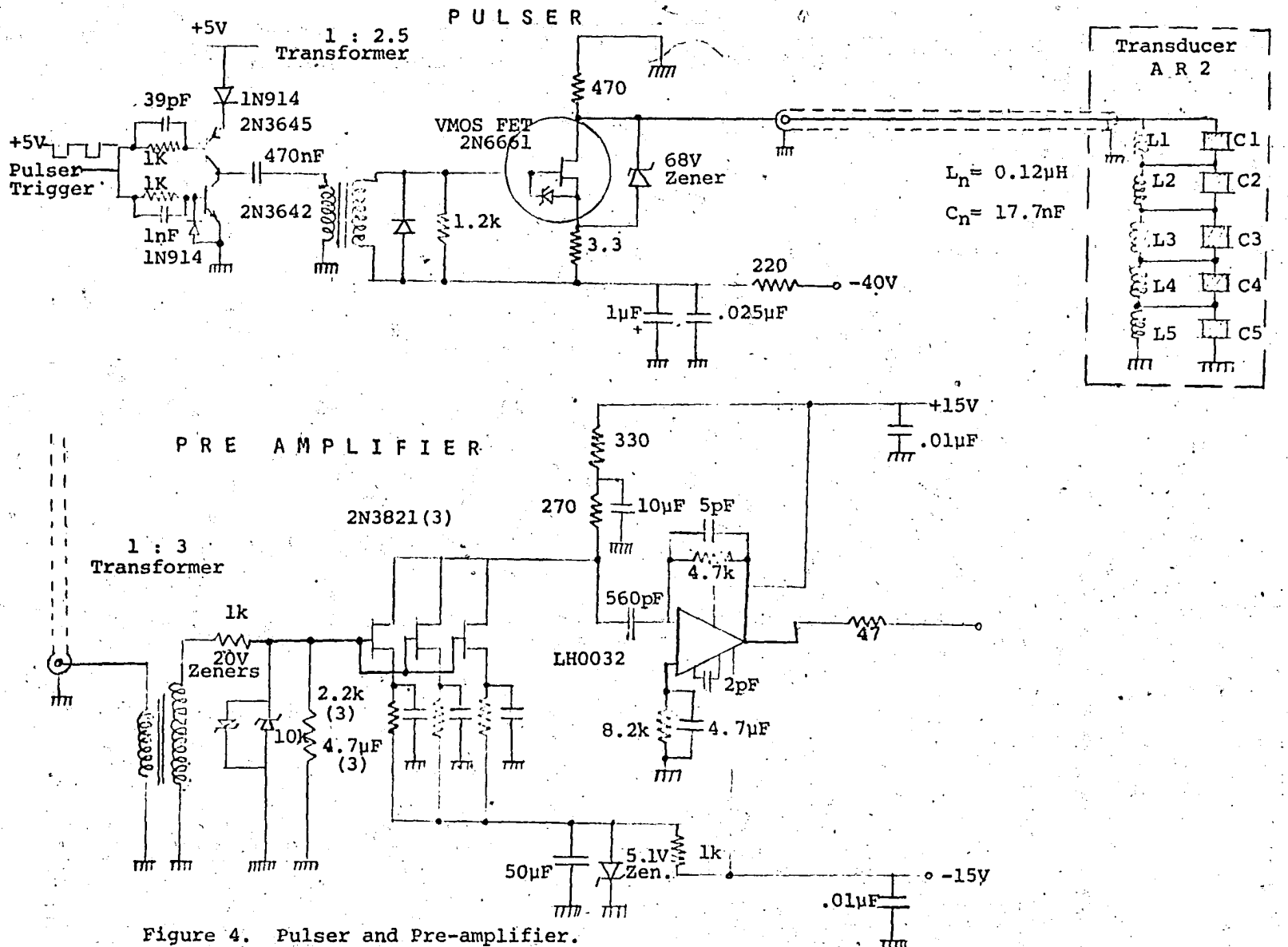

Figure 4. Pulser and Pre-amplifier.

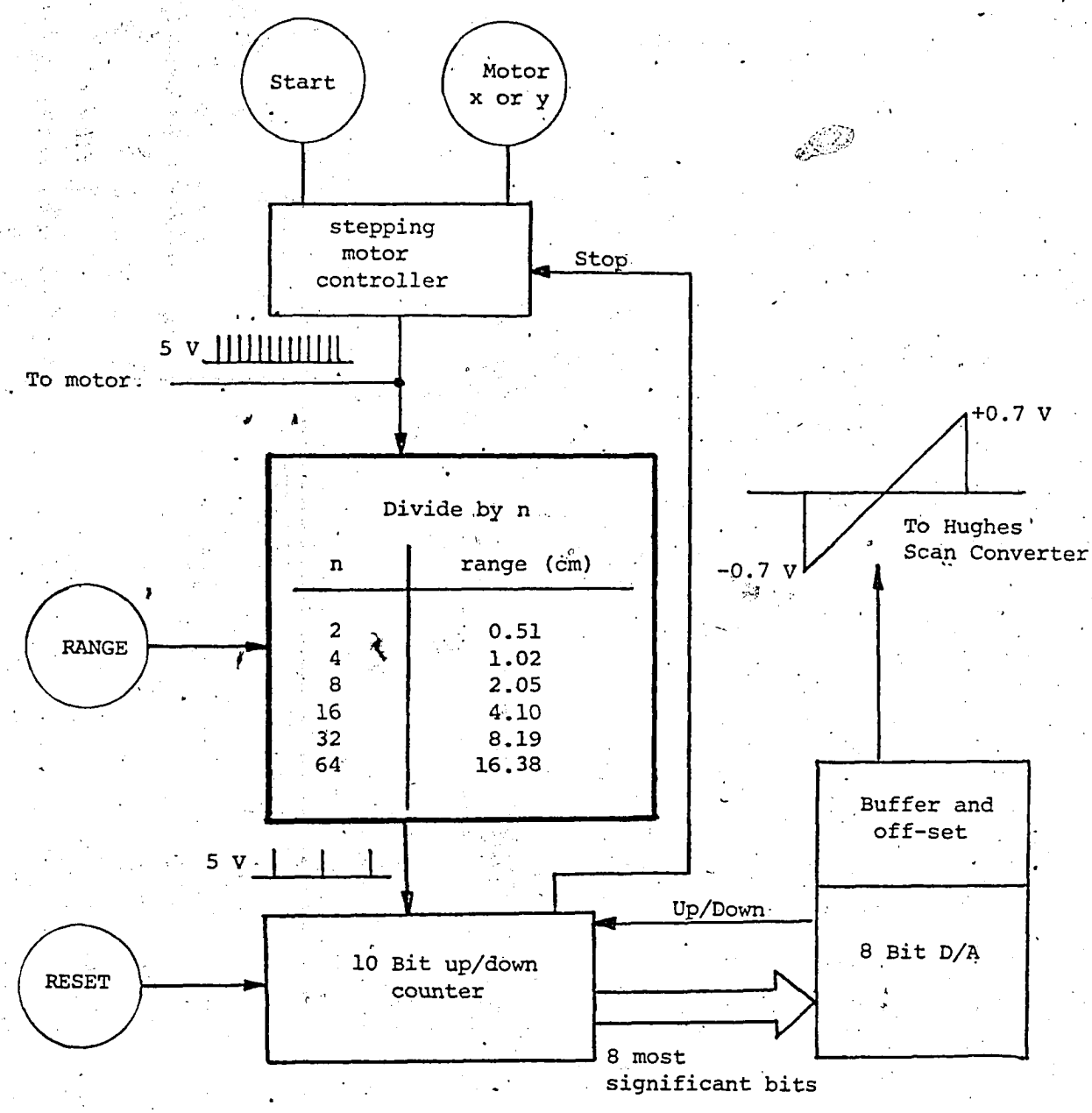

Figure 5. Motor control electronics.

Reproduced with permission of the copyright owner. Further reproduction prohibited without permission.

b) Transducer Motion

AR2 is mounted on two crossed linear slide assemblies (see Figure 1, Chapter 3). Both slides are moved by screws with a pitch of 1 mm/turn and are driven by stepping motors (M062, Superior Electric, Toronto). The stepping motors were operated in half step mode such that 400 steps move the transducer 1 mm.

A block diagram of the motor control circuitry is given in Figure 5. The distance that AR2 moves for a given scan (range) is controlled by a divide by n "gearbox" and a 10 bit up/down counter. When the latter counter reaches 1024 the stepping pulses are stopped. In the next scan the counter starts at 1024 and counts down to zero as the transducer returns to its original position. Ranges between 0.51 cm and 16.38 cm are available by changing n as indicated in Figure 5. For example, if n is 4, a total of (1024)·(4) = 4096 stepping pulses reach the motor resulting in a displacement of (4096)/(400 pulses/mm) = 1.02 cm.

The eight most significant bits of the 10 bit counter are fed to an 8 bit digital to analog (D/A) converter. The output of the D/A converter is buffered and offset such that the voltage output varies between -0.7 and +0.7 volts. This voltage swing is compatible with the horizontal input of the Hughes analog scan converter. Note that the voltage output to the scan converter (and hence the width of the viewed image) is independent of the range selected.

c) Freon Pump Controller

The Freon pump of the Demonstration Scanner is described in Section IIb of Chapter 3. The volume of Freon pumped in or out of the lens is proportional to the number of pulses applied to the pump motor. Figure 6 shows a block diagram of the Freon motor controller. The number of pulses to be delivered to the motor are entered on thumbwheel switches. When the start switch is activated, a clock

Reproduced with permission of the copyright owner. Further reproduction prohibited without permission.

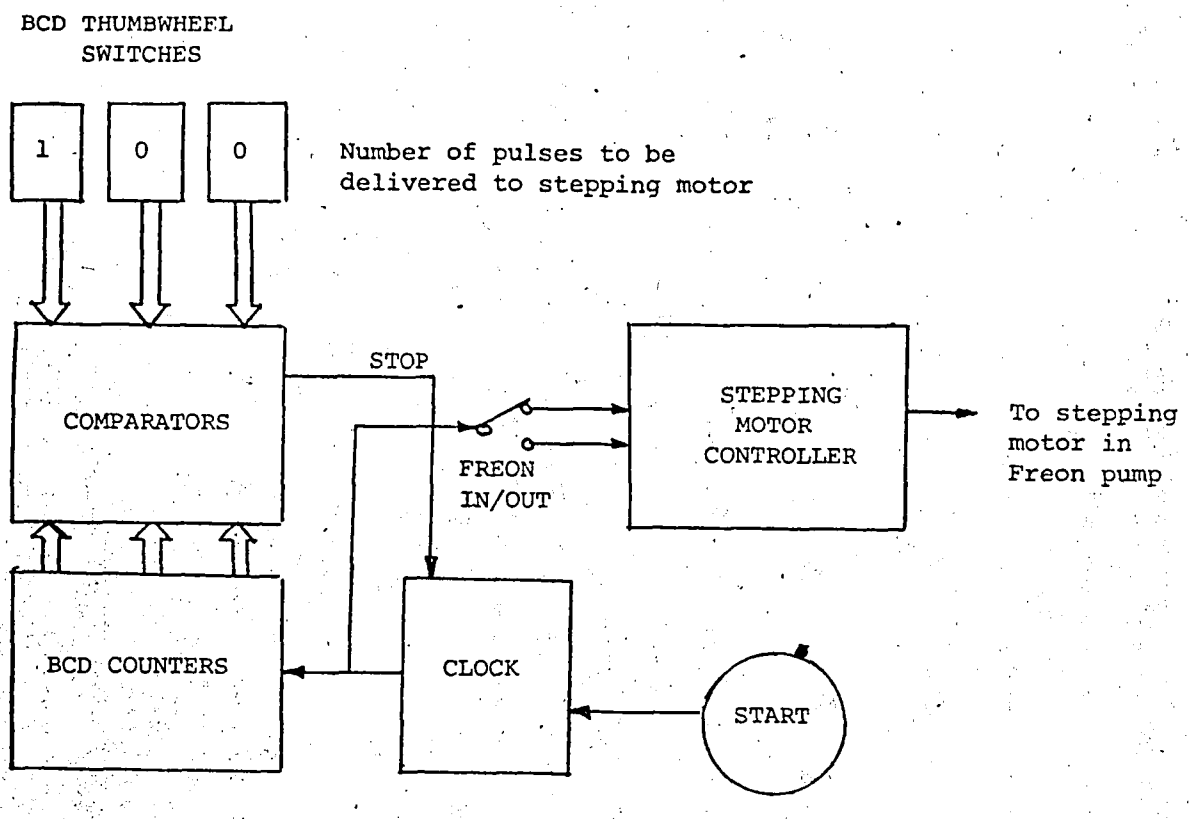

Figure 6. Freon pump controller

starts sending pulses to both a three digit binary coded decimal (BCD) counter and the stepping motor controller (STM 1001, Superior Electric, Toronto). When the values of the BCD counters are all equal to the values of the corresponding thumbwheel inputs a comparator generates a signal to stop the clock which in turn stops the motor.

d) Signal Gating

Signal gating is performed by the circuit given in Figure 7. A video gate, placed between the compression amplifier and scan converter, selects the information that is to be stored. The times at which the gate is to open, t_1, and close, t_2, are entered on sets of 4 digit thumbwheels. The timing sequence is activated by a trigger signal from the Breast II system which causes the 10 MHz clock to start. When the output of the counter is equal to t_1, a comparator triggers the

Reproduced with permission of the copyright owner. Further reproduction prohibited without permission.

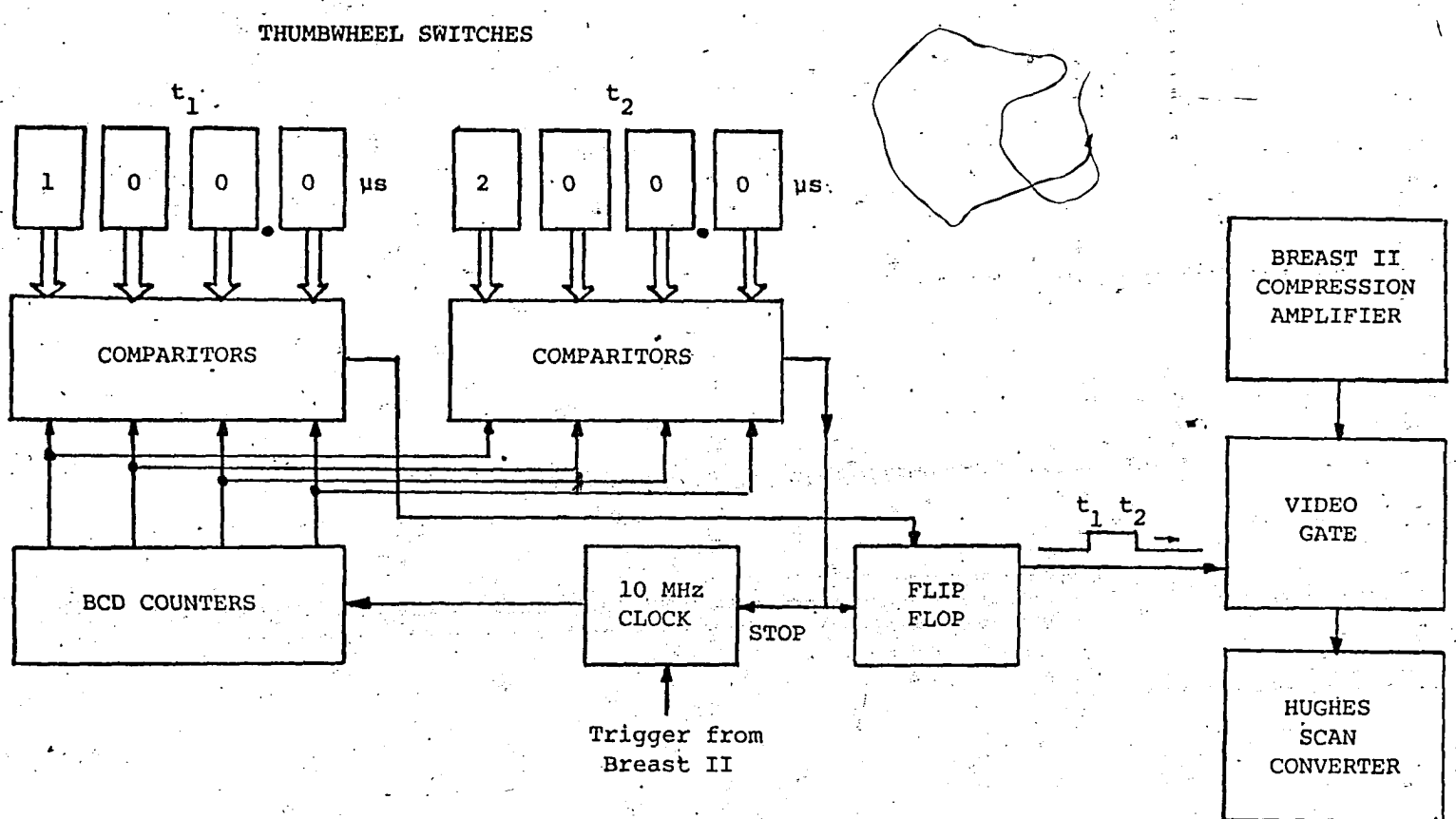

Figure 7. Gating electronics.

Reproduced with permission of the copyright owner. Further reproduction prohibited without permission.

flip-flop whose output goes high causing the gate to open. Video information is written on the scan converter until the counter has reached t_2, at which point a second comparator causes the flip-flop to go low, the gate to close, and the clock to stop. This process is repeated for each trigger cycle of the scanner. Zone focussed images exhibited no visible overlap of the zones or streaks from artefacts generated during the opening and closing of the gate.

Reproduced with permission of the copyright owner. Further reproduction prohibited without permission.

END

27·05·81

FIN

Reproduced with permission of the copyright owner. Further reproduction prohibited without permission.